



**POLITECNICO  
DI TORINO**

DEPARTMENT OF ELECTRONICS AND TELECOMMUNICATIONS  
Master degree in Electronic Engineering

Master Thesis

# Study of Field-Coupled Nanocomputing based on molecules for neural systems

**Supervisors**

Prof. Mariagrazia Graziano  
Prof. Gianluca Piccinini

**Candidate**

Giuliana Beretta

April 2020

# Abstract

Artificial neural networks (ANNs) have made tremendous progress, enabling the achievement of impressive results in artificial intelligence applications. In the last few years, the research highlighted the massive resource requirements of ANNs: contrarily to these, the human brain is capable of performing more general and complex tasks at a minuscule fraction of the power, time, and space required by state-of-the-art supercomputers. In parallel to this in recent years, the scaling process dictated by Moore's Law showed its future limitations, which led to the study and development of new ways to encode information. Among the extended scenario of proposed answers, there is a group of solutions classified as "Beyond CMOS" technology. In this context, the Field-Coupled Nanocomputing (FCN) is one of the most promising, thanks to its two intrinsic properties: ultra-small devices in large functional-density arrays, and low power dissipation.

The problem to be solved is related to the huge power consumption and space required by common ANNs. The research is trying to face the problem, working on the so-called spiking neural network (SNN), which should consume less power and occupy less area, performing the same task. This thesis work joins both ANNs and FCN paradigm, proposing

a model for an artificial neuron in the molecular implementation of the FCN paradigm. In this technology, the information is encoded in the charge distribution of a molecule, and the information propagation is enabled by the intermolecular electrostatic interaction, without the need for charge transport. The choice to use the molecular implementation derives from the fact that it has been shown that a molecule has a non-linear behaviour, capable of adding up the effects of surrounding molecules. The fact that a molecule has intrinsically the desired behaviour suggests that simple and compact structures can be obtained at the architectural level.

The methodology used to study the topic wants to be as general as possible. So starting from the neuron model, instead of using specific molecules and see if their features fit the goal, it has been chosen to work in terms of molecules transcharacteristics. This allows to define the properties a molecule should have to accomplish its task as a neuron. To simulate the molecular structure, a Self Consistent Electrostatic Potential Algorithm (SCERPA) is used, this tool analyses in an iterative way the molecule interactions.

The first fundamental result obtained in this work is the proof that the proposed structure actually behaves like an artificial neuron. The output switches when the sum of the weighted inputs reaches a certain threshold. In addition to this, the characteristics

that the input molecules must have to encode a certain weight have been defined. The properties that the output molecules must have to correctly propagate the information and to define the threshold for the output activation have also been identified.

The outcomes obtained confirm what was expected, namely that the molecules, for their intrinsic characteristics, lend themselves well to create an artificial neuron. The basic structure is very simple and compact when compared to the implementation of a “silicon neuron”. Moreover, the paradigm used permits to encode and transmit information without the use of current flow, being the information represented as the spatial charge distribution of a molecule, thus reducing the power consumption.

***Keywords:*** molecular Field-Coupled Nanocomputing (FCN), Neuromorphic Computing, Artificial Neurons, Artificial Neural Network (ANN)

*“Imparerai a tue spese che  
nel lungo tragitto della vita  
incontrerai tante maschere e pochi volti.”*  
– Luigi Pirandello

*A mio padre e mio fratello,  
gli unici due volti che ho incontrato.*



# Acknowledgements

Le persone che dovrei ringraziare per essere arrivata a concludere l'intero percorso universitario sono veramente tante e non riuscirei ad elencarle tutte in queste poche righe.

Prima di tutto intendo ringraziare i professori Mariagrazia Graziano e Gianluca Piccinini, non solo per la fiducia accordatemi accettando i ruoli di relatore e corelatore del presente lavoro, ruoli svolti con la loro consueta professionalità, ma soprattutto per avermi insegnato, già nei loro corsi, le qualità che un ingegnere deve avere sia dal punto di vista professionale che dal punto di vista umano.

Un sentito ringraziamento va poi a mio papà e a mio fratello, i quali hanno sempre creduto in me. In particolare li ringrazio per avermi concesso di dedicare tutta me stessa a ciò che più mi piaceva, sostenendomi moralmente ed anche economicamente, e per avermi dato la forza di superare tutte le difficoltà incontrate.

Ringrazio anche Yuri Ardesi per avermi aiutata quotidianamente nello sviluppo di questa tesi e non solo, per tutti i suoi suggerimenti pratici e per avermi insegnato ad ottimizzare tempi ed attività.

Infine, un enorme ringraziamento lo devo a tutti gli amici conosciuti in questi ultimi anni e non solo, per avermi dato preziosi consigli, per avermi sempre aiutata nel momento del bisogno e per i momenti di spensieratezza che hanno saputo regalarmi.



# Contents

|   |             |
|---|-------------|
| <b>Abstract</b>   | <b>i</b>    |
| <b>List of Figures</b>  | <b>ix</b>   |
| <b>List of Tables</b>   | <b>xv</b>   |
| <b>List of Acronyms</b>   | <b>xvii</b> |
| <b>1 Overview on Molecular FCN paradigm</b>                     | <b>1</b>    |
| 1.1 FCN and QCA as solutions for <i>Beyond CMOS</i> . . . . .   | 2           |
| 1.1.1 QCA basics . . . . .                                      | 3           |
| 1.1.2 QCA clock . . . . .                                       | 5           |
| 1.2 Molecular FCN . . . . .                                     | 8           |
| 1.2.1 Molecular FCN modelling . . . . .                         | 9           |
| 1.2.2 Molecular FCN technology . . . . .                        | 11          |
| <b>2 Brain-inspired computing</b>                               | <b>15</b>   |
| 2.1 Artificial Neural Networks (ANNs): fundamentals . . . . .   | 16          |
| 2.2 Spiking Neural Network (SNN) . . . . .                      | 18          |
| 2.3 Technology . . . . .  | 20          |
| <b>3 Molecular FCN for neuromorphic computation: some ideas</b> | <b>23</b>   |
| 3.1 Weight . . . . .  | 24          |
| 3.2 Sum . . . . .   | 24          |
| 3.3 Threshold and output signal . . . . .                       | 26          |
| 3.4 Outline . . . . .   | 27          |
| <b>4 Neuron inputs analysis</b>                                 | <b>33</b>   |
| 4.1 Step 0: the study of the first interface . . . . .          | 33          |
| 4.2 Step 1A: the study of the second interface . . . . .        | 44          |
| 4.3 Step 1B: the study of the third interface . . . . .         | 50          |

|          |   |           |
|----------|---|-----------|
| <b>5</b> | <b>Neuron output and connection with other neurons</b>        | <b>55</b> |
| 5.1      | Step 3: the influence of output molecules . . . . .           | 55        |
| 5.2      | Step 4: the study of the threshold . . . . .                  | 59        |
| 5.3      | Step 2: the effect of different molecules in the MV . . . . . | 62        |
| 5.4      | Step 5: toward neurons connected together . . . . .           | 66        |
| <b>6</b> | <b>Conclusion</b>   | <b>75</b> |
| <b>A</b> | <b>Molecules analysis with orca</b>                           | <b>77</b> |
| A.1      | Toward the characterization of a dendron . . . . .            | 77        |
| A.2      | <i>Modified</i> bisferrocene . . . . .                        | 81        |
|          | <b>Bibliography</b>   | <b>85</b> |

# List of Figures

|      |  |    |
|------|--|----|
| 1.1  | Transistor count and Moore’s Law, 1970-2018 [2]. . . . .   | 1  |
| 1.2  | Schematic of QCA cells: (a) QCA basic cell with the four quantum dots represented, (b) QCA cell in which two electrons occupy one of the main diagonal representing a logic ‘0’, (c) QCA cell in which two electrons occupy one of the main diagonal representing a logic ‘1’, (d) wire made of 5 QCA cells. . . . .                                       | 3  |
| 1.3  | A QCA majority logic gate. . . . .   | 4  |
| 1.4  | Logic functions implemented with QCA cells: (a) OR gate, obtained by a Majority gate with an input fixed to ‘0’, (b) AND gate, obtained by a Majority gate with an input fixed to ‘1’, (c) inverter gate implemented with QCA cells. . . . .   | 5  |
| 1.5  | Schematic of enriched QCA cells: (a) QCA basic cell with the six quantum dots represented, (b) QCA basic cell in the <i>Null state</i> or <i>Reset State</i> , (c) QCA basic cell in one of the two <i>stable states</i> . . . . .   | 6  |
| 1.6  | Schematic representation of the two possible situations related to the clock signal: when the <i>Clock</i> is active, or <i>Applied</i> , the cell stay in the <i>Null state</i> , whereas the <i>Clock</i> is not active, or <i>Released</i> , the cell configuration is stable and follow that of the input cell, usually called <i>Driver</i> . . . . . | 6  |
| 1.7  | Schematic representation of the information propagation as a pipeline: (a) trapezoidal clock signals overlapped to ensure correct propagation, (b) example of the first time steps in a wire. . . . .  | 7  |
| 1.8  | Conceptual molecule schematic: (a) position of the redundant charge in the logic ‘0’, (b) position of the redundant charge in the logic ‘1’, (c) position of the redundant charge in the <i>null</i> state. . . . .  | 8  |
| 1.9  | Bis-ferrocene molecule [28]. . . . .   | 9  |
| 1.10 | Figures of merit definitions: (a) electric field generated by the MUT on another molecule placed at a distance $d = w$ , (b) $V_{in}$ and $V_{out}$ definitions. . . . .   | 11 |
| 1.11 | Molecular wire implementation: (a) a substrate, for example a gold nanowire, onto which molecules are placed, (b) top view. . . . .  | 12 |
| 1.12 | Implementation of the electric fields involved in the computation (section view): (a) input voltage is generated by two electrodes placed on top of the trench, (b) the clock field is obtained by a potential difference between the top electrodes and the gold nanowire at the bottom of the trench. . . . .  | 12 |

|      |   |    |
|------|---|----|
| 1.13 | Clocked molecular FCN nanowire implementation. . . . .  | 13 |
| 1.14 | Clocked molecular FCN nanowire implementation: zoom in the separation of two electrodes. . . . .  | 13 |
| 1.15 | Schematic representation of some possible implementation defects: (a) vertical misalignment, (b) horizontal shift, (c) tilting. . . . .   | 14 |
| 2.1  | Schematic representation of a neuron in a biological system [35]. . . . .   | 16 |
| 2.2  | Schematic representation of a neuron in an artificial system, where $x_i$ are the inputs and $w_i$ are the weights associated to them. . . . .  | 17 |
| 2.3  | Examples of common activation functions in ANNs [36]: (a) sigmoid function, (b) tansig function, (c) step function, (d) shifted step function, (e) sign function, (f) linear function. . . . .  | 18 |
| 2.4  | The action potential. . . . .   | 19 |
| 2.5  | Schematic circuit of an integrate-and-fire neuron model [43]. . . . .   | 20 |
| 3.1  | Hysteresis phenomenon in a wire made of bisferrocene molecules [63]. . . . .  | 24 |
| 3.2  | Schematic model of a possible implementation of a neuron in molecular FCN, where $w_i$ represent the synaptic weight of the $i$ -th input wire. . . . .   | 25 |
| 3.3  | Input voltage versus aggregated charge transcharacteristic (VAC) for the bisferrocene molecule. . . . .   | 26 |
| 3.4  | Schematic representation of the two possibilities to implement the threshold: (a) applying an external voltage to the first molecule of the output wire, (b) using a particular molecule with an intrinsically shifted VACT. . . . .  | 27 |
| 3.5  | Scheme of the structure analysed in the step 0. . . . .   | 27 |
| 3.6  | Schemes of the analysed structures: (a) in the step 1A, (b) in the step 1B. . . . .   | 28 |
| 3.7  | Scheme of the structure analysed in the step 2. . . . .   | 29 |
| 3.8  | Representation of the two molecules used [29]: (a) diallyl-butane, (b) decatriene. . . . .  | 29 |
| 3.9  | Schemes of the analysed structures: (a) in the step 3, (b) in the step 4. . . . .   | 30 |
| 3.10 | Scheme of the structure analysed in the step 5. . . . .   | 31 |
| 4.1  | Transcharacteristics used to analyse the behaviour of the first interface: (a) asymmetric transcharacteristics, (b) symmetric transcharacteristics. . . . .   | 34 |
| 4.2  | Layout of the architecture studied in the step 0: (a) schematic representation, (b) SCERPA representation. . . . .  | 34 |
| 4.3  | $V_{in}$ - $V_{out}$ characteristic when using the <i>symmetric</i> transcharacteristics for the interface and $V_{out}$ is computed <i>without</i> the contribution of the driver voltage. . . . .   | 35 |
| 4.4  | $V_{in}$ - $V_{out}$ characteristic when using the <i>symmetric</i> transcharacteristics for the interface and $V_{out}$ is computed <i>with</i> the contribution of the driver voltage. . . . .  | 36 |
| 4.5  | $V_{in}$ - $V_{out}$ characteristic when using the <i>asymmetric</i> transcharacteristics for the interface: (a) $V_{out}$ is computed <i>without</i> the contribution of the driver voltage, (b) $V_{out}$ is computed <i>with</i> the contribution of the driver voltage. . . . . | 37 |

|      |  |    |
|------|--|----|
| 4.6  | Layout of the architecture designed to insert a symmetry in the structure.   | 38 |
| 4.7  | $V_{in}$ - $V_{out}$ characteristic when $V_{out}$ is computed <i>without</i> the contribution of the driver voltage: (a) using the <i>symmetric</i> transcharacteristics for the interface 1, (b) using the <i>asymmetric</i> transcharacteristics for the interface 1.   | 39 |
| 4.8  | $V_{in}$ - $V_{out}$ characteristic when $V_{out}$ is computed <i>with</i> the contribution of the driver voltage: (a) using the <i>symmetric</i> transcharacteristics for the interface 1, (b) using the <i>asymmetric</i> transcharacteristics for the interface 1.  | 40 |
| 4.9  | New transcharacteristics synthesized to analyse the behaviour of the first interface: (a) asymmetric transcharacteristics, (b) symmetric transcharacteristics.   | 41 |
| 4.10 | $V_{in}$ - $V_{out}$ characteristic when $V_{out}$ is computed <i>without</i> the contribution of the driver voltage: (a) using the new <i>symmetric</i> transcharacteristics for the interface 1, (b) using the new <i>asymmetric</i> transcharacteristics for the interface 1.   | 42 |
| 4.11 | $V_{in}$ - $V_{out}$ characteristic when $V_{out}$ is computed <i>with</i> the contribution of the driver voltage: (a) using the new <i>symmetric</i> transcharacteristics for the interface 1, (b) using the new <i>asymmetric</i> transcharacteristics for the interface 1.  | 43 |
| 4.12 | Transcharacteristics used to analyse the behaviour of the first part of the step 1, it was chosen the one represented with a continuous line: (a) asymmetric transcharacteristics, (b) symmetric transcharacteristics.   | 44 |
| 4.13 | $V_{in1}$ - $V_{out}$ characteristics for different values of $V_{in2}$ using the <i>symmetric</i> transcharacteristic $\alpha = 0.5$ for the interfaces: (a) when $V_{out}$ is computed <i>without</i> the contribution of the driver voltage, (b) when $V_{out}$ is computed <i>with</i> the contribution of the driver voltage. | 45 |
| 4.14 | $V_{in1}$ - $V_{out}$ characteristics for different values of $V_{in2}$ using the <i>asymmetric</i> transcharacteristic $\alpha = 0.5$ for the interfaces, when $V_{out}$ is computed <i>without</i> the contribution of the driver voltage.   | 46 |
| 4.15 | $V_{in1}$ - $V_{out}$ characteristics for different values of $V_{in2}$ using the <i>asymmetric</i> transcharacteristic $\alpha = 0.5$ for the interfaces, when $V_{out}$ is computed <i>with</i> the contribution of the driver voltage.  | 47 |
| 4.16 | Schematic representation on the four extreme possible configurations for the output when: (a) both $V_{in1}$ and $V_{in2}$ are positive, (b) $V_{in1}$ is positive and $V_{in2}$ is negative, (c) both $V_{in1}$ and $V_{in2}$ are negative, (d) $V_{in1}$ is negative and $V_{in2}$ is positive.                                  | 47 |
| 4.17 | Representation of a QCA cell with the dot numbered.  | 48 |
| 4.18 | Input-output characteristics when the <i>symmetric</i> transcharacteristics are used for the drivers.  | 49 |
| 4.19 | Example to control if the MV works correctly when two different transcharacteristics are used for the interface 1 and the interface 2.   | 49 |

|      |   |    |
|------|---|----|
| 4.20 | Layout plotted with SCERPA for the simulations in which driver 1 has a symmetric transcharacteristic with $\alpha = 0.1$ , whereas Drivers 2 and 3 have a symmetric transcharacteristic with $\alpha = 0.5$ : (a) all three drivers have an input voltage equal to $+0.3$ V, (b) drivers 1 and 3 have an input voltage equal to $+0.3$ V, whereas the second interface has $V_{in2} = -0.3$ V. . . . .  | 50 |
| 4.21 | Layout plotted with SCERPA for the simulations in which driver 1 has a symmetric transcharacteristic with $\alpha = 0.1$ , whereas Drivers 2 and 3 have a symmetric transcharacteristic with $\alpha = 0.5$ : (a) drivers 2 and 3 have an input voltage equal to $+0.3$ V, whereas the first interface has $V_{in1} = -0.3$ V, (b) drivers 2 and 3 have an input voltage equal to $+0.1$ V, whereas the first interface has $V_{in1} = -0.1$ V. . . . . | 51 |
| 4.22 | Simulation results to verify the maximum possible voltage on a molecule: (a) SCERPA layout of the wired MV tested, (b) input voltage on each molecule. . . . .  | 52 |
| 4.23 | Transcharacteristics that guarantee a linear behaviour in the range of possible voltages on a molecule: (a) asymmetric transcharacteristics, (b) symmetric transcharacteristics. . . . .  | 52 |
| 5.1  | Simulation results when one molecule is placed at the output: (a) 3D representation, (b) charge for each molecule excluding the drivers. . . . .  | 56 |
| 5.2  | Charge for each molecule excluding the drivers when: (a) two molecules are placed at the output, (b) eight molecules are placed at the output. . . . .  | 57 |
| 5.3  | Charge for each molecule excluding the drivers, in the case of well define logic value on the central cell of the MV, when: (a) eight molecules are placed at the output, (b) ten molecules are placed at the output. . . . .   | 57 |
| 5.4  | Layout of the structure with the molecules used specified. . . . .  | 58 |
| 5.5  | Simulation results when eight molecules are placed at the output, the first is a molecule with $\alpha = 0.1$ V whereas the other seven are bisferrocenes: (a) 3D representation, (b) charge for each molecule excluding the drivers. . . . .   | 58 |
| 5.6  | Simulation results when eight molecules are placed at the output, the first is a molecule with $\alpha = 0.1$ V whereas the other seven are bisferrocenes, and the logic value on the MV is weak: (a) first time step of the simulation, (b) second time step of the simulation. . . . .  | 59 |
| 5.7  | SCERPA layout of the structure used to study the threshold mechanism using the external voltages. . . . .   | 60 |
| 5.8  | Relation between the polarization of the cell composed by the two drivers which simulate the MV and the input voltage on the first molecule after the driver (blue) and on the second molecule (orange). . . . .  | 60 |

|      |  |    |
|------|--|----|
| 5.9  | Relation between the polarization of the cell composed by the two drivers which simulate the MV and the input voltage on the first and the second molecule after the driver, for the reference case (cyan and magenta) and for the case in which an external voltage equal to +0.2 V is applied on the first molecule (blue and red). . . . .  | 61 |
| 5.10 | Transcharacteristics synthesized to study the effect of molecules with one logic state stronger than the other to implement the threshold mechanism. The pairs of curves for the two logical dots are identified by the intensity of the color. . . . .  | 63 |
| 5.11 | Polarization of the cell composed by the two drivers versus the input voltage on the second driver when: (a) the first driver is shifted by 0.1 V and the second by -0.1 V, (b) the first driver is shifted by -0.1 V and the second by 0.1 V, (c) the first driver is shifted by 0.2 V and the second by -0.2 V, (d) the first driver is shifted by -0.2 V and the second by 0.2 V, (e) the first driver is shifted by 0.3 V and the second by -0.3 V, (f) the first driver is shifted by -0.3 V and the second by 0.3 V. . . . . | 64 |
| 5.12 | Study of the threshold mechanism using, as drivers, two bisferrocenes in which one of the iron atom is substituted by a cobalt atom: (a) SCERPA layout which highlight the 180° rotation of the first driver, (b) polarization versus the input voltage on the second driver. . . . .  | 65 |
| 5.13 | Study of the threshold mechanism using, as drivers, two bisferrocenes in which one of the iron atom is substituted by a cobalt atom: (a) SCERPA layout which highlight the 180° rotation of the second driver, (b) polarization versus the input voltage on the second driver. . . . .   | 66 |
| 5.14 | Layout of the complete neuron: (a) schematic representation, (b) SCERPA representation. . . . .  | 67 |
| 5.15 | Simulation result of the neuron structure when the central cell of the MV is composed of bisferrocene molecules, that is threshold is equal to zero. . . . .   | 68 |
| 5.16 | Simulation result of the neuron structure when: (a) the threshold is equal to -0.2 V, (b) the threshold is equal to +0.2 V. . . . .  | 68 |
| 5.17 | Schematic representation of the neuron layout with the interfaces connected to the drivers with short wires. . . . .   | 69 |
| 5.18 | Simulation result of the neuron structure when there is no threshold: (a) <i>input propagation</i> time step, (b) <i>output propagation</i> time step. . . . .   | 70 |
| 5.19 | Simulation result of the neuron structure when threshold is equal to -0.2 V: (a) <i>input propagation</i> time step, (b) <i>output propagation</i> time step. . . . .  | 71 |
| 5.20 | Simulation result of the neuron structure when threshold is equal to 0.2 V: (a) <i>input propagation</i> time step, (b) <i>output propagation</i> time step. . . . .   | 72 |
| A.1  | Ferrocene-Cobaltocene molecule: (a) plotted with Avogadro, (b) schematic representation. . . . .   | 78 |

|      |  |    |
|------|--|----|
| A.2  | VAC transcharacteristic of the Ferrocene-Cobaltocene molecule: (a) whole transcharacteristic, (b) enlargement of the central region. . . . .   | 79 |
| A.3  | Ferrocene-Cobaltocene molecule: (a) scheme that shows where point-charges have been positioned, (b) VAC transcharacteristic obtained in that case. . . . .   | 79 |
| A.4  | VAC transcharacteristic for: (a) Ferrocene-Cobaltocene molecule with five carbon atoms in the chain, (b) Ferrocene-Cobaltocene molecule with three carbon atoms in the chain. . . . .  | 80 |
| A.5  | Bis-ferrocene molecule. . . . .  | 81 |
| A.6  | VAC Transchatacteristics obtained from the ORCA data for the bisferrocene molecule when: (a) clock signal is equal to +2 V, (b) clock signal is equal to 0 V, (c) clock signal is equal to -2 V. . . . .   | 82 |
| A.7  | <i>Modified</i> bis-ferrocene molecule with one cobalt atom instead of an iron atom. . . . .   | 82 |
| A.8  | VAC Transchatacteristics obtained from the ORCA data for the bisferrocene molecule with one cobalt atom instead of an iron atom, when: (a) clock signal is equal to +2 V, (b) clock signal is equal to 0 V, (c) clock signal is equal to -2 V. . . . .         | 83 |
| A.9  | <i>Modified</i> bis-ferrocene molecule with both the iron atoms substituted with cobalt atoms. . . . .   | 84 |
| A.10 | VAC Transchatacteristics obtained from the ORCA data for the bisferrocene molecule with both the iron atoms substituted by cobalt atoms, when: (a) clock signal is equal to +2 V, (b) clock signal is equal to 0 V, (c) clock signal is equal to -2 V. . . . . | 84 |

# List of Tables

|     |   |    |
|-----|---|----|
| 1.1 | Truth table of the majority gate function. . . . .  | 4  |
| 1.2 | Truth table of the majority gate function, which highlights: the behaviour of an AND gate (cyan rectangle) if the fixed input (IN 1) is '0'; the behaviour of an OR gate (magenta rectangle) if the fixed input (IN 1) is equal to '1'. . . . . | 4  |
| 4.1 | Weights of the interface 1 when the symmetric transcharacteristics are used.  | 48 |
| 4.2 | Weights of the interfaces calculated with the last set of synthesized transcharacteristics. . . . .   | 53 |
| 5.1 | Absolute values of the voltage shift on the two molecules after the drivers when an external voltage is applied either on the first molecule or on the second. . . . .  | 62 |



# List of Acronyms

|                 |  |
|-----------------|--|
| <b>FCN</b>      | Field-Coupled Nano-computing                             |
| <b>IC</b>       | Integrated Circuit                                       |
| <b>ITRS</b>     | International Technology Roadmap for Semiconductors      |
| <b>MtM</b>      | More than Moore  |
| <b>BC</b>       | Beyond CMOS  |
| <b>CMOS</b>     | Complementary MOS  |
| <b>QCA</b>      | Quantum-dot Cellular Automata                            |
| <b>MoSQuiTo</b> | Molecular Simulator Quantum-dot cellular automata Torino |
| <b>AC</b>       | Aggregated Charge  |
| <b>EFGR</b>     | Electric Field Generated at the Receiver molecule        |
| <b>MUT</b>      | Molecule Under Test                                      |
| <b>VVT</b>      | $V_{in}$ - $V_{out}$ transcharacteristic                 |
| <b>VACT</b>     | $V_{in}$ -AC transcharacteristic                         |
| <b>VOM</b>      | $V_{out}$ Map  |
| <b>MQCA</b>     | Molecular Quantum-dot Cellular Automata                  |
| <b>CWZ</b>      | Cell Working Zone  |
| <b>SCERPA</b>   | Self-Consistent Electrostatic Potential Algorithm        |
| <b>ANN</b>      | Artificial Neural Network                                |
| <b>SNN</b>      | Spiking Neural Network                                   |
| <b>HNN</b>      | Hardware Neural Network                                  |
| <b>MV</b>       | Majority Voter   |



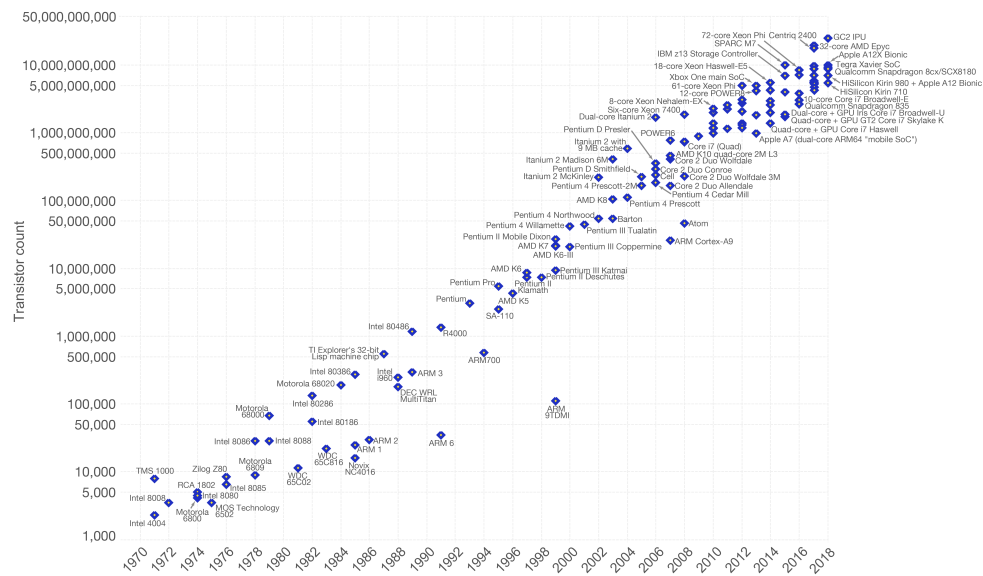
# Chapter 1

## Overview on Molecular FCN paradigm

The technological development of the last 50 years follow the rhythm of Moore's Law [1]. In its standard form, Moore's Law states that the number of transistors on an IC double about every two years, as shown in Figure 1.1. In order to define the long-term planning and the targets for the research and development, Moore's Law has been, more than anything else, an agreement between mainly three parties: software developers, hardware designers, and IC producers.

### Moore's Law – The number of transistors on integrated circuit chips (1971-2018)

Moore's law describes the empirical regularity that the number of transistors on integrated circuits doubles approximately every two years. This advancement is important as other aspects of technological progress – such as processing speed or the price of electronic products – are linked to Moore's law.



Data source: Wikipedia ([https://en.wikipedia.org/wiki/Transistor\\_count](https://en.wikipedia.org/wiki/Transistor_count))  
The data visualization is available at OurWorldInData.org. There you find more visualizations and research on this topic. Licensed under CC-BY-SA by the author Max Roser.

Figure 1.1: Transistor count and Moore's Law, 1970-2018 [2].

Moore's law can be expressed in another form, which underlines one of the physical barriers Silicon Industry is running into. It states that the minimum size within an integrated circuit, the channel length, reduces by 30% every three years. Gordon Moore itself stated in an interview that the size of the transistor, in terms of minimum dimension, is approaching the size of atoms which is a fundamental barrier [3].

The second huge limitations coming from shrinking transistors dimensions is related to power consumption. Until the past decade, for each technology node, both transistor count and frequency kept on increasing. Due to physical limitations on power dissipation, one of these two parameters had to slow down its trend. The choice has been for the frequency, which has been stopped to a few GHz in the last years [4].

Analysing the trend and the behaviour of the new equilibrium emerged in the last two decades, the requirement to find new solutions to the standard performance-addressed innovation stands out. In this sense, the ITRS report clearly defines the two paths that can be undertaken [4]:

**More than Moore (MtM)** which refers to the possibility to produce heterogeneous integrated systems, like Systems-on-Chip, in order to create complex systems that accomplish specific tasks. It's related to the differentiation of circuits functionalities [5];

**Beyond CMOS (BC)** which includes new technology paradigm and device principle [6].

## 1.1 FCN and QCA as solutions for *Beyond CMOS*

Some examples of the possible solutions proposed over the past decade as alternative information processing emerging research devices can be found in ITRS [4]. The FCN paradigm is one of these, offering a completely new approach to information coding and processing. Among all the possible implementations, molecular FCN is one of the most interesting. The paradigm wants to not use conduction to transmit information. The basic concept is thus to use devices not as current switches but as structured charges containers, that can influence each other through the coupling of electric fields. The theoretical principle is to encode information in electrons position and to have a region in which electrons can be hosted: quantum dots can be a possibility. The main advantages of this technology are:

- possibility to have small devices;
- without charge transport, there is no power consumption due to transmission of information, the only dissipation is due to the switching [7], [8];
- possibility to work at room temperature [9], [10].

### 1.1.1 QCA basics

The most common implementation of molecular FCN is based on the concept of Quantum-dot Cellular Automata (QCA), in which quantum dots are the low potential regions in which electrons are more likely to stay. The basic cell is a square in which there are four dots, as shown in Figure 1.2(a): electrons can move between dots through tunnelling. Assuming to have two electrons in the cells, due to Coulomb force electrons place more likely on the two diagonals [11], as shown in Figure 1.2(b) and Figure 1.2(c). Thus there are two possible arrangements associated with two possible logic values, and these states, called *ground states*, are equivalent from an energetic point of view.

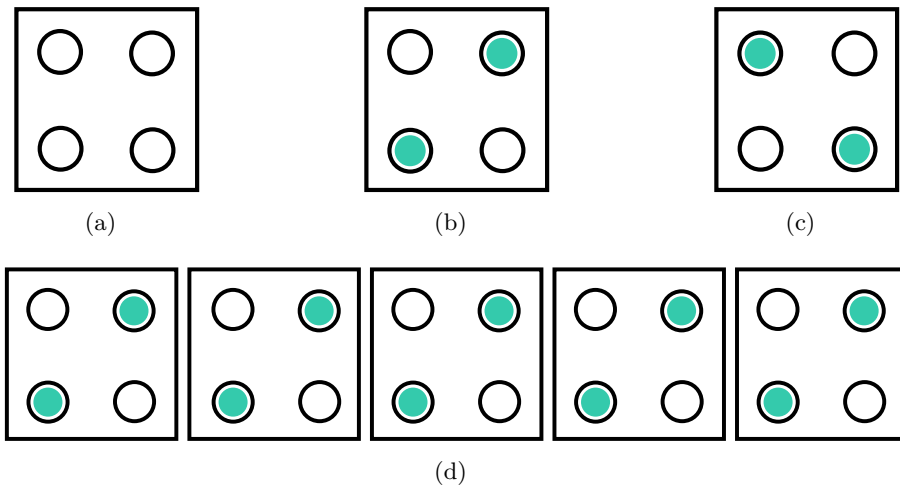


**Figure 1.2:** Schematic of QCA cells: (a) QCA basic cell with the four quantum dots represented, (b) QCA cell in which two electrons occupy one of the main diagonal representing a logic ‘0’, (c) QCA cell in which two electrons occupy one of the main diagonal representing a logic ‘1’, (d) wire made of 5 QCA cells.

To propagate the information, cells are placed one nearby the other with a correct distance, which depends on the technology, as shown in Figure 1.2(d). If one forces the first cell in one of the two possible arrangements, then all the other cells will assume the same configuration, to have the lowest possible energy. By changing the state of the first cell, all the others will change accordingly in a *domino* style. So information propagates without charge transfer through a pseudo-wire made of neighbouring cells. Information propagation requires only the switching within each cell, whose energy has been studied and is of the order of  $10^{-20}$  J [12]. Just to have an idea, the switch for a transistor requires minimum energy of the orders of  $10^{-18}$  J, so two orders of magnitude bigger [13].

Logic functions can be obtained by specific displacement of the cells. The basic gate is the three-input *Majority Voter*, shown in Figure 1.3, whose truth table is Table 1.1. It consists of three inputs converging on a computing cell. The state of the cell is

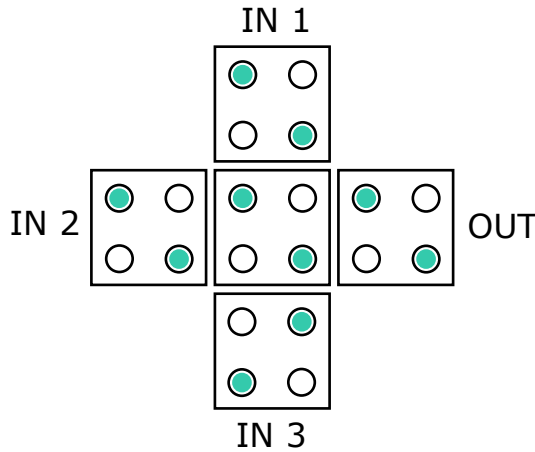


**Figure 1.3:** A QCA majority logic gate.

**Table 1.1:** Truth table of the majority gate function.

| IN 1 | IN 2 | IN 3 | OUT |
|------|------|------|-----|
| 0    | 0    | 0    | 0   |
| 0    | 0    | 1    | 0   |
| 0    | 1    | 0    | 0   |
| 0    | 1    | 1    | 1   |
| 1    | 0    | 0    | 0   |
| 1    | 0    | 1    | 1   |
| 1    | 1    | 0    | 1   |
| 1    | 1    | 1    | 1   |

determined by the state of the majority of the inputs [11].

Playing with the majority gate, it is possible to obtain both an AND gate and an OR gate. In fact, looking at the truth table of the majority gate, it is possible to see that fixing one of the three inputs, the remaining truth table is that of an AND or an OR, depending on the logic value of the fixed input, as highlighted in Table 1.2. The two resulting gates are shown in Figure 1.4(a) and Figure 1.4(b). The structure of an inverter, which is the simplest gate in CMOS technology, is not so easy to obtain. The implementation of an inverter is shown in Figure 1.4(c).

**Table 1.2:** Truth table of the majority gate function, which highlights: the behaviour of an AND gate (cyan rectangle) if the fixed input (IN 1) is ‘0’; the behaviour of an OR gate (magenta rectangle) if the fixed input (IN 1) is equal to ‘1’.

| IN 1 | IN 2 | IN 3 | OUT |
|------|------|------|-----|
| 0    | 0    | 0    | 0   |
| 0    | 0    | 1    | 0   |
| 0    | 1    | 0    | 0   |
| 0    | 1    | 1    | 1   |
| 1    | 0    | 0    | 0   |
| 1    | 0    | 1    | 1   |
| 1    | 1    | 0    | 1   |
| 1    | 1    | 1    | 1   |

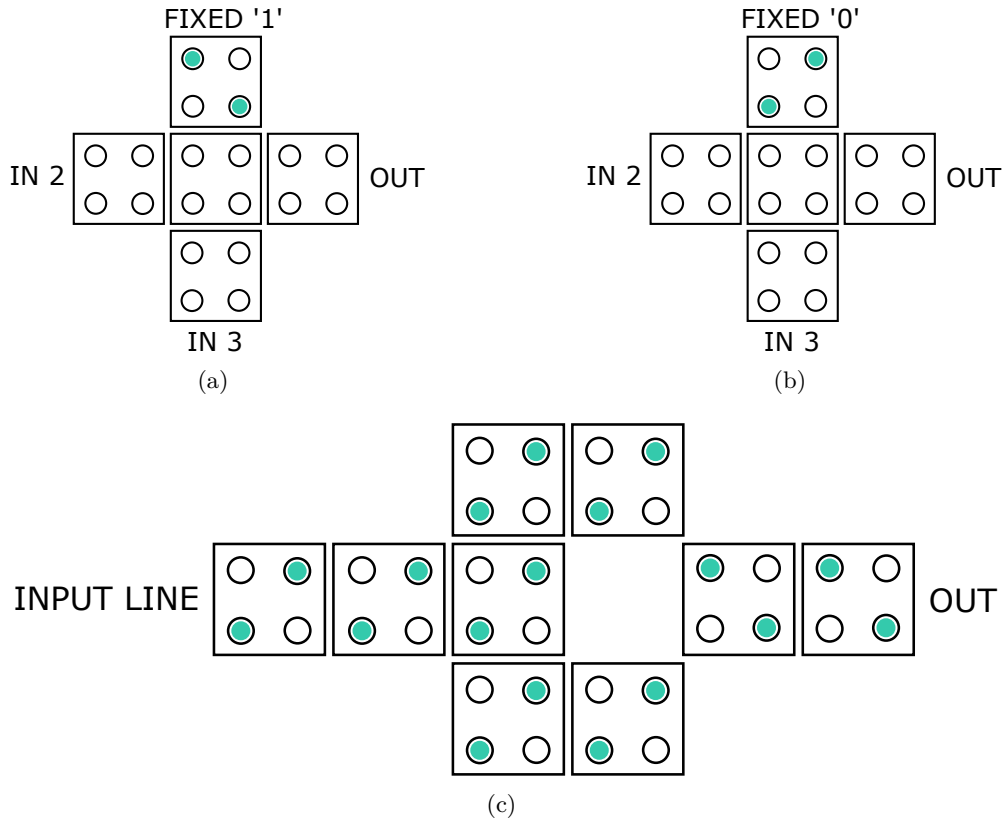


**Figure 1.4:** Logic functions implemented with QCA cells: (a) OR gate, obtained by a Majority gate with an input fixed to ‘0’, (b) AND gate, obtained by a Majority gate with an input fixed to ‘1’, (c) inverter gate implemented with QCA cells.

### 1.1.2 QCA clock

What has been assumed until now was:

- cell configuration can switch, so there is a *low potential barrier* between the two possible states;
- logic values are stable, so there is a *high potential barrier* between the two configurations;
- there is a direction of propagation, i.e. information goes from the left to the right;
- there is no loss of information during the propagation.

For what concerns the last point, it is true for a limited number of cells: overcome that maximum number of neighbouring cells, information gets lost. The main causes of this phenomenon are temperature and external noise. On the other hand, to solve the

first two questions that are in contrast, the cell must be enriched with a sort of *Enable*. This should, from one side, reduce the barrier for the switch and the propagation, and on the other side increase the barrier to have stable logic states. To do this, cells should have six dots [14], as shown in Figure 1.5(a).

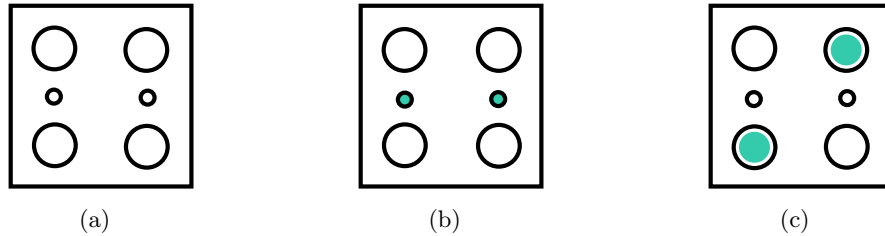


**Figure 1.5:** Schematic of enriched QCA cells: (a) QCA basic cell with the six quantum dots represented, (b) QCA basic cell in the *Null state* or *Reset State*, (c) QCA basic cell in one of the two *stable states*.

The new dots are regions where electrons can go only depending on the *enable signal*. In this case, charges are trapped in the central dots in an unstable state, called *Null state* or *Reset State*, so there is the need to apply an external electric field, as displayed in Figure 1.5(b). When the external field is released, charges are in a *stable state*, and the cell assumes the same configuration of the input. The external field is usually called *Clock*, and ideally is a square wave, as schematically shown in Figure 1.6.

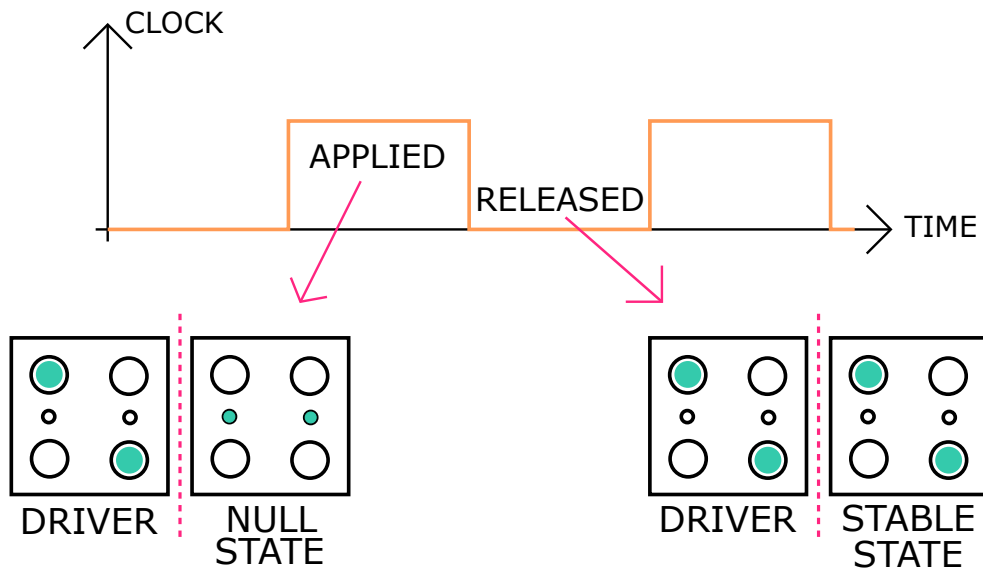
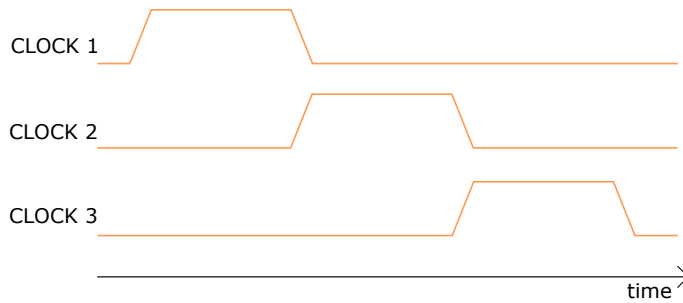


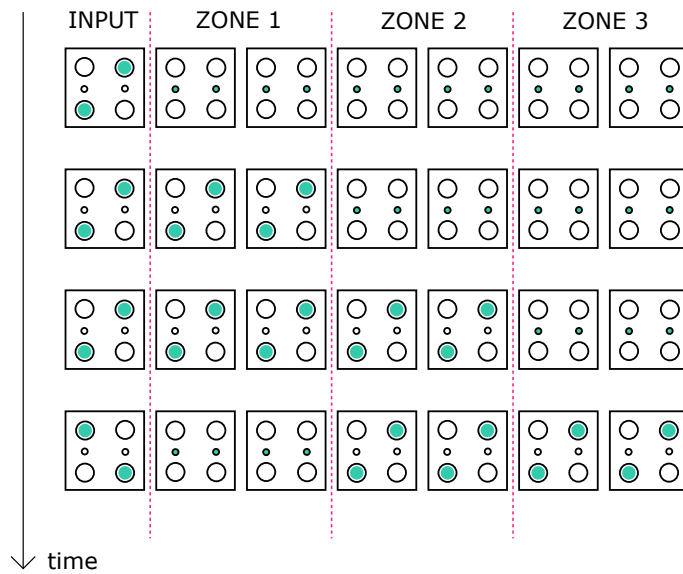
**Figure 1.6:** Schematic representation of the two possible situations related to the clock signal: when the *Clock* is active, or *Applied*, the cell stay in the *Null state*, whereas the *Clock* is not active, or *Released*, the cell configuration is stable and follow that of the input cell, usually called *Driver*.

In real situations, the assumption to work with a perfect square wave clock signal is not possible. The clock signal is an electric field that cannot switch instantaneously, thus actual signals are trapezoidal waves, as shown in Figure 1.7(a).

The last question to solve is related to the assurance of a correct propagation, for example in long wires. The circuit is thus organized in *zones* or bunches of cells [15]. The number of cells in each zone depends on the technology: each zone embraces a maximum number of cells, in order to assure no loss of information in a given condition. Each zone is associated with a different clock signal: clock signals are applied in sequence, so information propagates as in a pipeline, as shown in Figure 1.7(b). Moreover, using trapezoidal clock signals, the system works properly even in the presence of jitter. So, the overlaps of the clock signals are useful to avoid errors in the switching of the cells.



(a)



(b)

**Figure 1.7:** Schematic representation of the information propagation as a pipeline: (a) trapezoidal clock signals overlapped to ensure correct propagation, (b) example of the first time steps in a wire.

## 1.2 Molecular FCN

There are several possible physical implementations for QCA technology. Using metallic dots, which has two main issues: it works only at very low temperature and it is not so small but is useful if one is only looking for power consumption reduction [16], [17]. Another possibility is to use semiconductors heterostructures, which works with layers of different semiconductors and has been experimented [18]. The most used today is the magnetic implementation, which encodes information in the orientation of the magnetization of small magnets [19]. The last possibility is to use molecular implementation, which seems to be the most promising for the future. The advantages coming from the use of molecules to implement quantum dots are:

- the possibility to work at room temperature [9], [10];
- possibility to have very high-density circuits since molecules are, by definitions, the smallest systems capable of preserving the chemical composition and of determining the chemical-physical properties and behaviour;
- the possibility to exploit self-assembly, and thus no need for lithography [20], [21];
- the low power consumption of the switching mechanism [12];
- possibility to work at very high frequencies, up to about 1 THz [7], [22].

The conceptual molecule requires 3 dots, where a dot is a *redox* center [14]. In this way, it is possible to implement the two logic states and the null state, as shown in Figure 1.8.

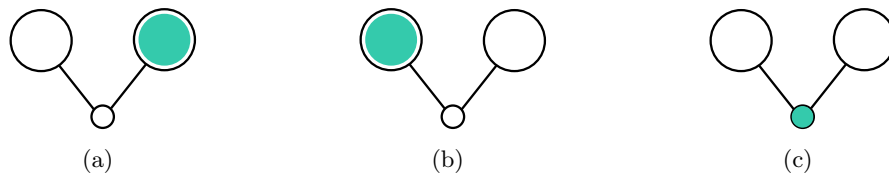


**Figure 1.8:** Conceptual molecule schematic: (a) position of the redundant charge in the logic ‘0’, (b) position of the redundant charge in the logic ‘1’, (c) position of the redundant charge in the *null* state.

There are many choices for the molecule type: some of these implement only three of the six dots [11], [23], others implement the four logic dots and present a fifth dot for the null state [9], [24], [25]. One of the most studied molecules for FCN is called bis-ferrocene, shown in Figure 1.9: it is composed of two ferrocene groups, a carbazole for the central dot and a thiol is used to anchor the molecule to a gold substrate [26], [27].

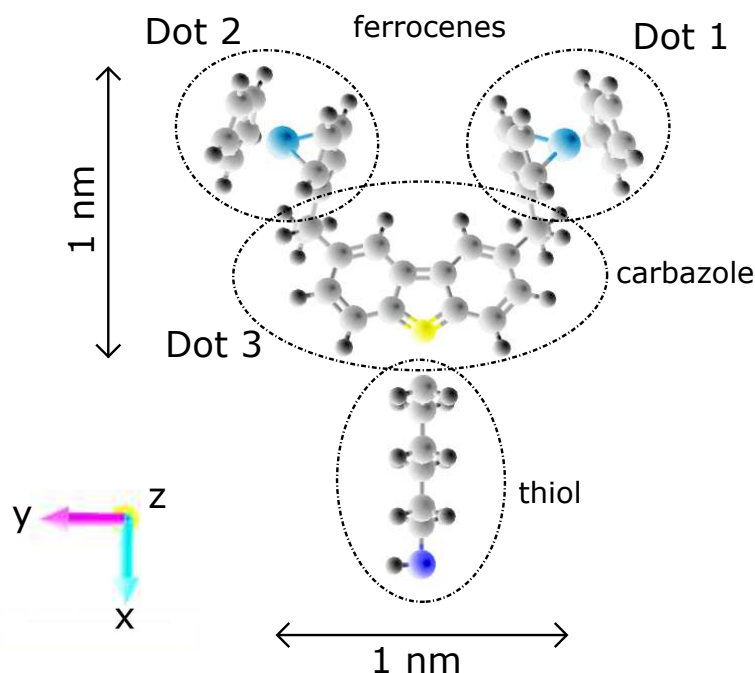


**Figure 1.9:** Bis-ferrocene molecule [28].

### 1.2.1 Molecular FCN modelling

One approach to studying molecular FCN is to use *ab initio* simulations. In any case, this is the reference and the starting point and is used to validate the system under study. However, it has some drawbacks. First, these simulations are CPU intensive and a lot of memory is required. Moreover, results are difficult to use from a device level point of view, because the outputs given are homo/lumo information, charges distribution, and so on. Finally, it is difficult to control the biasing conditions, as input electric field, clock electric field or technological parameter.

For all these reasons, a new approach has been proposed, which proposes new figures of merit and reduces the complexity of calculations, still maintaining a connection with the physical level. This approach, called MoSQuiTo (Molecular Simulator Quantum-dot cellular automata Torino) [29], is based on three stages:

1. analyse the molecule with *ab initio* simulations;
2. using the results of the first stage, post-process them and generate new figures of merit and characteristics of the device;
3. implement an algorithm at a higher level, to go toward the simulation of the circuit and the interactions among elements.

**First stage**

Molecules are described through the Z-matrix, which is the entry point of each *ab initio* simulation. After this, biasing conditions are set: electric field of an input driver, a clock signal or presence of other molecules, emulated by point charges. The direction of each field is defined and then the amount is spanned over a range of interest. The data generally obtained from these simulations are potential surfaces and charges associated to each atom.

**Second stage**

The second stage is used to elaborate the informations got from the previous step and to define new figures of merit which characterize the molecule at a higher level. These figures of merit are [29]:

**Aggregated charge (AC):** instead of having information on charges associated with each atom, it is preferred to have information related to each dot. The aggregated charge is the sum of all the charges in a dot and is centred in a point of interest, e.g. the Fe atoms of the ferrocene groups in Figure 1.9.

**Electric-field generated at the receiver molecule (EFGR):** a molecule with a certain charge distribution generates an electric field in the surrounding space, as shown in Figure 1.10(a). The EFGR is the electric field that influences a hypothetical molecule placed at a specific distance  $d = w$  from the molecule under test (MUT), where  $w$  is the distance between the two logic dots.

**$V_{in}$ - $V_{out}$  transcharacteristic (VVT):** molecules generate an electric field all around, but for propagation purposes, only the field between logic dots is of interest. It is thus possible to transform such field in an equivalent voltage, which is the integral of the electric field along a specific path. The input voltage is that defined between the two logic dots of the MUT, while the output voltage is the one defined on a fictitious molecule placed at a distance  $d = w$ , where  $w$  is the distance between the logical dots, as shown in Figure 1.10(b).

**$V_{in}$ -AC transcharacteristic (VACT):** to characterize a molecule it is possible also to use the aggregated charge of the MUT, instead of using the output voltage, and to relate it to the input voltage defined in the previous point.

**$V_{out}$  map (VOM):** represents the input voltage of a receiver molecule placed anywhere around the MUT.

**MQCA cell working zone (CWZ):** defines the region in which a molecule is supposed to work correctly if subjected to a proper electric field.

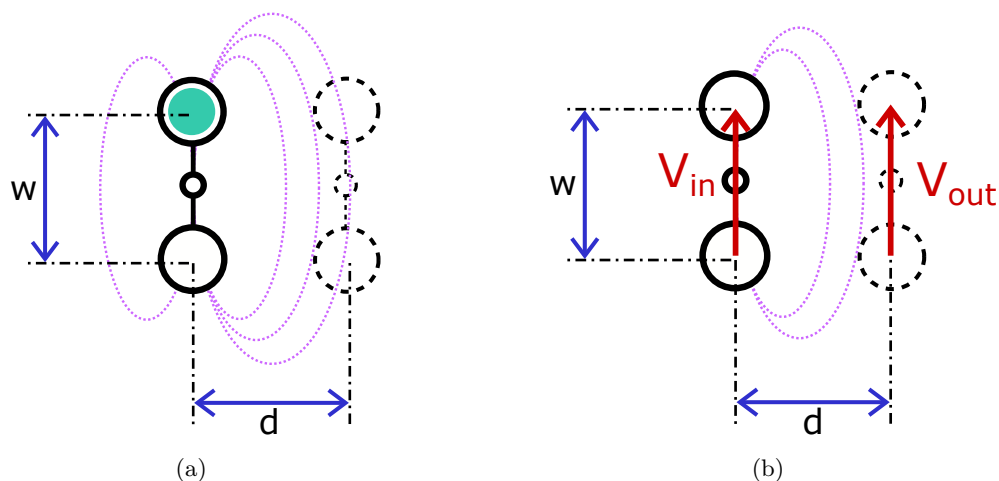


**Figure 1.10:** Figures of merit definitions: (a) electric field generated by the MUT on another molecule placed at a distance  $d = w$ , (b)  $V_{in}$  and  $V_{out}$  definitions.

### Third stage

At this point, all the elements to formalize an algorithm have been defined: it is called Self-Consistent Electrostatic Potential Algorithm (SCERPA) [30], and can be synthesized in three steps:

- initialization;
- molecular interaction computation;
- final charge distribution calculation.

In the initialization phase, information on molecule positions and initial conditions for the charges of each molecule are extracted. Moreover, drivers and clock configurations are defined in this step. The second stage consists of a self-consistent loop in which, for each time step, the effect of the drivers and the molecules are calculated and stored. When the convergence is reached, it is possible to go on with the last step, in which the final charge configuration is produced, other than all the graphs of the figures of merit explained before.

### 1.2.2 Molecular FCN technology

Regarding the analysis of the implementation of molecular FCN, fewer studies are found in the literature [31], [32]. The idea is to have a substrate on which molecules attach by mean of a tile, as shown in Figure 1.11.



**Figure 1.11:** Molecular wire implementation: (a) a substrate, for example a gold nanowire, onto which molecules are placed, (b) top view.

The main problem is that molecules have generally dimensions of 1-2 nm, so wires need to have the same dimensions and lithography based technology does not permit it. Moreover, independently on dimensions, it is difficult to have the precision needed to build angles, which would be necessary for a cross structure like that of the majority gate. Since the idea is to deposit molecules employing self-assembled monolayers (SAM), to have regular SAM, a precise wire is needed.

Another important thing that has to be managed is the generation of the electric fields needed to the computation, which is the clock field and the switching field of the input molecules. To do this, other wires are needed. Among all the possible solutions, the most reliable is the one represented in Figure 1.12. The molecules are placed in a trench, over a wire as seen before. On top of the two edges of the trench, there are other two electrodes. Applying a voltage between these two electrodes, an electric field is generated between them as in a capacitor, and thanks to the border effects even molecules are subjected to this field, as represented in Figure 1.12(a). It is impossible to influence only one molecule, depending on the dimension of the electrodes a certain number of molecules are subjected to the generated field.

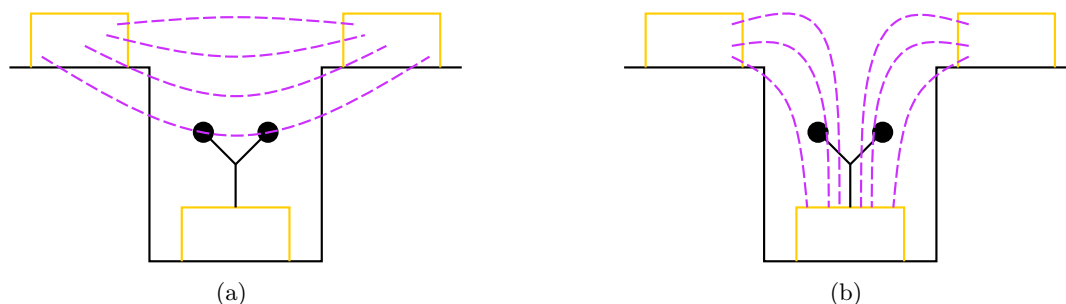


**Figure 1.12:** Implementation of the electric fields involved in the computation (section view): (a) input voltage is generated by two electrodes placed on top of the trench, (b) the clock field is obtained by a potential difference between the top electrodes and the gold nanowire at the bottom of the trench.

The same structure can be used also for the clock field, as shown in Figure 1.12(b). Applying a voltage between the electrodes on the top and at the bottom of the trench, a vertical electric field is generated over the molecule. The expected vertical field depends

on the aspect ratio of the trench.

The top view of the implementation of a clocked wire is shown in Figure 1.13. In real systems, neighbouring electrodes interfere with each other, the two fields overlap: the goal is to have constructive interference to not lose the information. Overlapping in time the clock signal waves solve also the issue concerning the overlap in space.

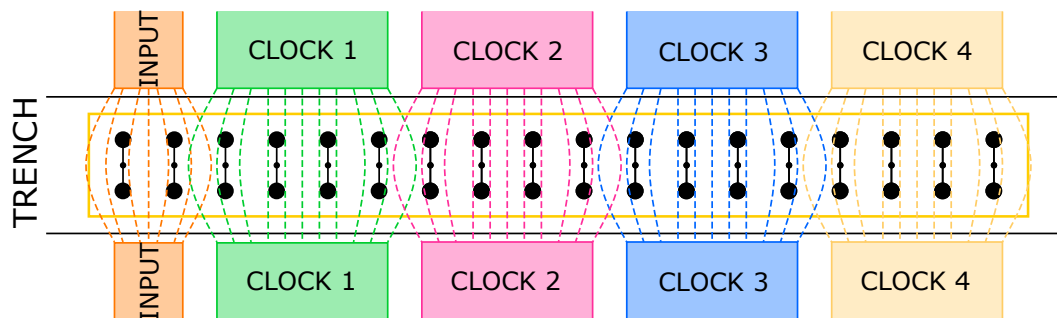


**Figure 1.13:** Clocked molecular FCN nanowire implementation.

Another problem emerges looking at the space between the electrodes, as shown in Figure 1.14. A separation of about 1 nm is desired, which is the order of magnitude of the distance between two molecules, but this is impossible to obtain. With a realistic separation, it is possible to see that some molecules are not associated to any electrode. Anyway, the presence of overlapped fields in space solves this resolution problem.

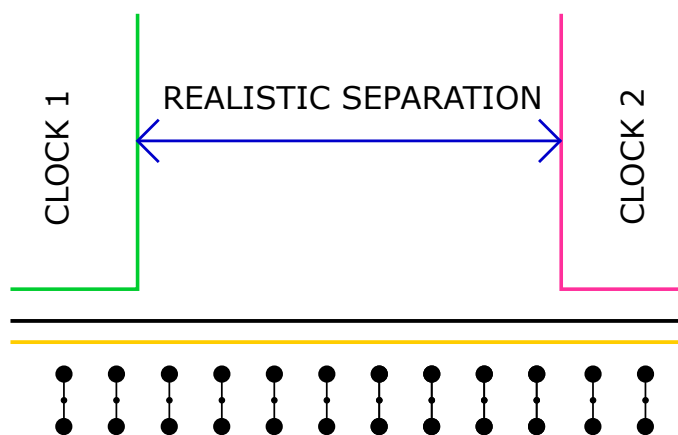


**Figure 1.14:** Clocked molecular FCN nanowire implementation: zoom in the separation of two electrodes.

From the information propagation point of view, there are many parameters involved. First of all, the parameters relative to the trench, so mainly height and width, which influence the application of the electric fields. Linked to this has to be mentioned also the separation of the electrodes, which depends on the precision of the production process. Even the limit of the width of the guiding wire is imposed by the lithography process. For

what concern the guiding wire there other two characteristics that influence information propagation: the lattice structure, which defines the regularity of the SAM anchoring, and the roughness, because the wire is not perfectly flat. In the case of a metal wire, both *inter-grain* and *intra-grain* irregularities have to be mentioned: grains are not all the same height and they are not perfectly smooth, as shown in Figure 1.15(a). Due to this, it is possible to have:

- vertical misalignment among molecules, Figure 1.15(a);
- horizontal shifts due to different anchoring points, Figure 1.15(b);
- tilting, due to defects and different grains orientation, Figure 1.15(c).

Finally, two more possible defects related to the SAM regularity are the presence of extra molecules not included in the design or the lack of some molecules, that can affect the propagation of the information.

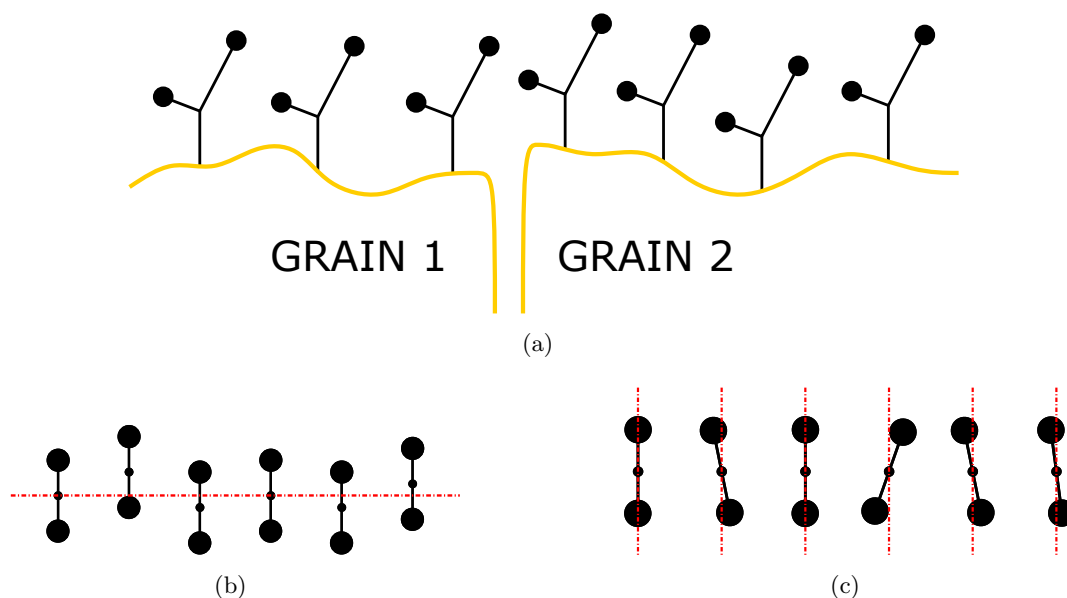


**Figure 1.15:** Schematic representation of some possible implementation defects: (a) vertical misalignment, (b) horizontal shift, (c) tilting.

## Chapter 2

# Brain-inspired computing

The idea of being able to make devices whose behavior resembled that of a human brain is now almost 80 years old. The first neural network model was proposed in 1943 by Warren McCulloch and Walter Pitts [33]. A neural network is a system that receives inputs, processes them and produces an output. The difference from a standard program depends on the approach to the problem that is submitted to it. In a classic program, the output is produced based on predefined choices, which the programmer has defined, following the problem-solving algorithm. It is in no way possible for a program to be able to process an input for which it has not been programmed.

A neural network, on the other hand, is not programmed in the common sense of the term but is trained for a specific task. This means that if the network is used to analyse images and find in which of these there is a house, the network is taught what an image is and then to process it, and subsequently images are presented to it in which there is a house. The neural network is left with the task of understanding what are the distinctive features of a house so that if it were given a new image, it would be able to recognize the presence or absence of a house on its own. From this simple example, it is immediately possible to understand that the strength of neural networks derives from having moved the complexity of the analysis of the inputs, from the programmer to the machine. Neural networks, therefore, do not execute programmed instructions but respond in parallel to the input model that is presented to them. There are no separate memory addresses for data storage: the information is contained in the general state of the network, which therefore represents the “knowledge” of the neural network itself.

The keyword here is *network*. In fact, a neural network is composed of a series of nodes, generally arranged on various levels, and a certain number of connections between the various nodes [34]. Each node, which in this case is called *artificial neuron*, is a simple computational unit whose task can be very simple, such as calculating the weighted sum of its inputs. The real strength lies in the complex connection of these nodes, which at a high level produces a network capable of performing very complex tasks, from patterns recognition to medical diagnosis.

One of the main advantages of a neural network is its ability to learn and model complex and often non-linear relationships, as occurs in the case of financial or behavioural

trends aimed at business. The other huge advantage is the ability of a neural network to generalize a problem, based on its training, and to deduce and predict relationships based on unseen data.

## 2.1 Artificial Neural Networks (ANNs): fundamentals

In an artificial neural network, the nodes are called “artificial neurons”. An artificial neuron is a system whose behaviour resembles that of a biological neuron. Most neurons are characterized by three regions, as shown in Figure 2.1:

**The soma** is the cell body, where the signals are processed and the necessary enzymes are produced.

**Dendrites** are branches whose main function is to receive incoming signals. They are therefore responsible for conducting stimuli from the periphery to the center. These structures amplify the surface of the neuron, allowing it to communicate with many other nerve cells.

**The axon** is a sort of extension, assigned to the transmission of signals from the center to the periphery. The axon is generally single, but it can have collateral ramifications allowing it to distribute the information in different destinations at the same time.

Biological neurons, therefore, receive signals through synapses located on the dendrites or the membrane. When the received signals are strong enough, therefore they exceed a certain threshold, the neuron “is activated” and emits a signal, called *action potential*, through the axon. This signal could be sent to another synapse and could “activate” other neurons.

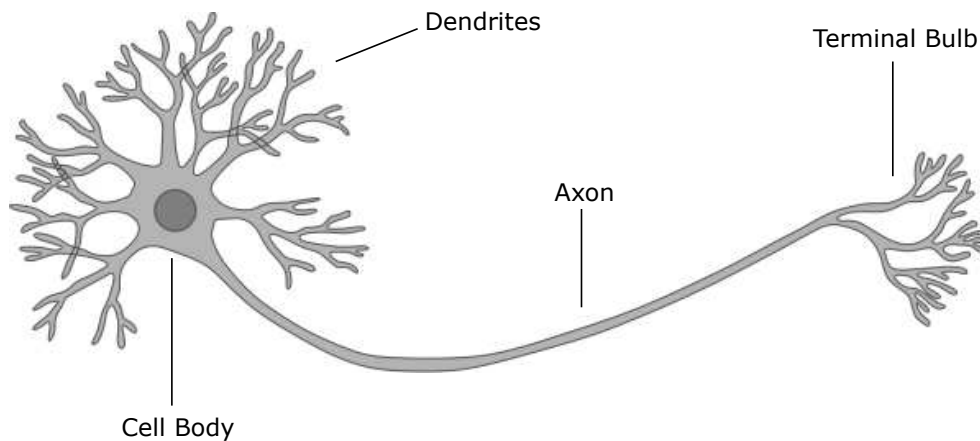


**Figure 2.1:** Schematic representation of a neuron in a biological system [35].

The complexity of biological neurons is highly abstracted when modelling artificial neurons. These essentially consist of inputs, which are multiplied by the weights that

represent the strength of the respective signals and then combined in a mathematical function that determines the activation of the neuron. Based on this, the output of the artificial neuron is calculated, sometimes relying on exceeding a certain threshold, as shown in Figure 2.2. ANNs combine artificial neurons to process information.

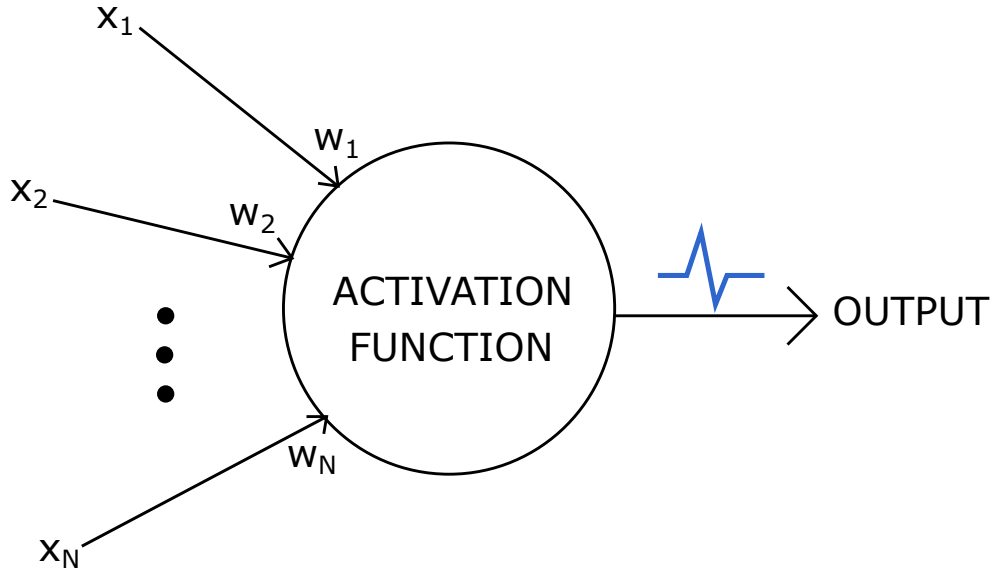


**Figure 2.2:** Schematic representation of a neuron in an artificial system, where  $x_i$  are the inputs and  $w_i$  are the weights associated to them.

The weight associated with each input is used to increase or decrease the influence of the associated input for the neuron. They can be both positive, in the case of excitatory signals, and negative, in the case of inhibitory signals. Depending on the weights, the processing of the information by the neuron will produce different effects on the output, and therefore by adjusting the value of the weights it is possible to “program” the output. In the case of large and complex networks, the task of adjusting the weights is carried out by specific algorithms, and it is nothing more than the training phase of the network [34].

In general, the total contribution of the inputs to a node coincides with the weighted sum of the inputs plus a bias term, as expressed in the equation (2.1)

$$s_k = \sum_{i=1}^N w_{ik} \cdot x_i + \theta_k \quad (2.1)$$

where  $s_k$  is the sum of the input for the node  $k$ ,  $N$  is the total number of inputs to the node,  $w_{ik}$  is the weight of the input  $i$  of the the node  $k$ ,  $x_i$  is the input signal and  $\theta_k$  is the offset.

In addition to this, there is normally a function that determines the activation of the output, based on the current status and the total contribution of the inputs. This function, called the *activation function*, is usually a non-decreasing function of the total

of the inputs. Threshold functions are normally used, such as the sign function or a sigmoid-like function, shown in Figure 2.3.

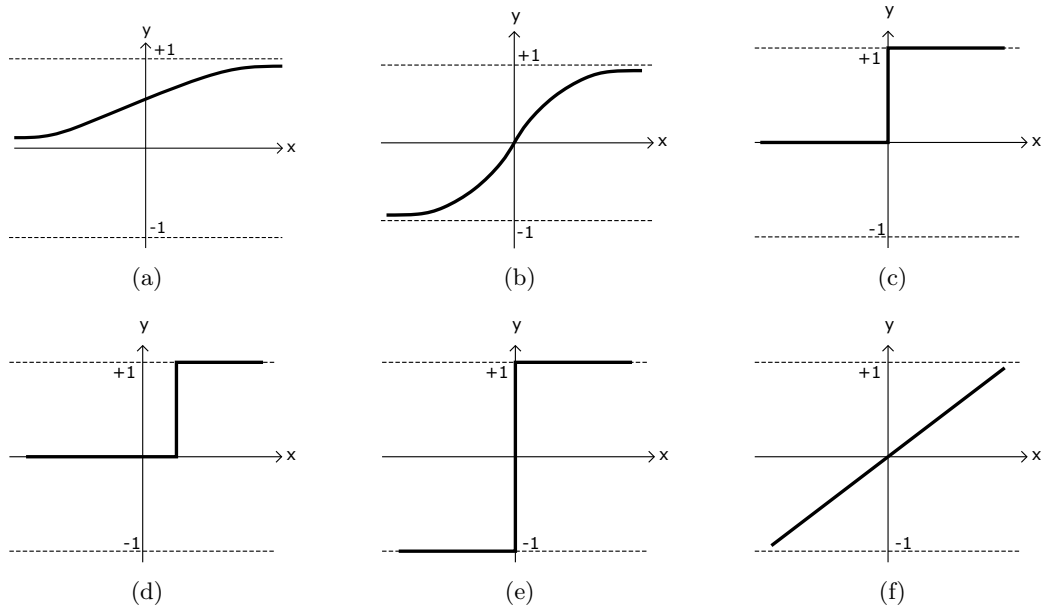


**Figure 2.3:** Examples of common activation functions in ANNs [36]: (a) sigmoid function, (b) tanh function, (c) step function, (d) shifted step function, (e) sign function, (f) linear function.

For what concern the connection types, ANNs can be basically divided into *feed-forward* networks, in which there are no feedback paths, and *recurrent* networks, in which feedback connections are present [37].

The last fundamental point concerns the training of the network. It consists, as already anticipated, in the optimization of the values of the weights associated with all the inputs of each node of the network. This can be done directly, by setting the various weights “manually”, or by providing sample input patterns and letting the weights vary according to some rule. The two main learning paradigms are [38], [39]:

- ***supervised learning*** in which an external teacher submits inputs to each of which is associated with an exit scheme;
- ***unsupervised learning*** in which the network is trained to recognize certain characteristics from the data. Subsequently, based on these characteristics, the network will be able to classify the new incoming data.

## 2.2 Spiking Neural Network (SNN)

Artificial neural networks generally take advantage of highly simplified neuron models. In the last decade, research has also focused on the creation of neuron models with a

function more similar to the biological one. Neurons in the human brain exhibit recurrent dynamic behaviour rather than static non-linearities: processing and communication take place through spike signals sparse over time. Neural networks that exploit this mechanism are called Spiking Neural Networks (SNNs).

The need to define new models, more similar to reality, derives from a critical analysis of common artificial neural networks: compared to the human brain they perform specific tasks consuming much more power and occupying a much larger area. In this sense, SNNs are much more efficient when compared with ANNs [40].

Over the past decade, several models of spiking neurons have been proposed on the basis of the very detailed Hodgkin-Huxley model [41], [42]. A widely used model is called the integrate-and-fire neuron. In this model, the neuron's behaviour is described through the trend of the membrane potential. The neuron receives excitatory or inhibitory inputs through synapses from neighbouring neurons. These inputs are weighed and modelled through an injected current or a change in membrane conductance. For each incoming spike, the membrane potential increases, while it decreases if no signals arrive. When a certain threshold is exceeded, the neuron generates an outgoing spike, which normally follows a refractory period during which the neuron is insensitive to other stimuli, as shown in Figure 2.4.

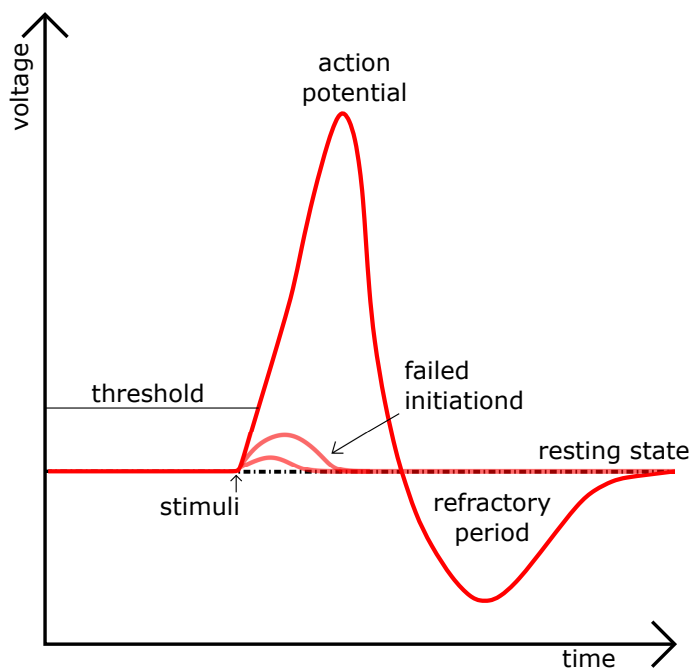


**Figure 2.4:** The action potential.

From an electronic point of view, this mechanism can be described with the circuit shown in Figure 2.5. On the left side, the input spike enters a low-pass filter which converts it in a current pulse  $I(t)$  that charges the capacitor. On the right, it is represented the equivalent of the soma, which can generate a spike when a threshold voltage  $\theta$  is

reached across the capacitor. The effect on the membrane potential  $v$  is described in the equation (2.2).

$$\tau_m \frac{\partial v}{\partial t} = -v(t) + R \cdot I(t) \quad (2.2)$$

where  $\tau_m$  is the time constant in which voltage extinguish.

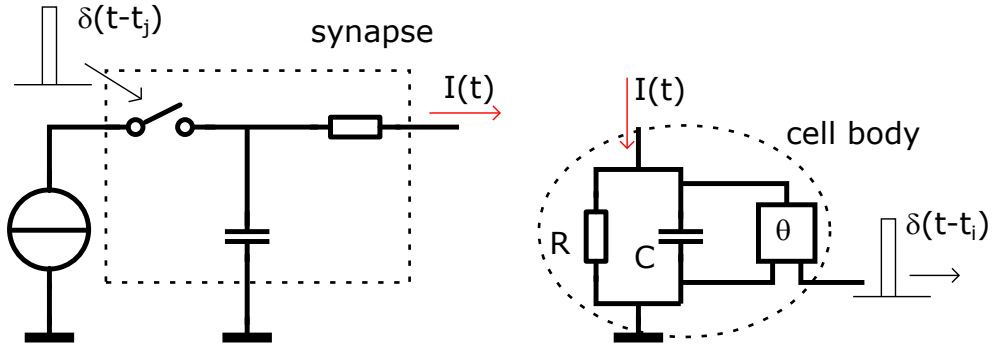


Figure 2.5: Schematic circuit of an integrate-and-fire neuron model [43].

## 2.3 Technology

For what concerns the hardware implementation of artificial neural networks, often called Hardware Neural Networks (HNNs), a very large number of architectures have been proposed, including digital, analog, and optical implementations. ANNs differ in terms of network topology, the number of levels, activation function, and so on. In addition to these distinctions, with regards to hardware implementations of neural networks, other parameters must be considered, including precision, data representation, and technology used [44].

HNNs made on chips are commonly called *neurochips*. In most cases, only some of the operations that the network has to perform are implemented on hardware, while the rest are performed by the system in which the neurochip is included. Several implementations of the neurochips have been made, including:

**Digital implementations:** generally realized in CMOS, with the advantage of the well-developed fabrication process. The main issue is related to the multiplication for the weights, which is normally slower than other operations [45], [46];

**Analog implementations:** present the advantage of smaller circuits if compared to the digital implementations, moreover some of the specific functions can be directly implemented with analog components [47], [48].

**Hybrid implementations:** use both digital and analog elements trying to exploit the best aspects of both technologies [49], [50].

**FPGA-based implementations:** offer quite easy reconfigurability, even if in terms of circuit density present lower performances [51], [52].

**SNN implementations:** given the advantages offered over the ANNs, several hardware solutions have recently been proposed that implement neuromorphic computing [53], [54].

**Non-electronic implementations:** in particular optical technology may solve some of the problems highlighted by electronic implementations. However, the absence of fast switches and large memories has slow down their development [55], [56]



## Chapter 3

# Molecular FCN for neuromorphic computation: some ideas

Most ANNs used for commercial use applications are implemented as software. However, hardware solutions have several advantages over software ones [57]. First, an ad hoc hardware solution is capable of optimizing computational power, allowing for faster execution. The cost falls on a large-scale production, therefore a hardware solution would be the most suitable choice in the case of neural networks in consumer products. Most of the hardware today allows execution with high real and non-simulated parallelism, increasing performance also in terms of fault tolerance. In addition to the advantages, the difficulty deriving from the irregularity and high connectivity of the neural networks complicates the work of the designers of HNN. Furthermore, particular attention must be paid to the accuracy of the design parameters, especially in the case of analog solutions.

In recent years, solutions in non-conventional technologies have been explored, to provide valuable alternatives to the standard implementations [58], [59]. For what concerns molecular FCN, the most complete solution was proposed in [60]. The authors suggest using *partial clocking* to implement the synaptic weight. This should be applied to the inputs of a Majority gate, so that the sum operation performed by the central cell of the Majority gate will take into account inputs differently, depending on the weights. The other solution they proposed to implement weights consists of replicate a signal so that redundancy will encode the strength, and thus the weight, of an input. To implement the threshold mechanism the authors in [60] proposed to combine fixed cells and the number of synaptic connections. When the threshold is reached, the output logic value change and propagate as if it were a sort of impulse.

In addition to those proposed in [60], several hypotheses for the realization of a neuron in molecular FCN technology have been advanced and analysed. In particular, various possibilities were considered for the implementation of the weights, the threshold, and the addition operation, which are some of the key elements for the realization of a structure that behaves like a neuron.

### 3.1 Weight

An idea to weigh the inputs of the neuron is to exploit a hysteresis phenomenon, which would allow having different reactions to the same signal in a controlled way. A similar mechanism is also exploited in some neural networks in standard technologies, as it allows quite simply to eliminate the multiplication operation, which is critical for of the complexity and therefore of execution time [61], [62]. In molecular FCN, a hysteresis phenomenon has been observed on a wire of bisferrocenes, as schematically shown in Figure 3.1, where  $P_D$  is the driver polarization and  $\bar{P}$  is the average wire polarization, defined as

$$\bar{P} = \frac{1}{N} \sum_{i=1}^N P_i \quad (3.1)$$

$$P_i = \frac{Q1 + Q3 - Q2 - Q4}{Q1 + Q2 + Q3 + Q4} \quad (3.2)$$

and  $Q_j$  is the charge of the j-th dot in a QCA cell.

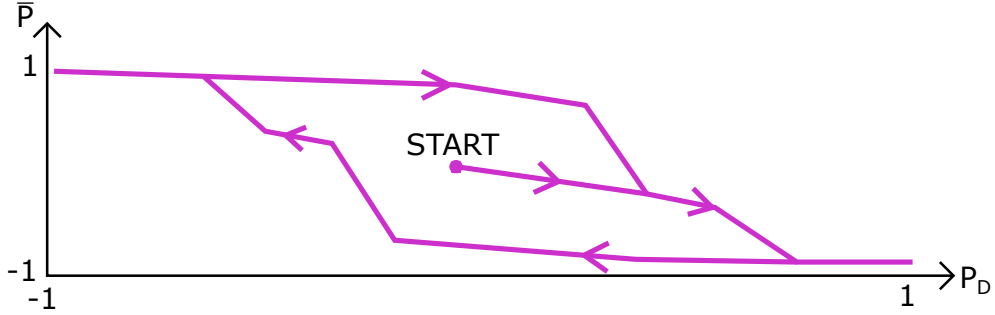


**Figure 3.1:** Hysteresis phenomenon in a wire made of bisferrocene molecules [63].

This result means that a wire once reached a stable configuration, opposes a certain resistance to change its configuration. Normally this mechanism is bypassed through the use of the clock signal, which can reset the wire before the next input signal is provided. In a neural network, this phenomenon can instead prove useful.

Another possibility is to use particular molecules with more than one mobile electron inside it, i.e. dioxide, trioxide molecules, and so on. Or neutral molecules in which a certain number of electrons move from one logical dot to another. In this way, depending on the number of mobile electrons present in the molecule, it would be possible to encode more or less large weights: the greater the number of electrons located in a dot, the greater the maximum output voltage that is generated on the receiver molecule.

### 3.2 Sum

As for the implementation of the addition operation, one possibility is to use a majority gate. The majority function is nothing more than a threshold logic function in which

the weight of the inputs is the same and is unitary [64]. The threshold, in this case, is the minimum number of inputs that allow the output to switch. The advantage derives from the fact that the majority voter in molecular FCN is a basic gate, the behaviour of which has been widely studied in the literature. Furthermore, by functionalizing the inputs of the majority voter, perhaps using molecules whose behaviour is that described in Section 3.1, it is also possible to vary the weight of the various inputs.

Another possibility may be the use of branched molecules to collect electrons in one point and use it as a driver for the output wire, as schematically shown in Figure 3.2.

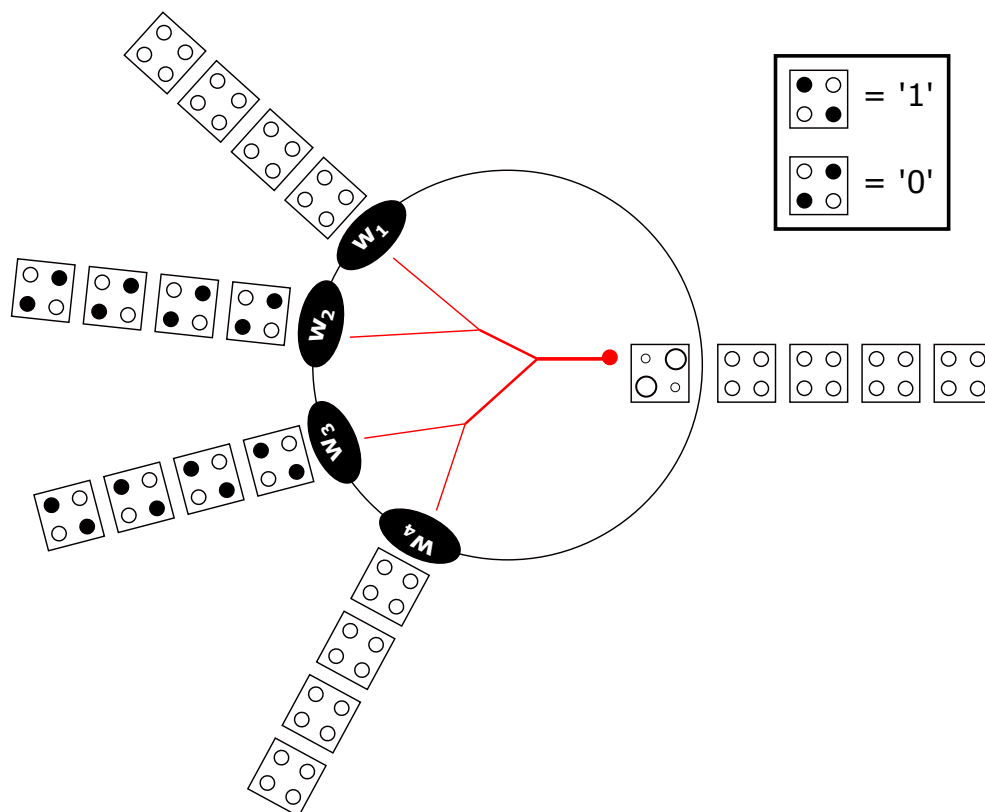


**Figure 3.2:** Schematic model of a possible implementation of a neuron in molecular FCN, where  $w_i$  represent the synaptic weight of the  $i$ -th input wire.

In this case, synapses could be either a separated molecule that based on its input voltage generates an electric field along the branch favouring the accumulation of electrons near the output wire, or a particular termination of the branched molecule itself. These branched molecules could be similar to the so-called *dendrons*, which are described in [65], [66]. One of the particularly interesting properties is that the whole behaviour of the dendrimer is dominated by the functional groups on the molecular surface. Therefore, depending on the terminal groups, it is possible to obtain, in this case, different weights.

### 3.3 Threshold and output signal

Before talking about the threshold, it was necessary to reflect on what the rest value of an *axon* should be. One possibility could be to keep the connection wire always reset, or with the charge concentrated in dot 3. However, since the activation of the neuron, and therefore of the axon, depends on a logical value, it should be possible to control the electrodes that generate the clock field through a logic signal encoded on the molecules. Relating the two is not at all simple, therefore it is more reasonable to use the logical value zero as the rest value of the line.

A couple of solutions are also possible for the implementation of the threshold mechanism. First, the most reasonable idea is to implement the threshold value in the input voltage of the first molecule on the output branch. Therefore the threshold would be the value of the input voltage on that molecule such as to switch the logical value from zero to one, that is, from the rest value to the activation value. Normally, for example for bisferrocene, the input voltage for which there is a logical one is slightly above zero, as seen in Figure 3.3.

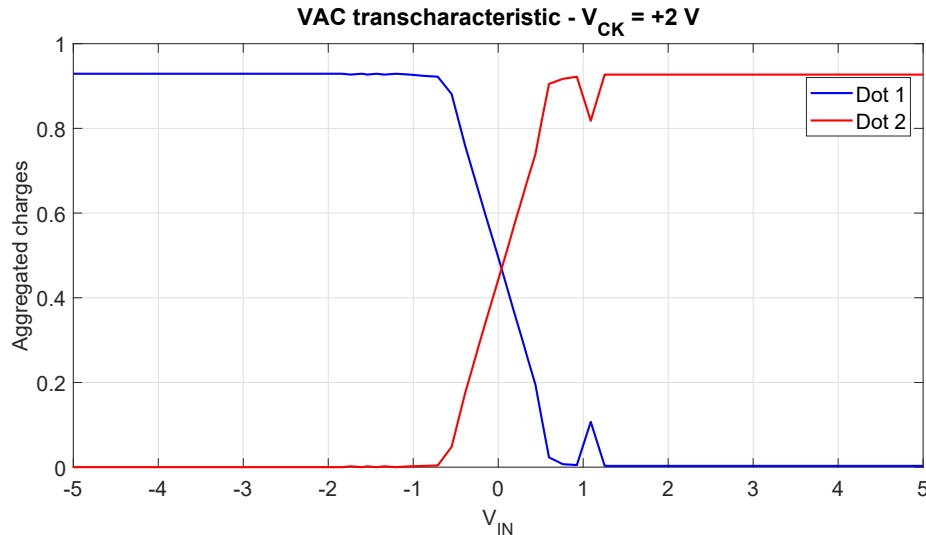


**Figure 3.3:** Input voltage versus aggregated charge transcharacteristic (VAC) for the bisferrocene molecule.

Moving the threshold means making one logical state more or less “strong” than the other. To have a threshold value different from about zero, it is possible, for example, to apply an external voltage, which overlaps the input voltage, to shift the VACT to the right or left, depending on the direction of the external voltage, by a quantity proportional to the module of this voltage, as shown schematically in Figure 3.4(a). The need to apply an external voltage on a molecule can be substituted by a molecule that has intrinsically one of the two states more probable than the other, maybe because it is monostable rather than bistable with asymmetric logic states, as shown in Figure 3.4(b).

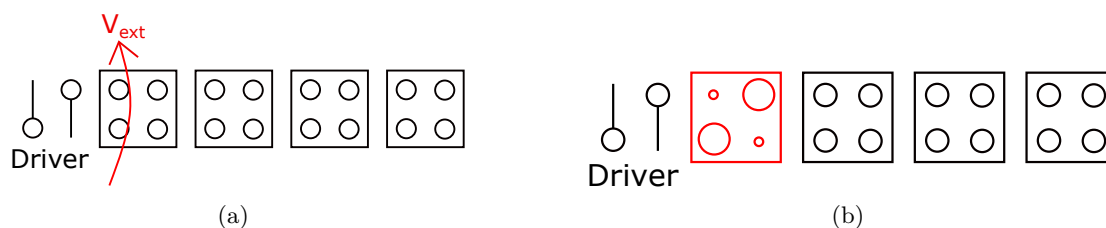


**Figure 3.4:** Schematic representation of the two possibilities to implement the threshold: (a) applying an external voltage to the first molecule of the output wire, (b) using a particular molecule with an intrinsically shifted VACT.

### 3.4 Outline

Based on the ideas that have been previously exposed, an approach has been outlined to demonstrate that it is possible to obtain neuromorphic behaviour using molecular FCN technology. The approach was divided into several steps, briefly described below, to study one aspect at a time, starting from the inputs up to a structure with several neurons connected. Steps 0 and 1 analyse the impact of the inputs and are described in detail in Chapter 4. Steps from 2 to 5 analyse the behaviour of the output, the threshold mechanism, and the relation between different neurons connected. These are explained in detail in Chapter 5.

#### Step 0

It was decided to work with a Majority Voter (MV) structure for the sum, in which the molecules of the central cell are two bisferrocene molecules placed at 1 nm distance from each other. First, only one of the three interfaces to the inputs has been added, the one at the top, as shown in Figure 3.5.

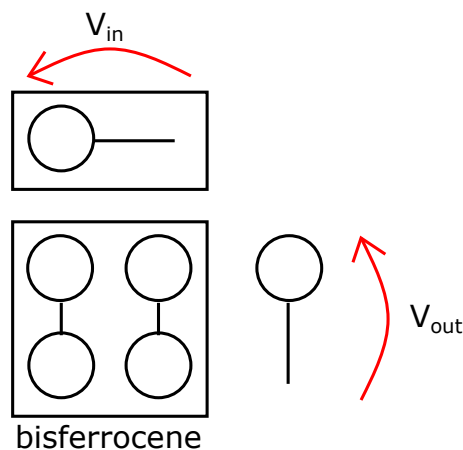


**Figure 3.5:** Scheme of the structure analysed in the step 0.

For the interface molecule, several transcharacteristics have been used, created ad hoc. These transcharacteristics can be divided into two classes, which have been called:

**Symmetric:** these molecules are oxidized, thus the aggregates charge span between 0 and 1, or 0 and 2, and so on. The weight is encoded in the saturation charge. The geometry used is the same of the bisferrocene, and the counter-ion which balances the total charge has been placed on dot 4;

**Asymmetric:** these molecules are neutral, so the total charge is equal to zero without the need of a counter-ion. The weight is encoded in the saturation charge. Even in this case, the geometry used for the molecules was the same as the bisferrocene.

In this step has been studied the relation between the input voltage  $V_{in}$  on the interface molecule and the output voltage  $V_{out}$  on a fictitious molecule placed at 1 nm distance from the MV central cell, with 1 nm as a distance between the two logic dots.

### Step 1

Once the system with a single input was characterized, the others were added in sequence: first, the interface 2 located under the computational cell of the MV as shown in Figure 3.6(a), and then the interface 3 located on the left of the central cell of the MV as shown in Figure 3.6(b).

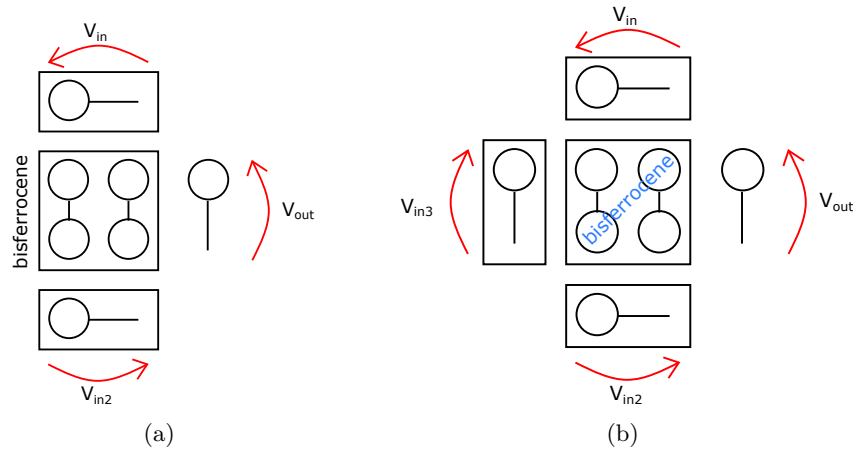


**Figure 3.6:** Schemes of the analysed structures: (a) in the step 1A, (b) in the step 1B.

Even in this case, we wanted to work with both the class of transcharacteristics, symmetric and asymmetric. The expectations are to be able to make a weighted sum of the input voltages, and also to determine the weights related to the transcharacteristics used. The system can be described through the equation (3.3)

$$V_{out} = f(m_1 \cdot V_{in1} + m_2 \cdot V_{in2} + m_3 \cdot V_{in3}) \quad (3.3)$$

where  $V_{ini}$  is the input voltage of the  $i$ -th interface,  $V_{out}$  is the output voltage on the fictitious molecule and  $m_i$  are the weights related to the three interfaces. The function  $f$  is a non-linear relation between the output and the total effect of the inputs on the MV. To obtain each weight value, inputs are switched on one at a time, so the relation between input and output is exactly the weight of the active input.

## Step 2

In step 2 we wanted to analyze the behavior of the MV with molecules other than bisferrocene in the central cell, as shown in Figure 3.7.

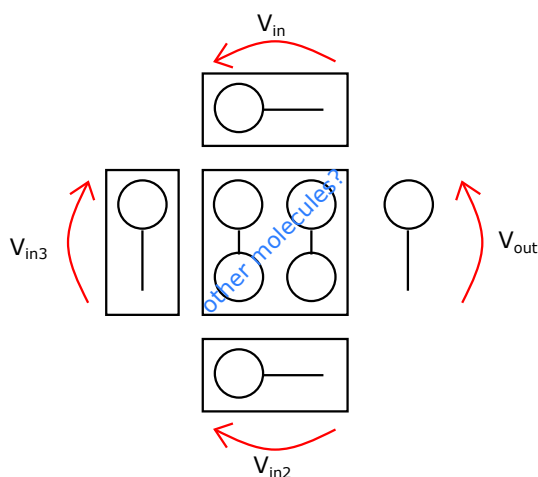


**Figure 3.7:** Scheme of the structure analysed in the step 2.

The aim is to determine which characteristic suits the role best, and which therefore offers the best results. The two molecules that have been thought to be used are diallyl-butane, shown in Figure 3.8(a), and decatriene, shown in Figure 3.8(b).

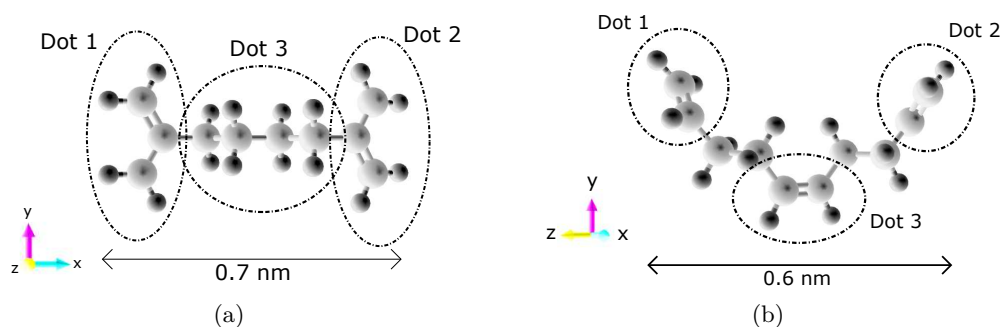


**Figure 3.8:** Representation of the two molecules used [29]: (a) diallyl-butane, (b) decatriene.

### Step 3 and Step 4

In these two steps the effect of molecules on the output branch was studied, as shown in Figure 3.9(a) in the case of a single molecule, and the threshold mechanism was studied, as shown schematically in Figure 3.9(b).

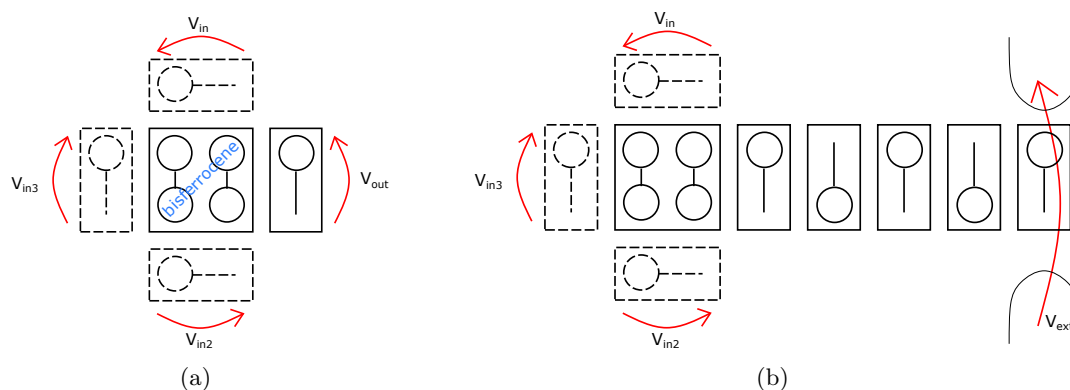


**Figure 3.9:** Schemes of the analysed structures: (a) in the step 3, (b) in the step 4.

Studying the system in the presence of outgoing molecules allows us to understand how and to what extent they affect the system. In fact, in general, each molecule affects all the others, in both directions. So the molecules on the output branch also affect the MV molecules, just as the molecules on the MV including the drivers influence the output branch. In this case, the dotted drivers mean that from this point onwards it is possible that the molecules must be divided into different clock zones, both because the number of molecules involved grows, and because mutual influence may cause the system to not work.

As for the threshold, it was decided to work in terms of an external voltage applied for the sake of simplicity. It is, in fact, presumable that the effect of external voltage is the same as an asymmetric molecule in the sense that the two logical states are not equivalent from the energetic point of view. Even in this case, we thought about the type of molecule best suited to the role and how information propagation should take place, also to connect with another neuron.

### Step 5

As the last step, once it was demonstrated that the behavior of the analyzed structure is comparable with that of an artificial neuron, it was decided to try to connect some of them, in a structure like the one shown in Figure 3.10. It is important, besides studying the structure of the neuron itself, to understand if and how things change when it is connected to other similar ones. Also because one of the characteristics of a neural network is precisely the high connectivity between neurons, and the ability to perform complex tasks if connected.

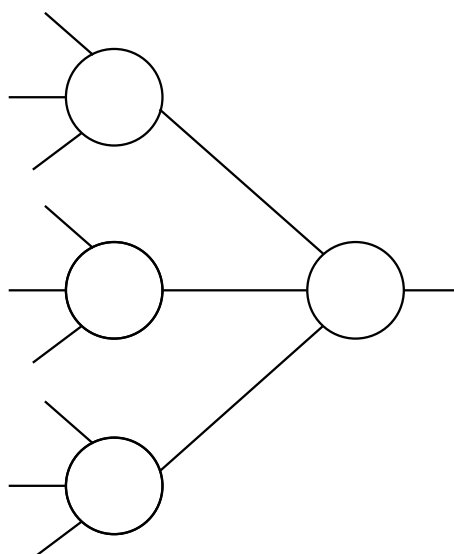


**Figure 3.10:** Scheme of the structure analysed in the step 5.

The approach just described allows one to understand if it is possible first to make neuromorphic computation in FCN molecular technology, and also to understand what are the key elements thanks to which it is possible to do it. All this from a purely computational point of view, in fact, most of the time we think in terms of trans-characteristics of molecules created ad hoc to perform a certain task. The parallel approach to this, which however requires much longer analysis times, involves studying real molecules from their electrostatic behaviour in the presence of specific electric fields. The results and analyses made from this point of view are described in Appendix A.



## Chapter 4

# Neuron inputs analysis

As mentioned in the previous chapter, the approach used was meant to study the structure from the point of view of behaviour at the architectural level. SCERPA was used to carry out all the simulations [30]. This algorithm receives the layout and some specifications of the circuit to be studied. Through the transcharacteristics of the molecules, usually obtained from *ab initio* simulations, it calculates the interaction between the molecules of the circuit and produces the final charge distribution on them. The strength of this algorithm lies in the high precision of the results provided, based on the results of *ab initio* simulations, and in the short times in which these are produced, not having to solve complex equations thanks to the definition of new figures of merit.

To study the architecture that will be presented below, one functionality has been added to SCERPA, which is the possibility of working with different types of molecules within the same circuit. The possibility of choosing the type of each molecule also extends to the drivers, so that driver molecules can be used to simulate the interfaces: in this way, in addition to the voltage value, it is also possible to choose the type of response that the inputs can give. Another feature that has been added to SCERPA consists in being able to apply fixed external voltages on each molecule of the circuit, which will come in handy later when the simulations are carried out to study the modification of the threshold on the output branch.

### 4.1 Step 0: the study of the first interface

Most of the transcharacteristics used do not correspond to a real molecule but have been synthesized *ad hoc*. As mentioned in the previous chapter, two classes of transcharacteristics have been used for the interface, defined as asymmetric and symmetric. These are shown in Figure 4.1(a) and Figure 4.1(b), respectively. These curves are all relatives to the case in which the clock signal favour the presence of the charge in the logic dots. From Figure 4.1 is also possible to notice that the words symmetric and asymmetric refer to the extreme values of the aggregated charge with respect to zero. In the two figures there are many curves because for each of the two classes five different transcharacteristics have been synthesized, each of which is characterized by two curves:

one for Dot 1, represented in a shade of blue, and one for Dot 2, drawn in a shade of red. The intensity of the color, dark or light, allows to associate the curves relating to the two dots for a specific interface, and in any case, for each of the five synthesized transcharacteristics, the extreme values assumed by the aggregate charge are the same, even if they are opposite.

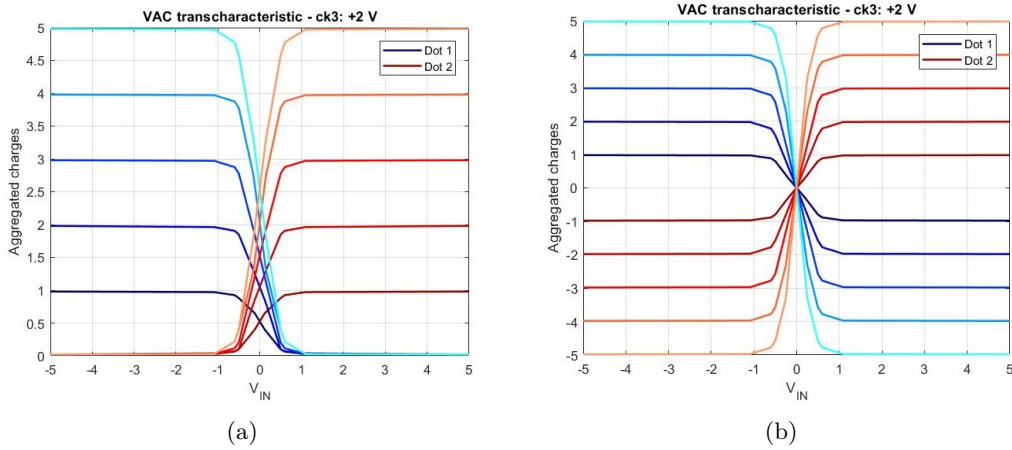


**Figure 4.1:** Transcharacteristics used to analyse the behaviour of the first interface: (a) asymmetric transcharacteristics, (b) symmetric transcharacteristics.

As previously mentioned, the central cell of the MV is made up of two bisferrocene molecules, as shown in Figure 4.2. In Figure 4.2(b) the 3D layout obtained with SCERPA is shown. To calculate the output voltage, a dummy molecule was inserted, which is sensitive to the charge distribution on the other molecules from which  $V_{out}$  is obtained, but does not affect the system in any way, having always null charged on its Dots.

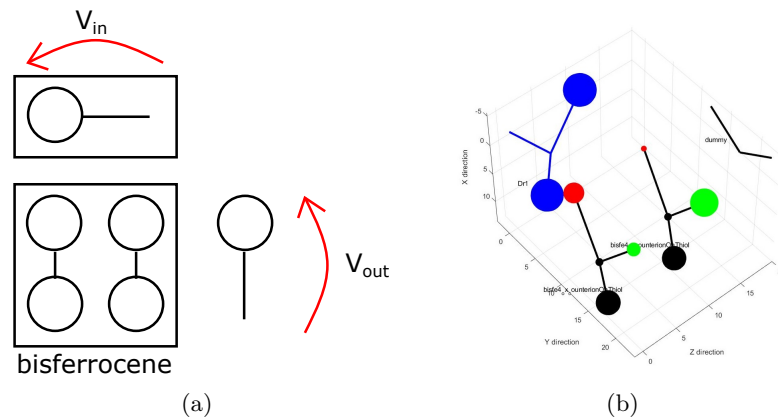


**Figure 4.2:** Layout of the architecture studied in the step 0: (a) schematic representation, (b) SCERPA representation.

The relationship between  $V_{\text{in}}$  and  $V_{\text{out}}$  was therefore simulated, using the transcharacteristics shown above at the interface. It was preferred to calculate the output voltage in two different cases, with and without the voltage contribution given by the driver itself. This allows distinguishing what is the effect due to the computation on the MV and what instead depends on the input voltage. The clock signal throughout this chapter will always be equal to  $+2\text{ V}$ , i.e. it favours the presence of charge in the logic dots.

The  $V_{\text{in}}-V_{\text{out}}$  characteristics relating to the cases in which the symmetric transcharacteristics for the interface have been used are shown in Figure 4.3, in which  $V_{\text{out}}$  does not take into account the driver voltage, and in Figure 4.4, in which instead also the effect of the driver on the dummy molecule is superimposed. To distinguish the various curves in the legend, the extreme values of the charge that logic dots can assume are written.

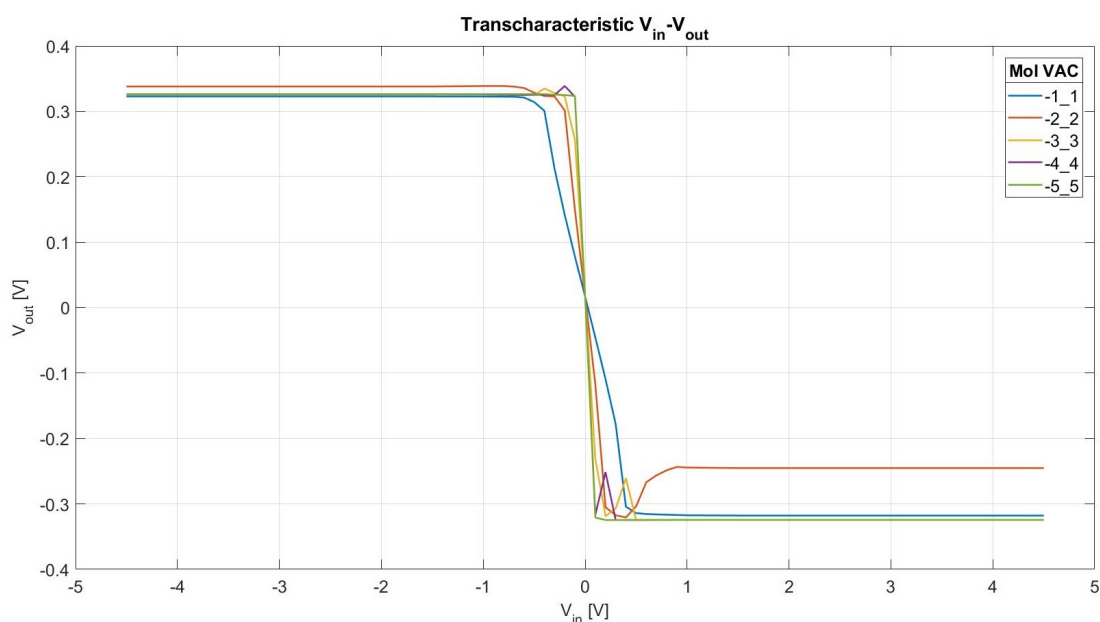


**Figure 4.3:**  $V_{\text{in}}-V_{\text{out}}$  characteristic when using the *symmetric* transcharacteristics for the interface and  $V_{\text{out}}$  is computed *without* the contribution of the driver voltage.

The curves where there is no driver contribution to  $V_{\text{out}}$  are in line with what can be expected. It should be noted that the greater the maximum charge possible on the two logic dots of the interface, the greater the slope of the output voltage. The inverting mechanism is coherent with the standard behaviour of molecules in molecular FCN. In fact, if we consider QCA cells composed of a single molecule, it would be like having an inverter cascade. In this case, the output voltage is calculated on the first molecule of a hypothetical cell placed at the output, and not on the second, from which the inverting behaviour.

As regards the trend of the output voltage, in which the contribution given by the

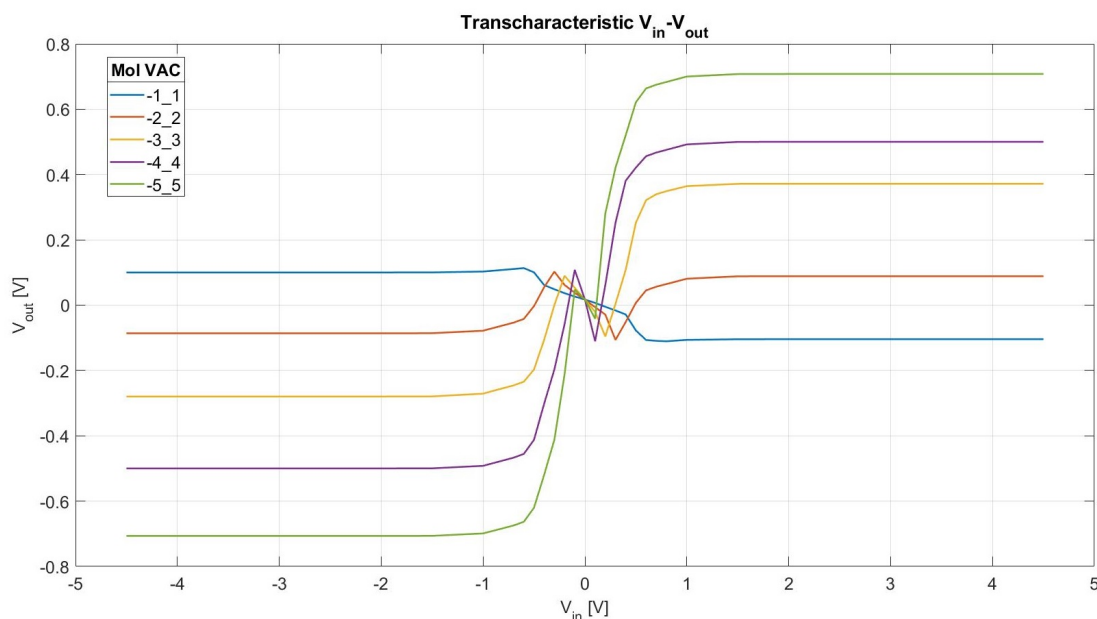
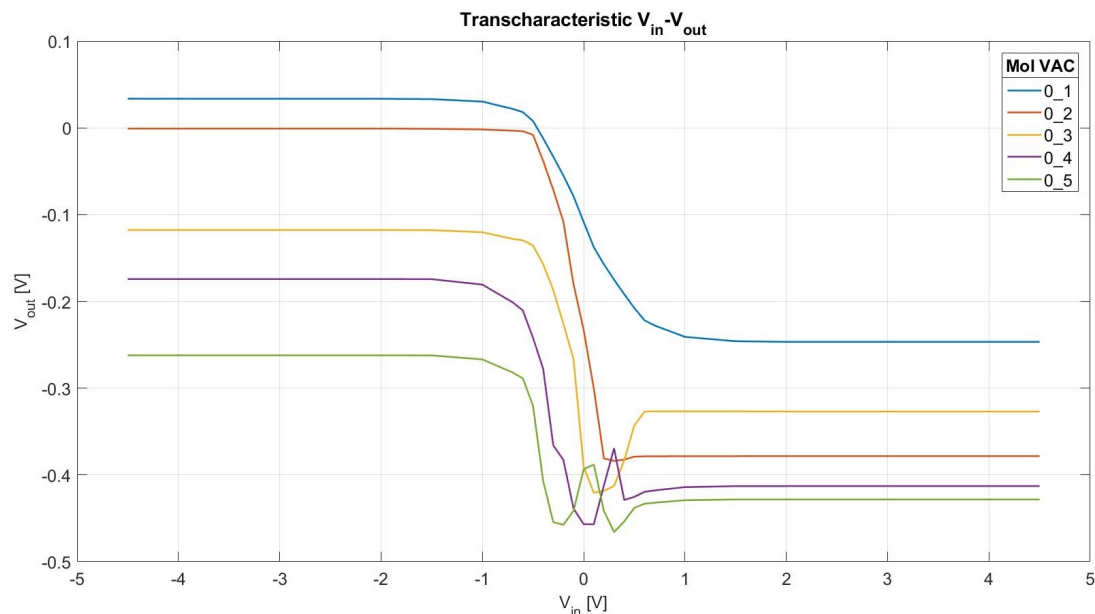


**Figure 4.4:**  $V_{in}-V_{out}$  characteristic when using the *symmetric* transcharacteristics for the interface and  $V_{out}$  is computed *with* the contribution of the driver voltage.

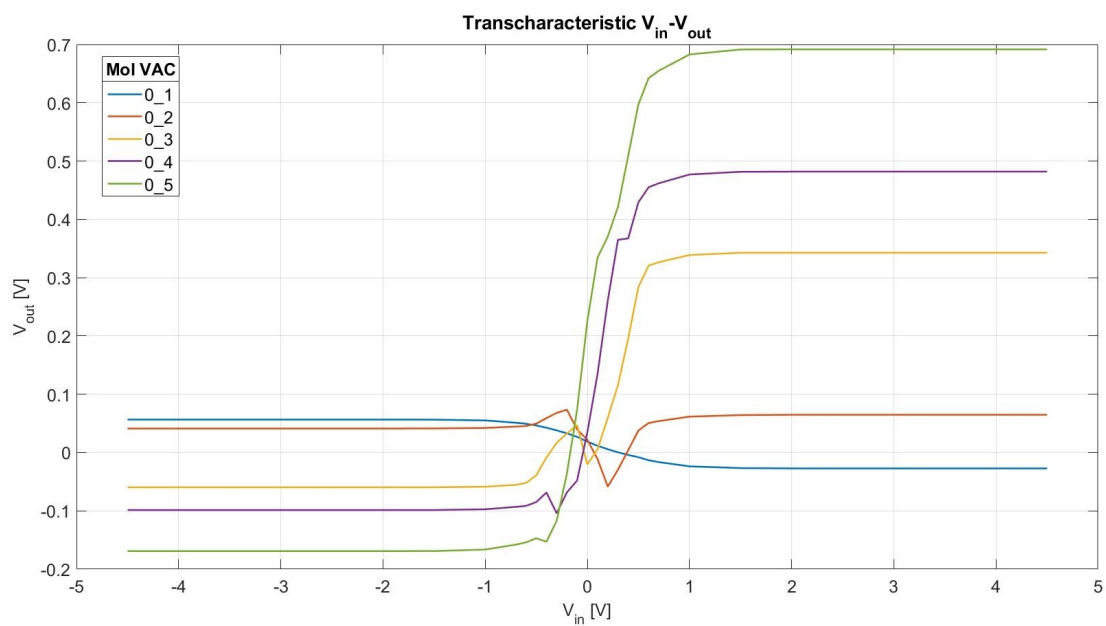
interface is also added, it is seen that the behaviour changes whereas the output voltage is more inclined to follow the voltage on the driver. The enormous influence of the interface directly on the output was foreseeable, since the charge distribution generates an electric field all around, which grows as the charge concentration increases at a point in space.

Figure 4.5(a) and Figure 4.5(b) show the  $V_{in}-V_{out}$  curves if the asymmetric transcharacteristics for the interface are used, without and with the contribution of the driver in calculating the output voltage, respectively. In the first case, that is when the driver's contribution is absent on the dummy molecule, it can be seen that the curves are made differently than before: the maximum and minimum values of the output voltage are very different from each other if different interfaces are used, unlike before where the saturation values were more or less constant between the various cases. Furthermore, practically all curves are always negative.

If the driver's contribution to the  $V_{out}$  is also added, as can be seen from Figure 4.5(b), the incorrect trend highlighted even in the case of symmetric characteristics occurs again, underlining that in any case, the driver's contribution is not negligible.



(a)



(b)

**Figure 4.5:**  $V_{in}-V_{out}$  characteristic when using the *asymmetric* transcharacteristics for the interface: (a)  $V_{out}$  is computed *without* the contribution of the driver voltage, (b)  $V_{out}$  is computed *with* the contribution of the driver voltage.

Summing up what has been observed. For the cases in which the driver contribution is superimposed on the output voltage, with both symmetric and asymmetric transcharacteristics at the interface, the influence of the driver voltage is huge and leads to the inversion of most curves. For the cases in which the driver contribution is not added on the output voltage:

- ✓ if symmetric transcharacteristics are used for the interface, the behaviour is correct;
- ✗ if asymmetric transcharacteristics are used, the majority of the curves are always negative, and the extreme values of  $V_{out}$  are not the same in all the cases.

The last written problem, given that it occurs only when using asymmetric transcharacteristics, suggests that a certain symmetry is needed in the system. It is therefore presumable that by putting interface two, even if turned off, the problem will be solved. By adding the second interface, the layout becomes that shown in Figure 4.6.

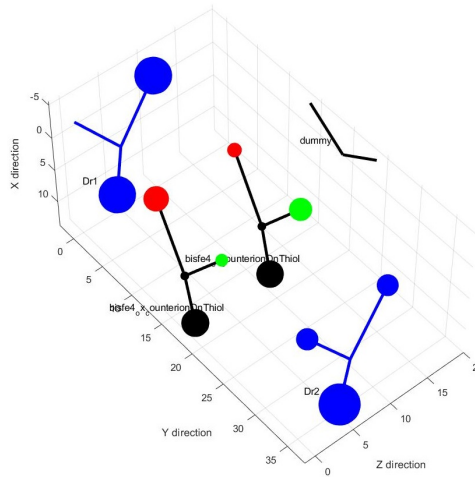
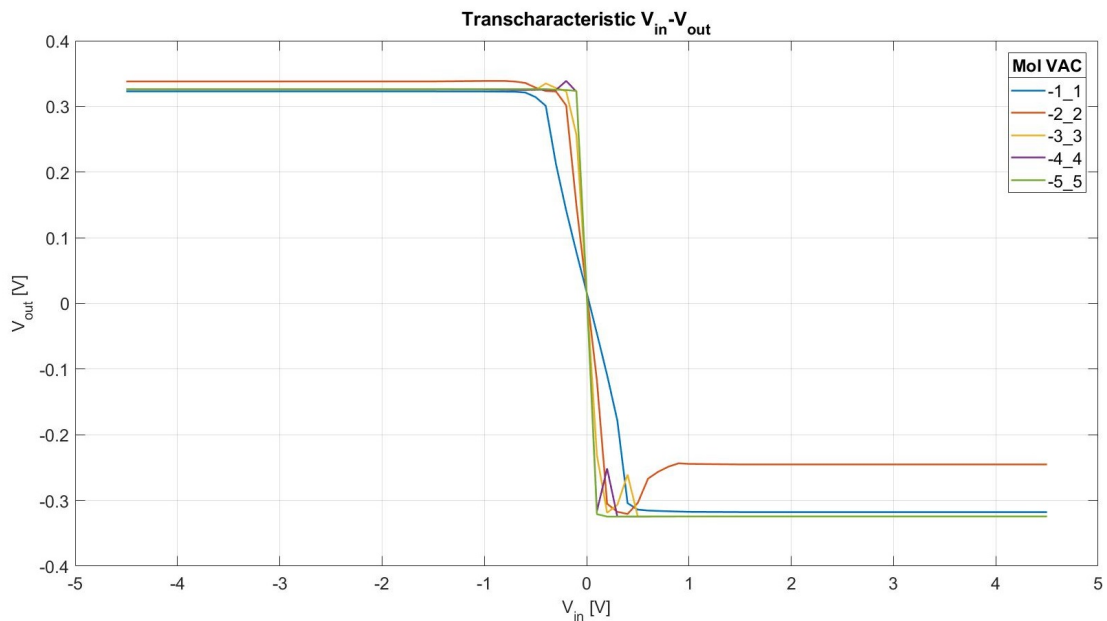
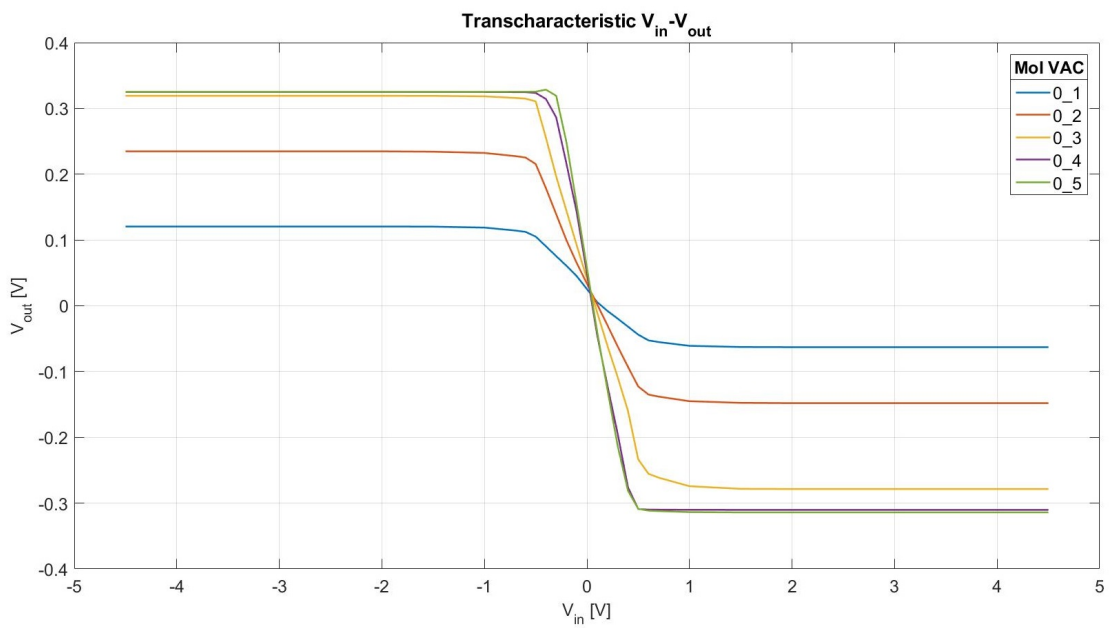


**Figure 4.6:** Layout of the architecture designed to insert a symmetry in the structure.

The same simulations described above were made, but with the second interface placed. Nevertheless, even in this case, only the input voltage on Driver 1 has changed, while the input voltage on the second interface is left constant equal to zero. Looking at the results obtained, shown in Figure 4.7(a) and Figure 4.7(b), respectively for the case in which the symmetric and asymmetric characteristics were used, it can be seen that in both cases the curves now have roughly the same trend. It can be seen, in Figure 4.7(b), that the curves are now symmetric with respect to  $V_{out}$  equal to zero, and the only thing that varies between the different characteristics is the extreme values assumed by the output voltage. For the case in which the contribution of the drivers to calculate the output voltage is also considered, the situation has not improved, the influence is still strong, as can be seen in Figure 4.8(a) and Figure 4.8(b) for the case in which symmetric and asymmetric transcharacteristics are used for the interfaces, respectively.



(a)



(b)

**Figure 4.7:**  $V_{in}-V_{out}$  characteristic when  $V_{out}$  is computed *without* the contribution of the driver voltage: (a) using the *symmetric* transcharacteristics for the interface 1, (b) using the *asymmetric* transcharacteristics for the interface 1.

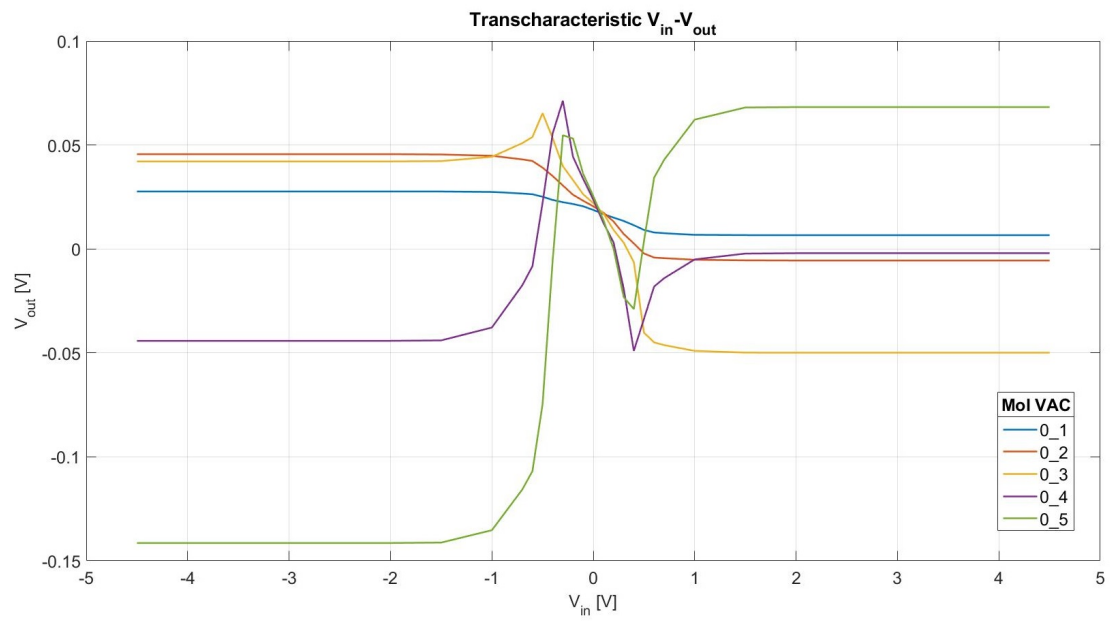
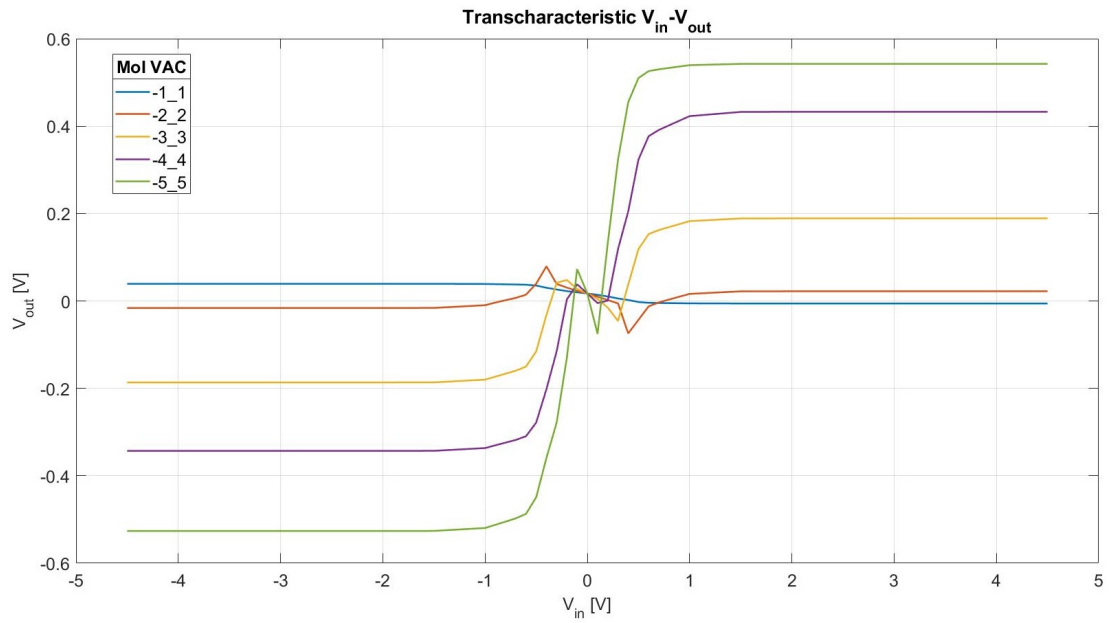


**Figure 4.8:**  $V_{in}$ - $V_{out}$  characteristic when  $V_{out}$  is computed *with* the contribution of the driver voltage: (a) using the *symmetric* transcharacteristics for the interface 1, (b) using the *asymmetric* transcharacteristics for the interface 1.

By observing the behaviour of  $V_{\text{out}}$  in the case in which the driver effect is considered in the calculation, it is understood that the problem is all the more evident the greater the extreme values of the aggregate charge. Furthermore, analysing the behaviour in the case in which the output voltage does not take into account the contribution of the interface, it is seen that what really changes is the slope of the central linear section, while the maximum and minimum values of the aggregate charge of the interfaces affect relatively the central cell of the MV. This led to thinking about changing the transcharacteristics to be used for the interfaces. It was decided to change only the slope between the different curves, instead of the maximum and minimum values. The new transcharacteristics are shown in Figure 4.9. Even in this case, symmetric and asymmetric characteristics were considered. The curves in the shades of blue represent the trend of the charge on Dot 1, whereas those in the shades of red show the behaviour of the charge on Dot 2. Here too, the intensity of the color, light or dark, allows associating the various curve pairs.

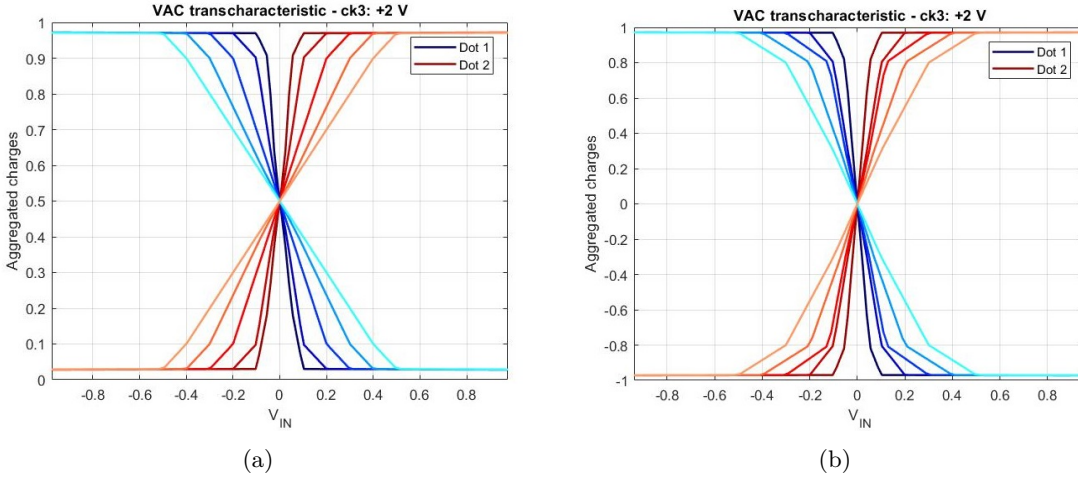
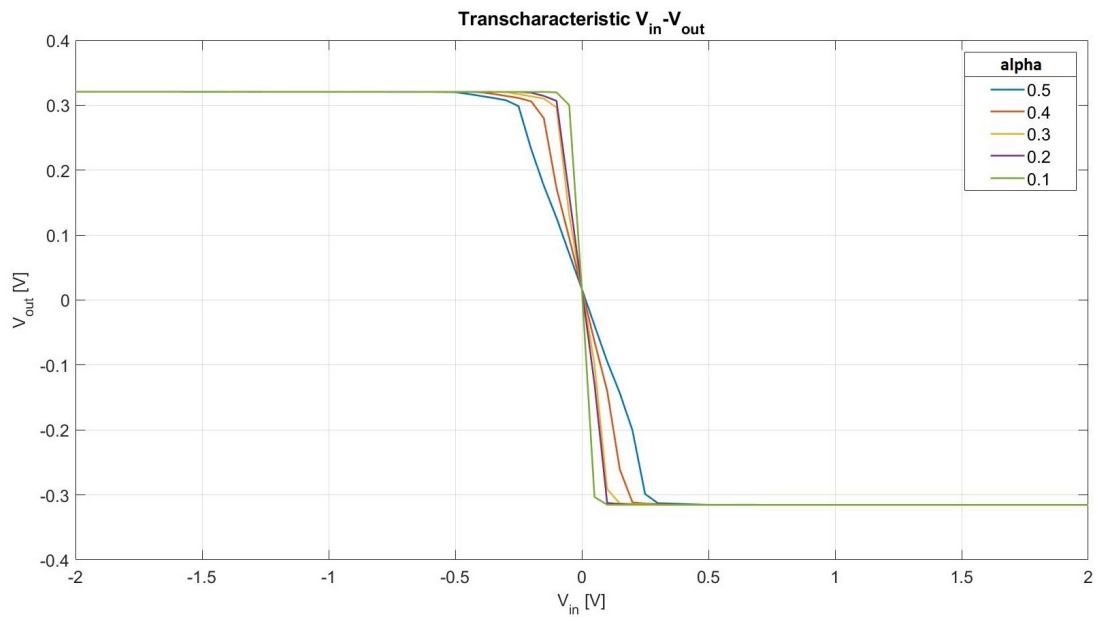


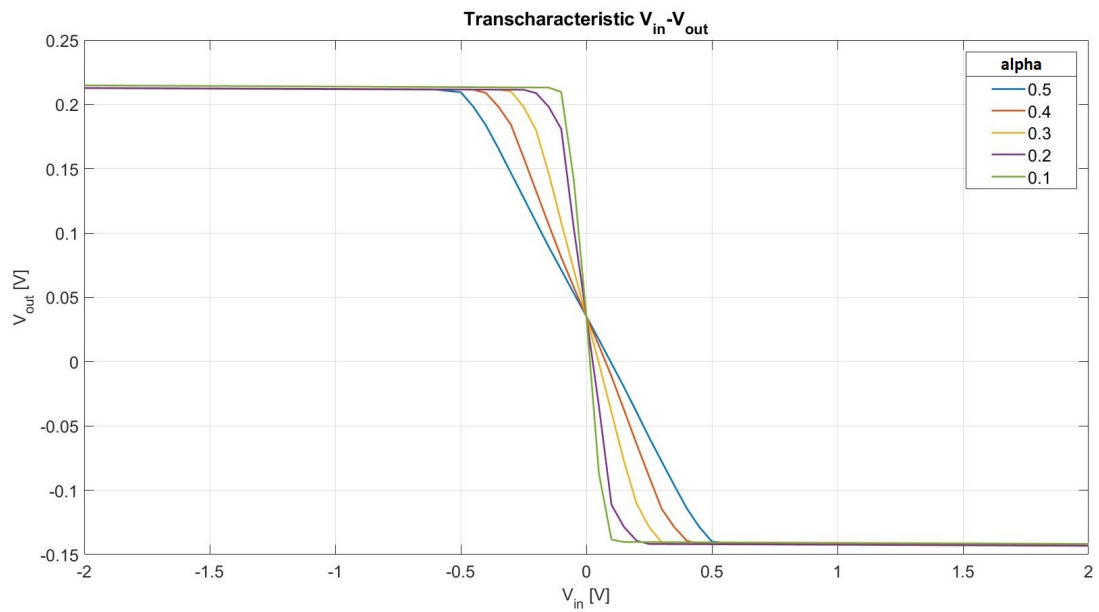
**Figure 4.9:** New transcharacteristics synthesized to analyse the behaviour of the first interface: (a) asymmetric transcharacteristics, (b) symmetric transcharacteristics.

In Figure 4.10(a) and in Figure 4.10(b) the  $V_{\text{in}}-V_{\text{out}}$  curves are shown if the driver effect is not considered. It can be observed that between the various transcharacteristics only the slope of the central section changes, while the maximum and minimum values assumed by the output voltage are the same in all cases. The various curves are distinguished in the legend according to the value of the input voltage  $V_{\text{in}}$  in which the aggregate charge reaches saturation in the transcharacteristics of Figure 4.9: this value has been called *alpha*.

The real difference obtained using these new transcharacteristics is visible when the effect of the driver to calculate  $V_{\text{out}}$  is also considered. As shown in Figure 4.11(a) and Figure 4.11(b), the behaviour is now the same as when  $V_{\text{out}}$  does not take into account the effect of the driver. The only differences are the range of values assumed by the output voltage and the presence of overshoots when using symmetric transcharacteristics.

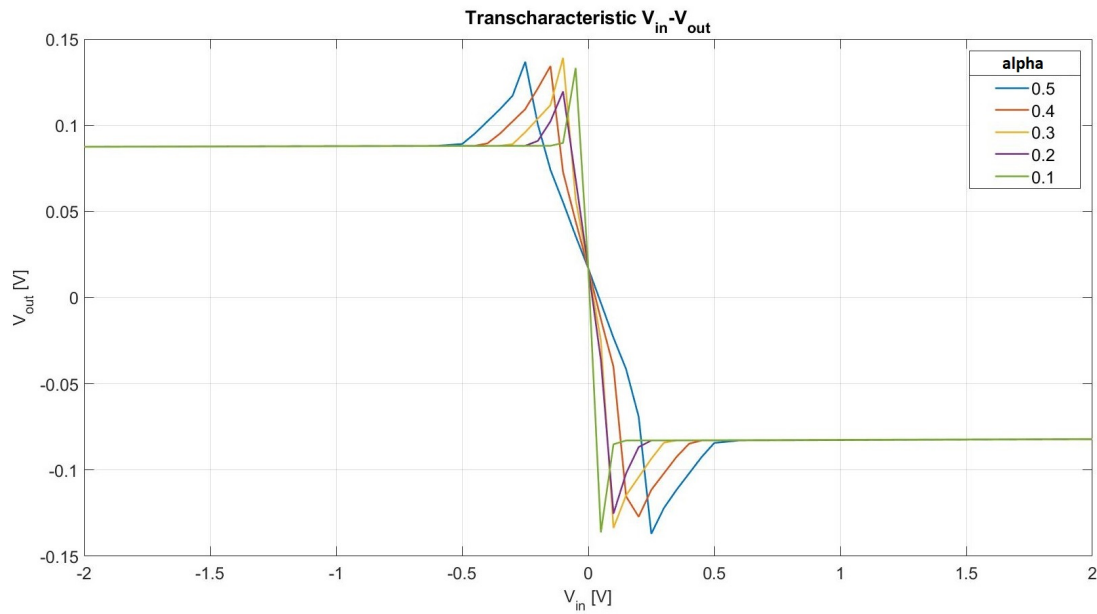


(a)

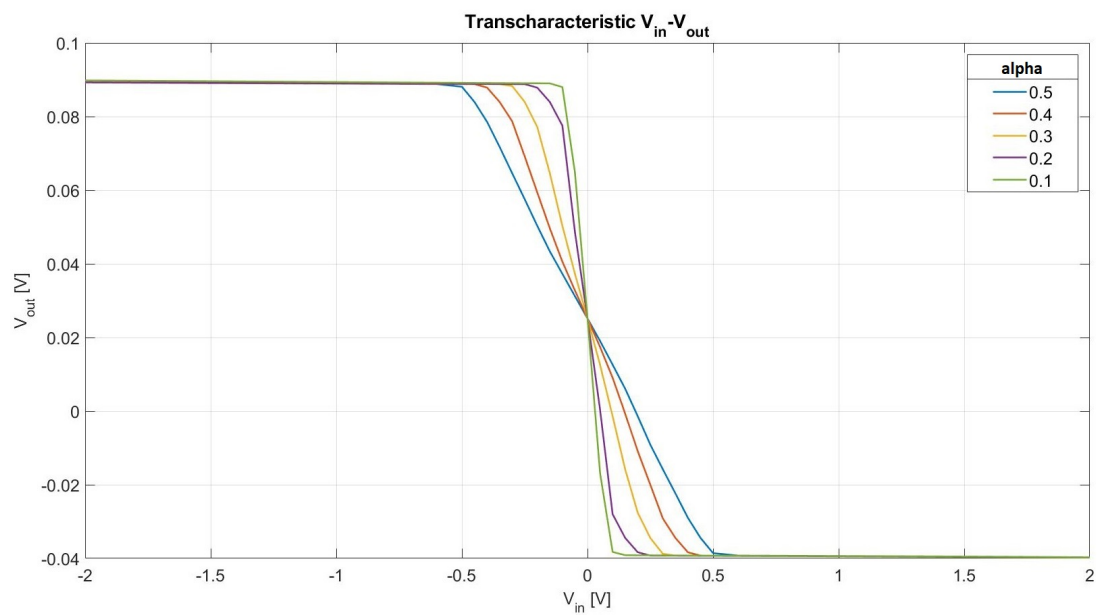


(b)

**Figure 4.10:**  $V_{in} - V_{out}$  characteristic when  $V_{out}$  is computed *without* the contribution of the driver voltage: (a) using the new *symmetric* transcharacteristics for the interface 1, (b) using the new *asymmetric* transcharacteristics for the interface 1.



(a)



(b)

**Figure 4.11:**  $V_{in} - V_{out}$  characteristic when  $V_{out}$  is computed *with* the contribution of the driver voltage: (a) using the new *symmetric* transcharacteristics for the interface 1, (b) using the new *asymmetric* transcharacteristics for the interface 1.

## 4.2 Step 1A: the study of the second interface

For the first part of step 1, the layout is always the same as in Figure 4.6, but in this case, the input voltage on the second interface is different from zero. For both drivers the same transcharacteristic was used, in particular the one with alpha equal to 0.5 was chosen, as shown in Figure 4.12(a) and Figure 4.12(b) for the asymmetric and symmetric cases, respectively.

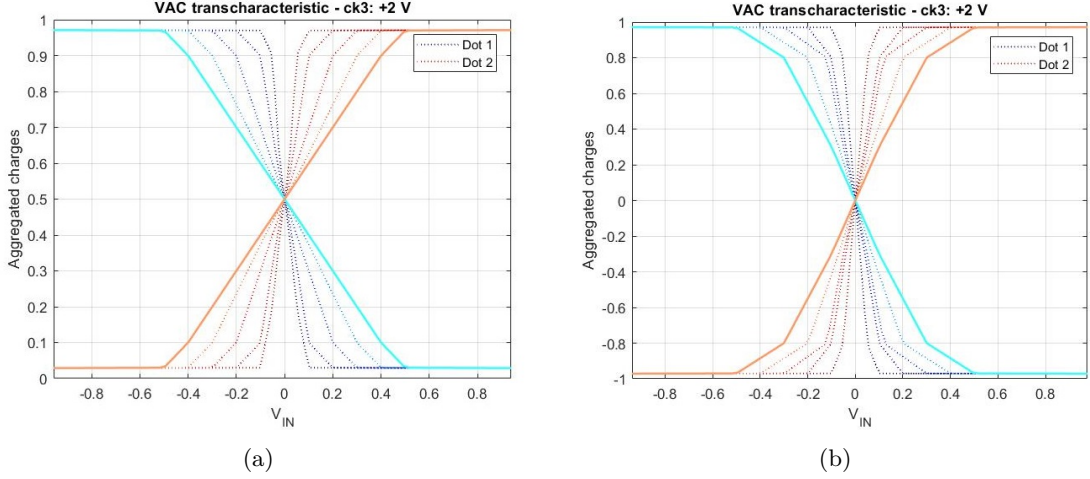


**Figure 4.12:** Transcharacteristics used to analyse the behaviour of the first part of the step 1, it was chosen the one represented with a continuous line: (a) asymmetric transcharacteristics, (b) symmetric transcharacteristics.

It has been chosen to plot the output voltage  $V_{out}$  with respect to the input voltage on the first interface  $V_{in1}$ , for different values of the input voltage on the second interface  $V_{in2}$ , to see how the second driver changes the previously obtained curve. The results obtained when the symmetric transcharacteristic  $\alpha = 0.5$  was used for the interfaces are shown in Figure 4.13(a), for the case in which the effect of the driver was not considered to calculate the output voltage, and in Figure 4.13(b), for the case in which also the voltages given by the drivers are used for the calculation of  $V_{out}$ .

From Figure 4.13(a) it can be seen that in the central linear section the behaviour is of the type

$$V_{out} = m_1 \cdot V_{in1} + m_2 \cdot V_{in2} \quad (4.1)$$

where  $m_1$  and  $m_2$  are the weights of the two interfaces. In Figure 4.13(b) the behaviour of the central linear section remains the same, within certain limits, however at the extremes of the characteristic the behaviour is still influenced by the voltage of the drivers.

## 4.2. Step 1A: the study of the second interface

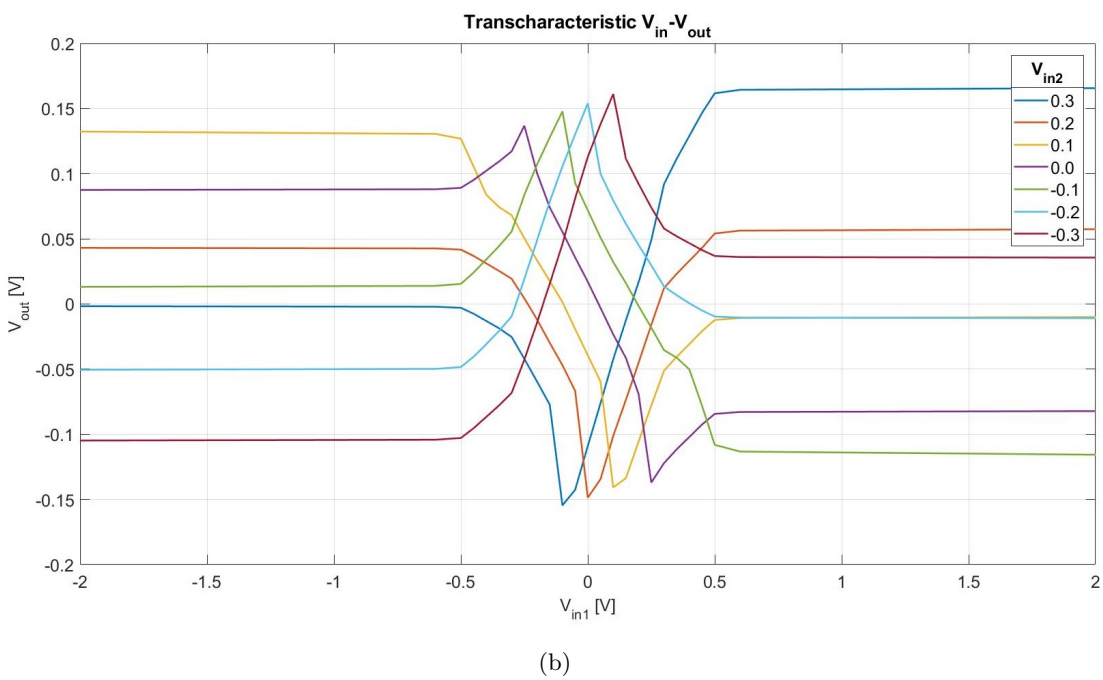
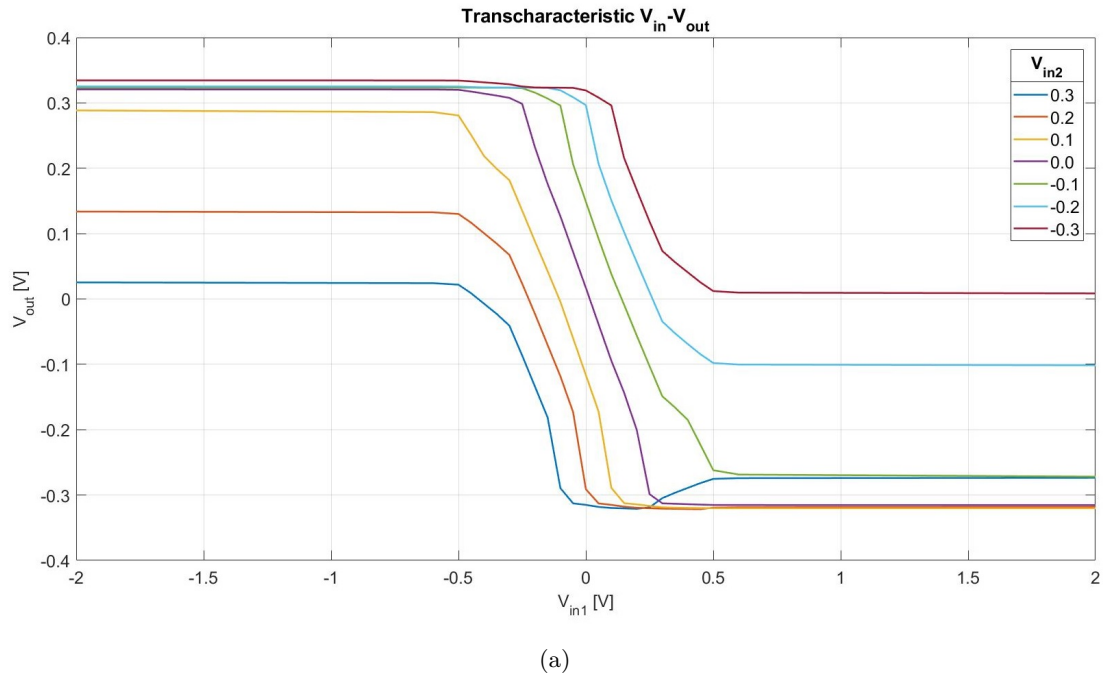


**Figure 4.13:**  $V_{in1}-V_{out}$  characteristics for different values of  $V_{in2}$  using the *symmetric* transcharacteristic  $\alpha = 0.5$  for the interfaces: (a) when  $V_{out}$  is computed *without* the contribution of the driver voltage, (b) when  $V_{out}$  is computed *with* the contribution of the driver voltage.

In Figure 4.14 and Figure 4.15 are shown the results of the same simulations, but performed with the asymmetric  $\alpha = 0.5$  transcharacteristic for the interfaces. Here, in both the cases in which the contribution of the drivers is and is not considered for the calculation of  $V_{out}$ , the curves in the central linear section follow equation (4.1), and in the lateral part of the graph, there is no superposition between the various characteristics.

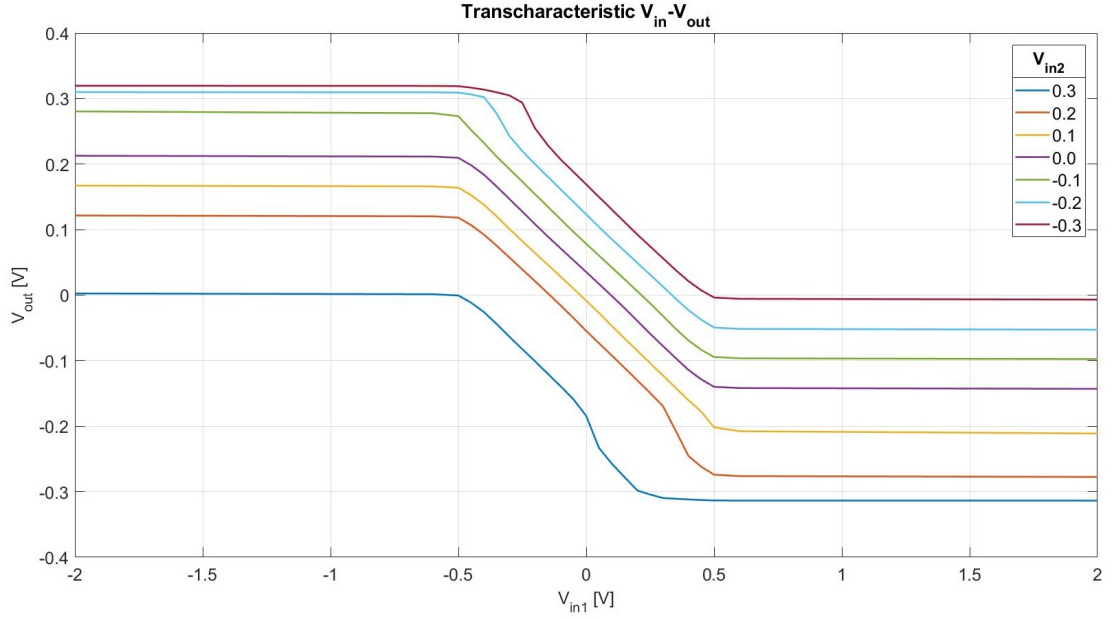


**Figure 4.14:**  $V_{in1}$ - $V_{out}$  characteristics for different values of  $V_{in2}$  using the *asymmetric* transcharacteristic  $\alpha = 0.5$  for the interfaces, when  $V_{out}$  is computed *without* the contribution of the driver voltage.

From these simulations, the behaviour appears to be qualitatively correct. In fact, focusing for example on Figure 4.14, on the curves for which  $V_{in2} = \pm 0.3$  V, four possible configurations can be observed:

1. both  $V_{in1}$  and  $V_{in2}$  are positive,  $V_{out}$  should saturate toward positive values, but for the inversion mechanism saturates at negative values;
2.  $V_{in1}$  is positive and  $V_{in2}$  is negative, the two drivers provide opposite logic information, and  $V_{out}$  tends to zero;
3. both  $V_{in1}$  and  $V_{in2}$  are negative,  $V_{out}$  should saturate toward negative values, but for the inversion mechanism saturates at positive values.
4.  $V_{in1}$  is negative and  $V_{in2}$  is positive, the two drivers provide opposite logic information, and  $V_{out}$  tends to zero;

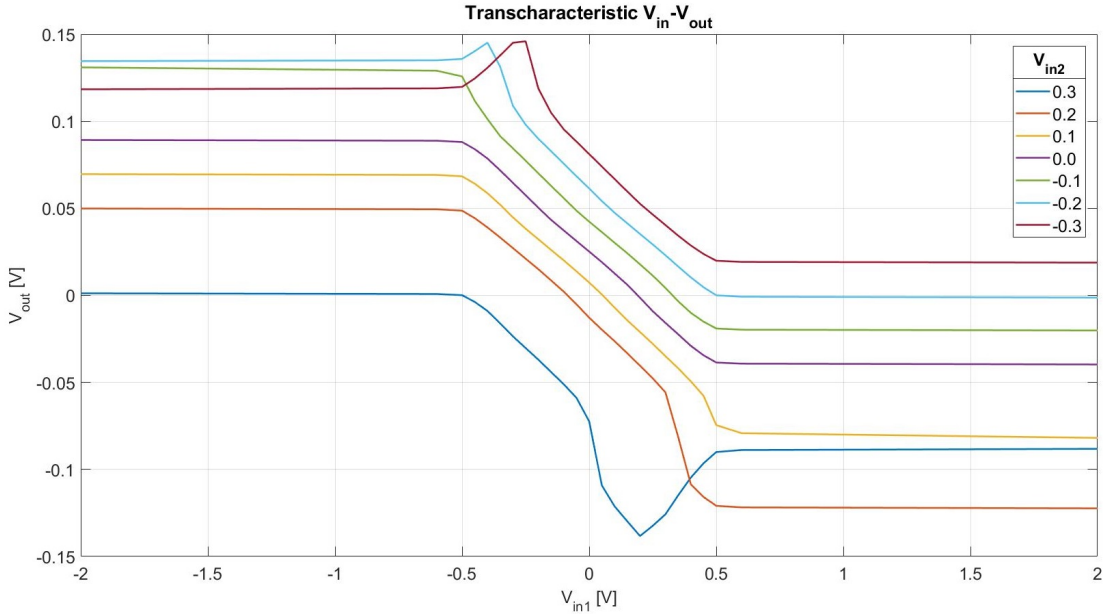


**Figure 4.15:**  $V_{in1}$ - $V_{out}$  characteristics for different values of  $V_{in2}$  using the *asymmetric* transcharacteristic  $\alpha = 0.5$  for the interfaces, when  $V_{out}$  is computed *with* the contribution of the driver voltage.

These four configuration can be schematically represented as in Figure 4.16, in particular: case (1) corresponds to Figure 4.16(a), case (2) corresponds to Figure 4.16(b), case (3) corresponds to Figure 4.16(c), and case (4) corresponds to Figure 4.16(d).

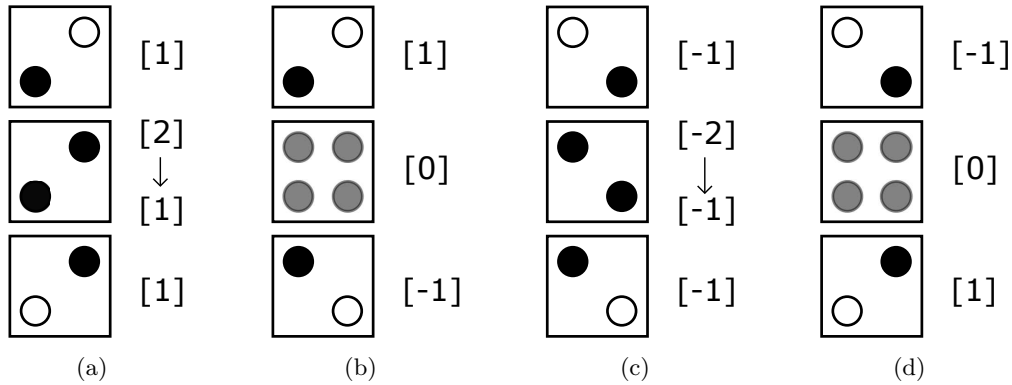


**Figure 4.16:** Schematic representation on the four extreme possible configurations for the output when: (a) both  $V_{in1}$  and  $V_{in2}$  are positive, (b)  $V_{in1}$  is positive and  $V_{in2}$  is negative, (c) both  $V_{in1}$  and  $V_{in2}$  are negative, (d)  $V_{in1}$  is negative and  $V_{in2}$  is positive.

The simulations that have been done so far, show that the behaviour is qualitatively

correct, however, they are not very intuitive for two reasons: it is not spontaneous to associate a voltage to a logical value and the relationship between the input voltage and output voltage is inverting. It was therefore thought to change the variables involved, in particular the one that describes the output behaviour. Instead of using the voltage on a fictitious molecule located downstream of the MV, it was decided to use the polarization  $P_{MV}$  of the central cell of the MV, the one composed of the two bisferrocene molecules. This quantity is defined as

$$P_{MV} = \frac{(Q_1 + Q_4) - (Q_2 + Q_3)}{\sum_{i=1}^4 Q_i} \quad (4.2)$$

where  $Q_i$  is the charge on the  $i$ -th dot of the cell, as shown in Figure 4.17. Moreover, it has been decided to normalize the input with respect to the maximum input value, which is  $V_{MAX} = 0.4$  V [29].

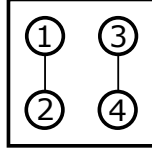


**Figure 4.17:** Representation of a QCA cell with the dot numbered.

In Figure 4.18 is shown the transcharacteristic when symmetric curves are used for the drivers. The layout is again the one represented in Figure 4.6 and the input voltage on the interface 2 is equal to zero.

In this case, since only one driver is switched on, the relation between input and output is the one below

$$P_{MV} = f \left( m_1 \cdot \frac{V_{in1}}{V_{MAX}} \right) \quad (4.3)$$

This means that in the region in which the characteristics are linear, it is possible to evaluate the weight  $m_1$  dividing the output by the input. In Table 4.1 are listed the obtained values.

**Table 4.1:** Weights of the interface 1 when the symmetric transcharacteristics are used.

| alpha | $m_1$ |
|-------|-------|
| 0.1   | 7.41  |
| 0.2   | 3.80  |
| 0.3   | 3.61  |
| 0.4   | 2.21  |
| 0.5   | 1.47  |

Assuming that the influence of the interface 2 is the same as that of the interface 1 since they are located the same way, it has been done one example to see if the MV polarizes correctly. This is shown in Figure 4.19. In particular, it has been tried to use two

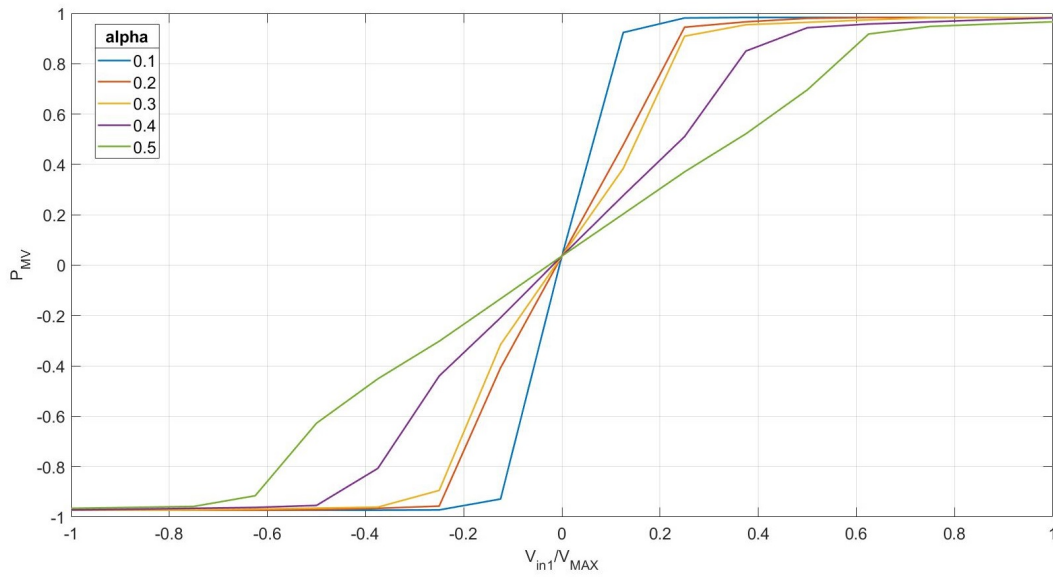


**Figure 4.18:** Input-output characteristics when the *symmetric* transcharacteristics are used for the drivers.

different characteristics for the two interfaces: driver 1 has the symmetric transcharacteristic with  $\alpha$  equal to 0.3, whereas for the second driver  $\alpha$  is equal to 0.1. The input voltage has the same absolute value for both drivers equal to 0.1 V but opposite sign, to verify that the output follows the input with the greatest weight. Indeed, it can be seen that the central cell of the MV has the same logical information as driver 2.

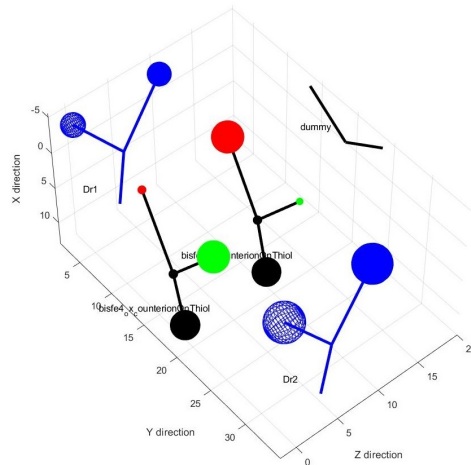


**Figure 4.19:** Example to control if the MV works correctly when two different transcharacteristics are used for the interface 1 and the interface 2.

### 4.3 Step 1B: the study of the third interface

This step involves adding the third interface. First of all, some examples have been made, to see the qualitative results. In all the following examples, a symmetrical transcharacteristic with  $\alpha = 0.1$  has always been used for interface one, whereas the other two interfaces both have a symmetrical transcharacteristic with  $\alpha = 0.5$ . Among the various examples, only the input voltage on the three interfaces was changed, so that it was easy to understand what is the logical value expected on the output.

As a first example, it has been tried to put the same input voltage  $V_{in} = +0.3$  V on all three drivers, i.e. all three drivers have the same logical information. At the output, as can be seen from Figure 4.20(a), the logical information is coherent with that of the three inputs. In the second example, the sign of the voltage on the driver 2 has been changed. Since the voltage has the same absolute value for all the inputs, adding the weights with the correct sign, it can be seen that the logical output information must be the same represented by the drivers 1 and 3, but “weaker” than in the previous case. This actually happens, as shown in Figure 4.20(b).

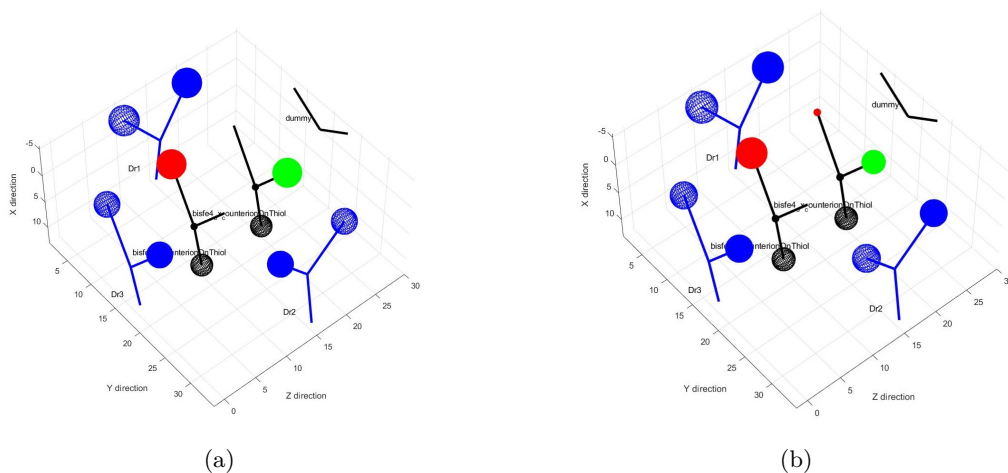


**Figure 4.20:** Layout plotted with SCERPA for the simulations in which driver 1 has a symmetric transcharacteristic with  $\alpha = 0.1$ , whereas Drivers 2 and 3 have a symmetric transcharacteristic with  $\alpha = 0.5$ : (a) all three drivers have an input voltage equal to  $+0.3$  V, (b) drivers 1 and 3 have an input voltage equal to  $+0.3$  V, whereas the second interface has  $V_{in2} = -0.3$  V.

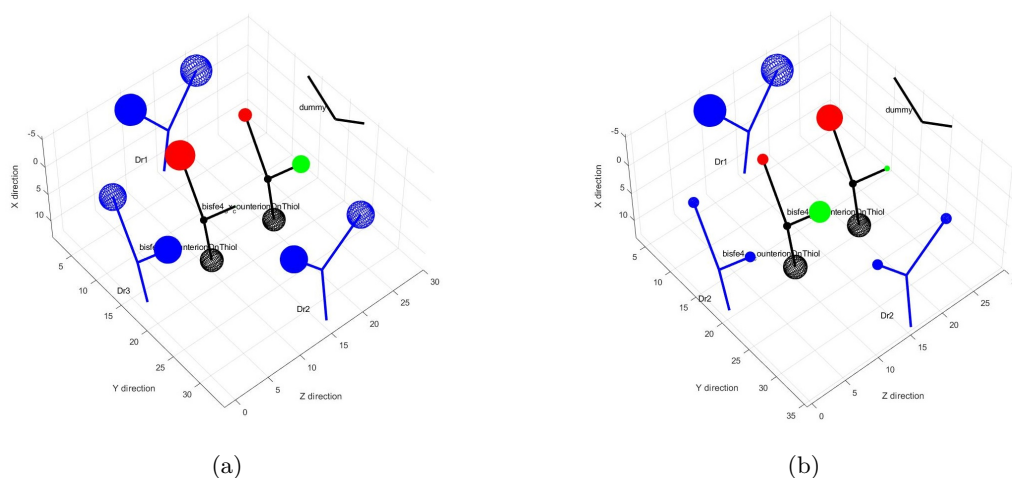
As the last example, it was decided to try to see if the mechanism works even in cases where only one strong entry wins over the other two, thus going beyond the classic behaviour of a majority voter. Therefore, compared to the first example of this section, the sign of the voltage on the first driver has been changed. Since interface 1 has a weight of 7.41, while the other two have a weight of 1.47 each, the output should assume the logical value of driver 1. However, this does not happen, as can be seen from

Figure 4.21(a).

By trying to repeat the same example, using a voltage that allows all three interfaces to work in the linear region, it can be seen from Figure 4.21(b) that the output correctly follows the logical information represented by interface 1 only. Furthermore, by calculating  $P_{MV}$  from the charge distribution on the central cell of the MV from the simulation,  $P_{MV} = -0.484$  is obtained. On the other hand, trying to calculate  $P_{MV}$  from the weighted sum of the inputs, one gets

$$P_{MV} = m_1 \cdot V_{in1} + m_2 \cdot V_{in2} + m_3 \cdot V_{in3} = -0.447 \quad (4.4)$$

where the difference comes from the rounded values of the weights.



**Figure 4.21:** Layout plotted with SCERPA for the simulations in which driver 1 has a symmetric transcharacteristic with  $\alpha = 0.1$ , whereas Drivers 2 and 3 have a symmetric transcharacteristic with  $\alpha = 0.5$ : (a) drivers 2 and 3 have an input voltage equal to  $+0.3$  V, whereas the first interface has  $V_{in1} = -0.3$  V, (b) drivers 2 and 3 have an input voltage equal to  $+0.1$  V, whereas the first interface has  $V_{in1} = -0.1$  V.

These examples have shown that in order to work properly, it must be ensured that all interfaces work in the linear region. This means that with the current transcharacteristics, the input voltage should be between  $\pm 0.1$  V. As this limits the system a lot, it has been thought to impose a limit on the possible transcharacteristics instead of on the voltage. Previously it has been said that the maximum input voltage on a molecule is  $0.4$  V. However, this is true if there are no other molecules present in the surroundings. Since the system will have to be connected with other elements, the maximum voltage that can be generated on a molecule is greater. Connection wires have therefore been added before the interfaces, as shown in Figure 4.22(a), and it has been seen that

$$-1 \text{ V} < V_{in} < +1 \text{ V} \quad (4.5)$$

as shown in Figure 4.22(b).

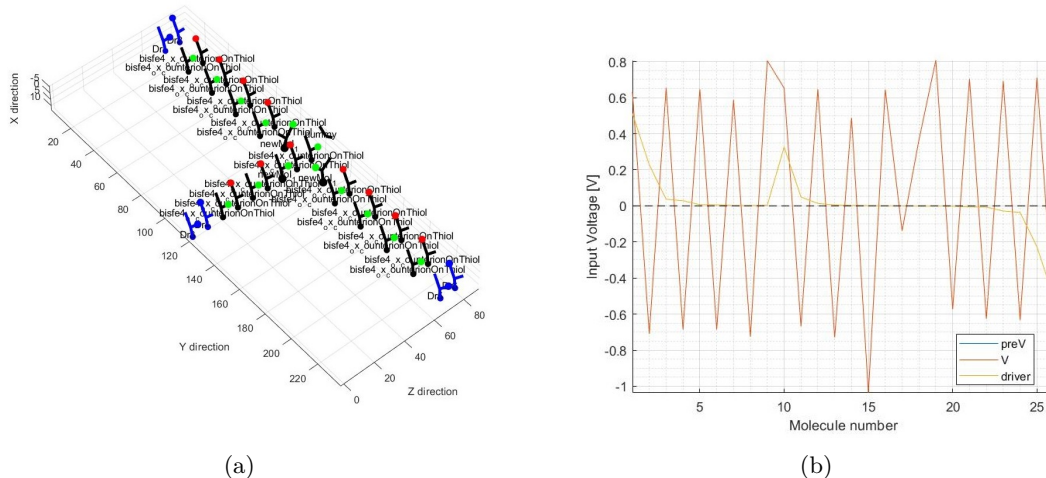


**Figure 4.22:** Simulation results to verify the maximum possible voltage on a molecule: (a) SCERPA layout of the wired MV tested, (b) input voltage on each molecule.

Therefore, new transcharacteristics have been synthesized which present a linear behaviour in the voltage range just highlighted. Here too it has been chosen to continue to present both asymmetric and symmetric transcharacteristics, shown respectively in Figure 4.23(a) and Figure 4.23(b).

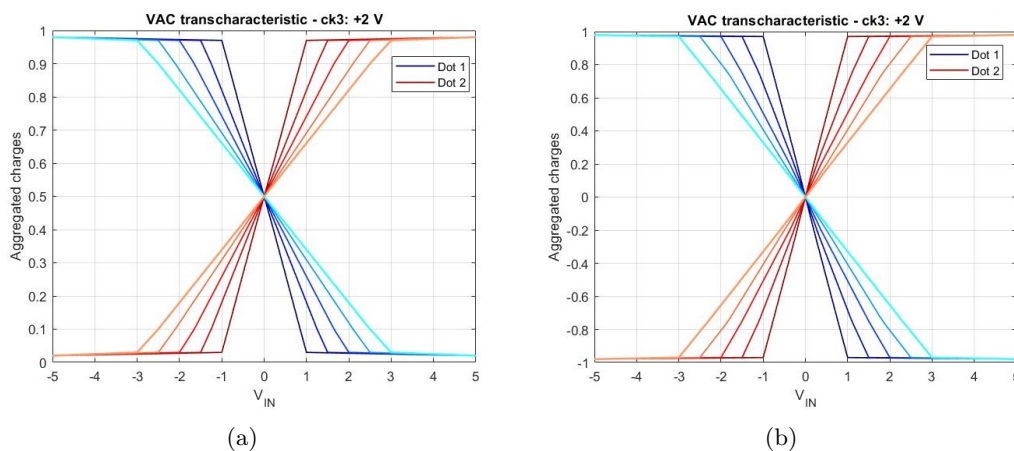


**Figure 4.23:** Transcharacteristics that guarantee a linear behaviour in the range of possible voltages on a molecule: (a) asymmetric transcharacteristics, (b) symmetric transcharacteristics.

The weights of the three interfaces were calculated when the various transcharacteristics are used. To do this, one driver at a time was turned on, and the ratio between the output and the input was calculated. The values found are listed in Table 4.2.

**Table 4.2:** Weights of the interfaces calculated with the last set of synthesized transcharacteristics.

| ALPHA | SYMMETRIC |        |        | ASYMMETRIC |        |        |
|-------|-----------|--------|--------|------------|--------|--------|
|       | $m_1$     | $m_2$  | $m_3$  | $m_1$      | $m_2$  | $m_3$  |
| 1     | 1.2630    | 1.2630 | 1.2630 | 0.5981     | 0.5981 | 0.6653 |
| 1.5   | 0.9110    | 0.9110 | 0.9110 | 0.4071     | 0.4071 | 0.3934 |
| 2     | 0.6775    | 0.6775 | 0.6775 | 0.3064     | 0.3064 | 0.2960 |
| 2.5   | 0.5034    | 0.5034 | 0.5034 | 0.2425     | 0.2425 | 0.2331 |
| 3     | 0.4193    | 0.4193 | 0.4057 | 0.2019     | 0.2019 | 0.1966 |

In the case of asymmetric transcharacteristics, and in one case also of symmetric transcharacteristics, it is seen that the value of the weight at interface 3 is slightly different from the others. This can be justified by the fact that the position with respect to the two central molecules of the MV is different, therefore the influence that the driver has on these also slightly changes.



## Chapter 5

# Neuron output and connection with other neurons

In this chapter, the issues concerning the presence of molecules at the exit and the concept of the threshold are studied in depth. In particular, the discussion will follow a logical rather than temporal path, for this reason, Step 2 has been moved after Section 5.2 where the threshold mechanism is discussed.

### 5.1 Step 3: the influence of output molecules

First, the effect of the presence of output molecules was investigated. Since each molecule influences the neighbouring ones by changing their charge distribution, it is important to understand whether the molecules on the output branch influence the calculation of the total input contribution. As a first simulation, only one bisferrocene molecule was added, as shown in Figure 5.1(a). Asymmetric characteristics have been used for all the examples in this section. In this case, the inputs were chosen so that the polarization on the MV was weak, in the sense that the charge is not distributed mainly along one of the two diagonals, but is present on all four dots of the central cell of the MV. In this example in particular, the configuration of the inputs is

#### INTERFACE 1 :

- $\alpha = 1 \text{ V} \rightarrow m_1 = 0.5981$
- $V_{IN1} = -1 \text{ V}$

#### INTERFACE 2 :

- $\alpha = 3 \text{ V} \rightarrow m_2 = 0.2019$
- $V_{IN2} = +1 \text{ V}$

#### INTERFACE 3 :

- $\alpha = 3 \text{ V} \rightarrow m_3 = 0.1966$
- $V_{IN3} = +1 \text{ V}$



another or four in the first phase and four in the next, the final effect is the same.

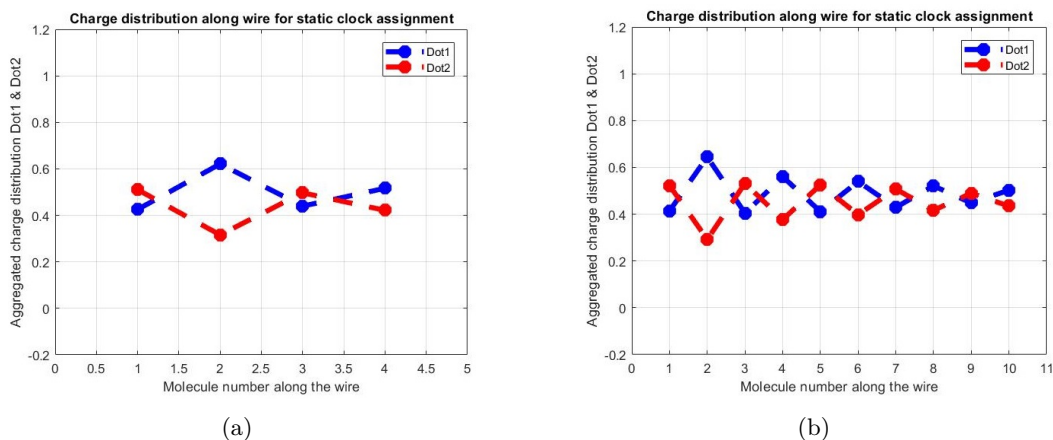


**Figure 5.2:** Charge for each molecule excluding the drivers when: (a) two molecules are placed at the output, (b) eight molecules are placed at the output.

Then, leaving eight molecules at the output, it was tried to see if, with a combination of inputs that gave a well-defined logical state, the molecules showed a bistable behaviour. The combination of the inputs is thus the same as before, but with all the input voltages positive. In Figure 5.3(a) the charge on the logical dots of each molecule is shown, and it is clear that the information tends to decay, despite the charge on the first two molecules, those at the center of the MV, is well separated. By adding molecules, the feedback effect of each of these allows the charge to saturate, in fact with ten molecules at the output of the MV the molecules exhibit a bistable behaviour, as shown in Figure 5.3(b).

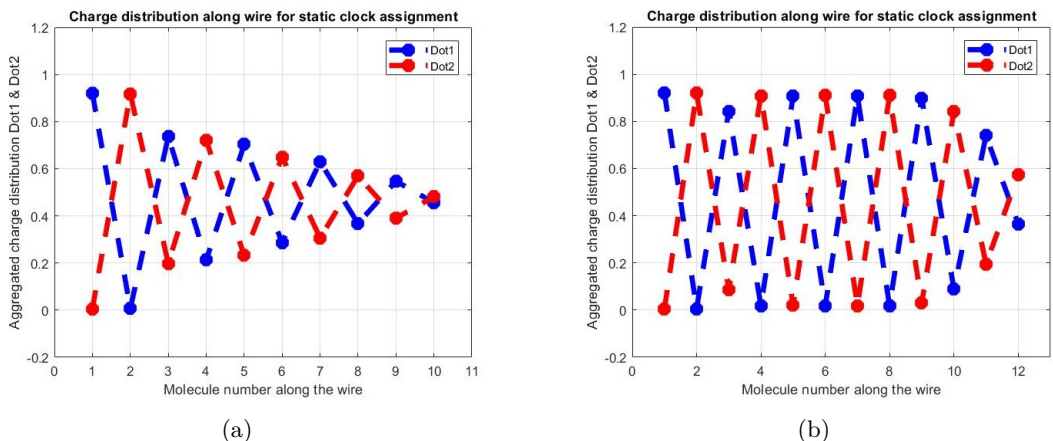


**Figure 5.3:** Charge for each molecule excluding the drivers, in the case of well define logic value on the central cell of the MV, when: (a) eight molecules are placed at the output, (b) ten molecules are placed at the output.

After that, it has been tried to insert, just after the central cell of the MV, a molecule with a very steep transcharacteristic. It has been inserted a molecule with  $\alpha = 0.1$  V, so the structure becomes the one shown in Figure 5.4. It has been tried to see if, with this molecule before the output wire, the propagation would have improved.

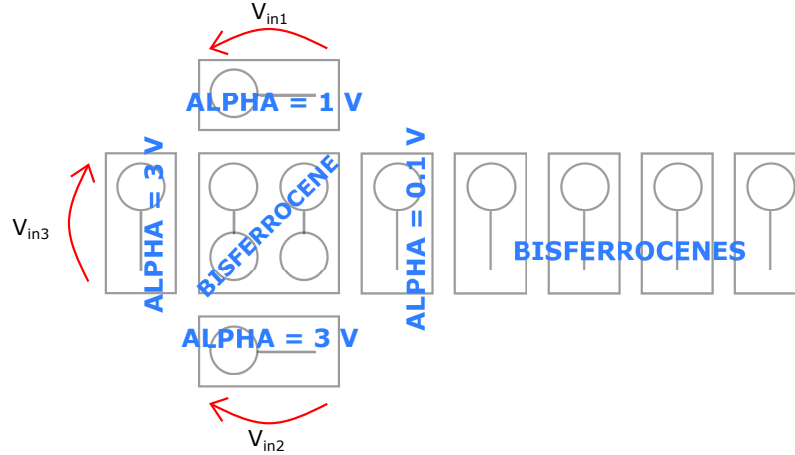


**Figure 5.4:** Layout of the structure with the molecules used specified.

The first case analysed was the one in which the three inputs voltages are the same, and therefore the logical information contained on the central cell of the MV is well defined. Putting only eight molecules at the output, the behaviour of the molecules was bistable, contrary to what was previously found. As it can see from Figure 5.5, by inserting the molecule with  $\alpha = 0.1$  V just after the two in the center of the MV, the output molecules propagate the information with bistable behaviour.

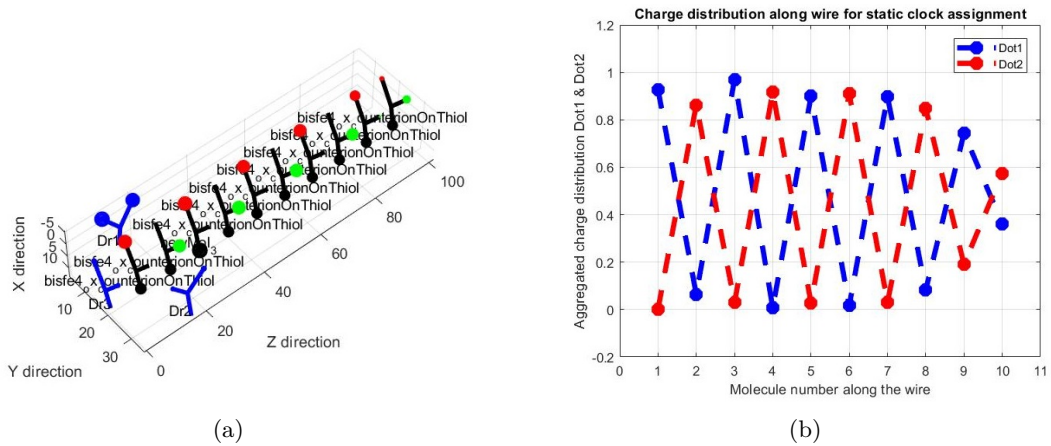


**Figure 5.5:** Simulation results when eight molecules are placed at the output, the first is a molecule with  $\alpha = 0.1$  V whereas the other seven are bisferrocenes: (a) 3D representation, (b) charge for each molecule excluding the drivers.

It has been tried to verify if, even in the case of a logical value not well defined on the MV, the output propagation improves in the presence of a molecule with  $\alpha = 0.1$  V. The input voltage on interface 1 has therefore changed to -1 V, as in the first examples of this section. The results obtained are shown in Figure 5.6. As can be seen from Figure 5.6(b) in this case the molecules in the output wire propagate the information with a bistable behaviour, as can be deduced by the strong separation of the charge in the logic dots. Thus a molecule with a very steep transcharacteristic acts like a *saturator*, since it can encode a very well define logic value even when its input voltage is small.

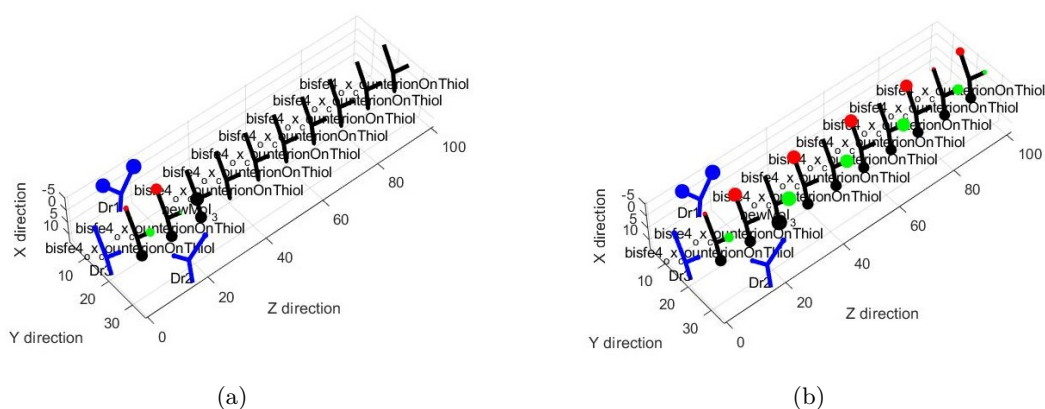


**Figure 5.6:** Simulation results when eight molecules are placed at the output, the first is a molecule with  $\alpha = 0.1$  V whereas the other seven are bisferrocenes, and the logic value on the MV is weak: (a) first time step of the simulation, (b) second time step of the simulation.

## 5.2 Step 4: the study of the threshold

As already mentioned in Chapter 3, one of the possible ways to represent the threshold is by using an external voltage applied on a molecule. At the moment, the logical information and the value of the weighted sum of the inputs are represented in terms of polarization. To link this information and the external voltage, it was decided to use a structure like the one shown in Figure 5.7, in which there are two drivers, which simulate the behaviour of the MV, and two molecules at the output. Having replaced the MV with two driver molecules it is easier to make complete characterizations: by setting the input voltage on the two drivers, opposite in sign and equal in absolute value, and spanning from -1 V to +1 V, it is possible to obtain a polarization between -1 and +1.

It was decided to work initially with all bisferrocenes, both for the drivers and the output molecules. In the first case analysed, no external voltage was applied, and characterization was carried out to subsequently be able to compare the results obtained with this case, which from now on will be called the “reference case”.

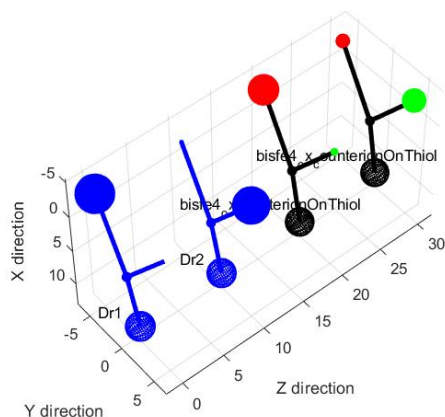


**Figure 5.7:** SCERPA layout of the structure used to study the threshold mechanism using the external voltages.

The input voltage on the two molecules after the drivers was calculated, as shown in Figure 5.8. If an external voltage is applied, what is expected is a vertical shift of both curves, even if the external voltage is applied only on one molecule. In fact, for the feedback mechanism, if the input voltage on one molecule is higher (or lower), on the other molecule the voltage will be lower (or greater), therefore the shifts will be in opposite directions.

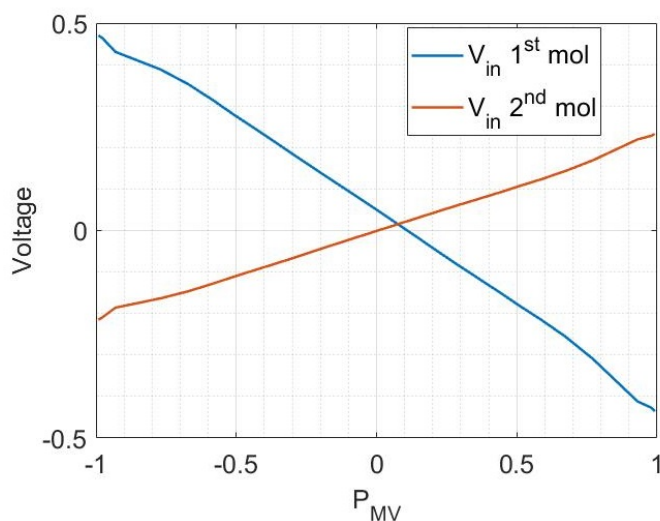


**Figure 5.8:** Relation between the polarization of the cell composed by the two drivers which simulate the MV and the input voltage on the first molecule after the driver (blue) and on the second molecule (orange).

Different external voltage values were used, ranging from +0.3 V to -0.3 V. The external voltage was first applied to the first molecule after the drivers and the average shift of the new voltage curve obtained for the different polarizations was calculated. An example of the graph obtained, in the case of external voltage equal to +0.2 V applied on the first molecule after the drivers, is shown in Figure 5.9. The same thing was then repeated with the same values, however applying the external voltage on the second molecule after the drivers, to see if there was any difference in the position of the molecule on which the external voltage is applied. As can be seen from Figure 5.9, since a positive voltage has been applied on the first molecule, the relative curve is shifted upwards. Conversely, the shift on the second molecule is in the opposite direction, since the charge in adjacent molecules is arranged diametrically, leading to opposite voltages in the sign.

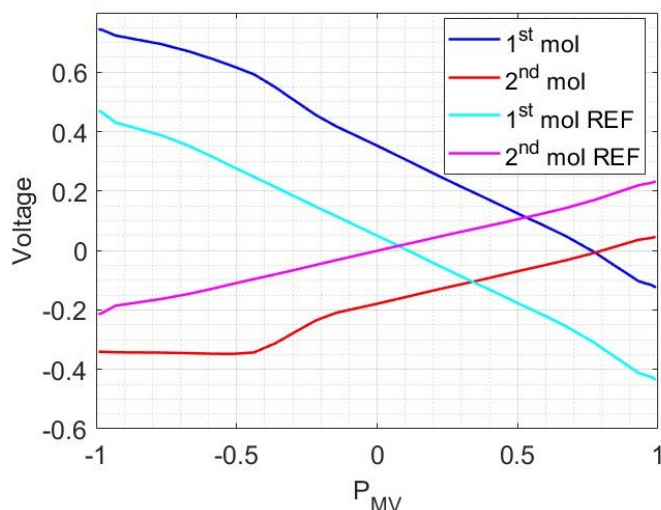


**Figure 5.9:** Relation between the polarization of the cell composed by the two drivers which simulate the MV and the input voltage on the first and the second molecule after the driver, for the reference case (cyan and magenta) and for the case in which an external voltage equal to +0.2 V is applied on the first molecule (blue and red).

Table 5.1 lists the average values of the shift (in absolute value) of the voltages on the two molecules after the drivers, both in the case in which the external voltage is applied on the first of the two molecules and in the case in which it is applied on the second.

By observing the results obtained in the various cases, it can be seen that the shift value equal to that set with the external voltage is present on the molecule on which  $V_{\text{ext}}$  is not applied. This is justified by the superposition of the effects and the presence of a feedback mechanism. In fact, the external voltage is added to that due to the drivers. Moreover, the higher the input voltage on a molecule, the higher the output voltage generated, which is nothing more than a contribution to the input voltage on

**Table 5.1:** Absolute values of the voltage shift on the two molecules after the drivers when an external voltage is applied either on the first molecule or on the second.

| $V_{\text{ext}}$ [V] | $V_{\text{ext}}$ on 1 <sup>st</sup> molecule |                          | $V_{\text{ext}}$ on 2 <sup>nd</sup> molecule |                          |
|----------------------|--|--------------------------|--|--------------------------|
|                      | 1 <sup>st</sup> mol. [V]                     | 2 <sup>nd</sup> mol. [V] | 1 <sup>st</sup> mol. [V]                     | 2 <sup>nd</sup> mol. [V] |
| +0.30                | 0.45   | 0.25                     | 0.29   | 0.46                     |
| +0.25                | 0.38   | 0.22                     | 0.24   | 0.39                     |
| +0.20                | 0.31   | 0.18                     | 0.18   | 0.31                     |
| +0.15                | 0.23   | 0.14                     | 0.14   | 0.23                     |
| +0.10                | 0.16   | 0.10                     | 0.09   | 0.16                     |
| +0.05                | 0.08   | 0.05                     | 0.05   | 0.08                     |
| -0.05                | 0.08   | 0.05                     | 0.05   | 0.08                     |
| -0.10                | 0.15   | 0.09                     | 0.09   | 0.16                     |
| -0.15                | 0.23   | 0.13                     | 0.14   | 0.24                     |
| -0.20                | 0.30   | 0.17                     | 0.19   | 0.32                     |
| -0.25                | 0.37   | 0.21                     | 0.23   | 0.39                     |
| -0.30                | 0.44   | 0.24                     | 0.27   | 0.46                     |

the adjacent molecule. So also the input voltage on the molecule on which the external voltage is not present increases, which in turn increases the input voltage on the other molecule. Although this suggests that the threshold is dependent on the layout, in reality, the problem can easily be bypassed when a saturator is introduced. In fact, it would lead to only two situations: polarization 1 or -1 depending on the sign of its input voltage, which mainly depends on the two drivers, that is, on the weighted sum, and the external voltage applied, that is, the threshold. The small contributions due to the other molecules would become negligible, and in any case, agree with the logical information already assumed.

### 5.3 Step 2: the effect of different molecules in the MV

Another way to implement the threshold mechanism, as mentioned in Chapter 3, is to use molecules with a stronger state than the other. Furthermore, to solve the question related to the mechanism explained in the previous section, in which it was observed that the shift was greater than that fixed with the external voltage, it was decided to use that kind of molecules as drivers in the configuration of Figure 5.7. Looking at the complete structure, the central cell of the MV in a single step would calculate the total contribution of the inputs and compare it with the threshold.

Having a molecule with a logical state stronger than the other means having a VACT that does not pass through the origin. In fact, in this way, one would have a logical state for a wider range of voltages and the other for a reduced range. Depending on the direction of the shift, the strongest state is related to either a logical one or a logical zero. Some new transcharacteristics have therefore been synthesized, shifted to the right

or left of the zero, as shown in Figure 5.10. Since the cell is composed of two molecules that oppositely distribute the charge, the two characteristics used for that two molecules do not have to be the same. If on the first molecule one wants to strengthen the situation that presents the charge on Dot 1, on the adjacent molecule it has to strengthen the case in which the charge is on Dot 2. In practice, this means that, for example, if a transcharacteristic with a shift equal to  $+0.3$  V is used on the first molecule, on the other one the transcharacteristic with a shift equal to  $-0.3$  V must be used.

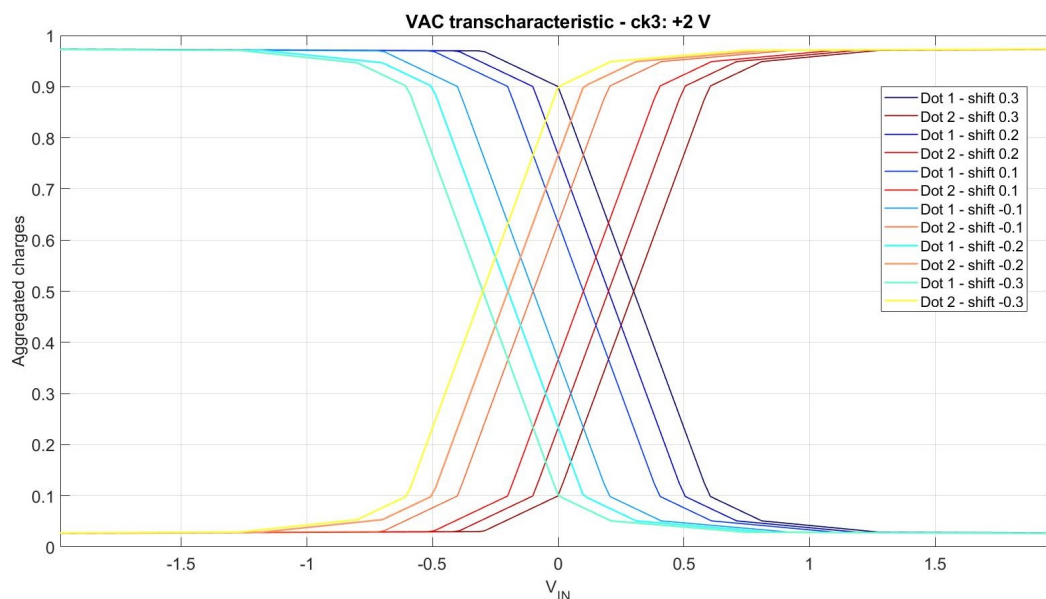


**Figure 5.10:** Transcharacteristics synthesized to study the effect of molecules with one logic state stronger than the other to implement the threshold mechanism. The pairs of curves for the two logical dots are identified by the intensity of the color.

To verify whether the assumptions made work, it was thought to plot the polarization of the cell made up of the two drivers versus the input voltage on one of them. In particular, it was chosen to use the input voltage on the second driver to not have inversion. Nevertheless, since the voltage on the first driver is equal in absolute value and opposite in sign to that applied on the second driver, the polarization of the cell versus the voltage on the first driver would be simply symmetrical to the axis  $V_{in} = 0$  V. In Figure 5.11 are shown the curves obtained for the polarization on the two drivers, which is always compared with the case in which two bisferrocene molecules are used.

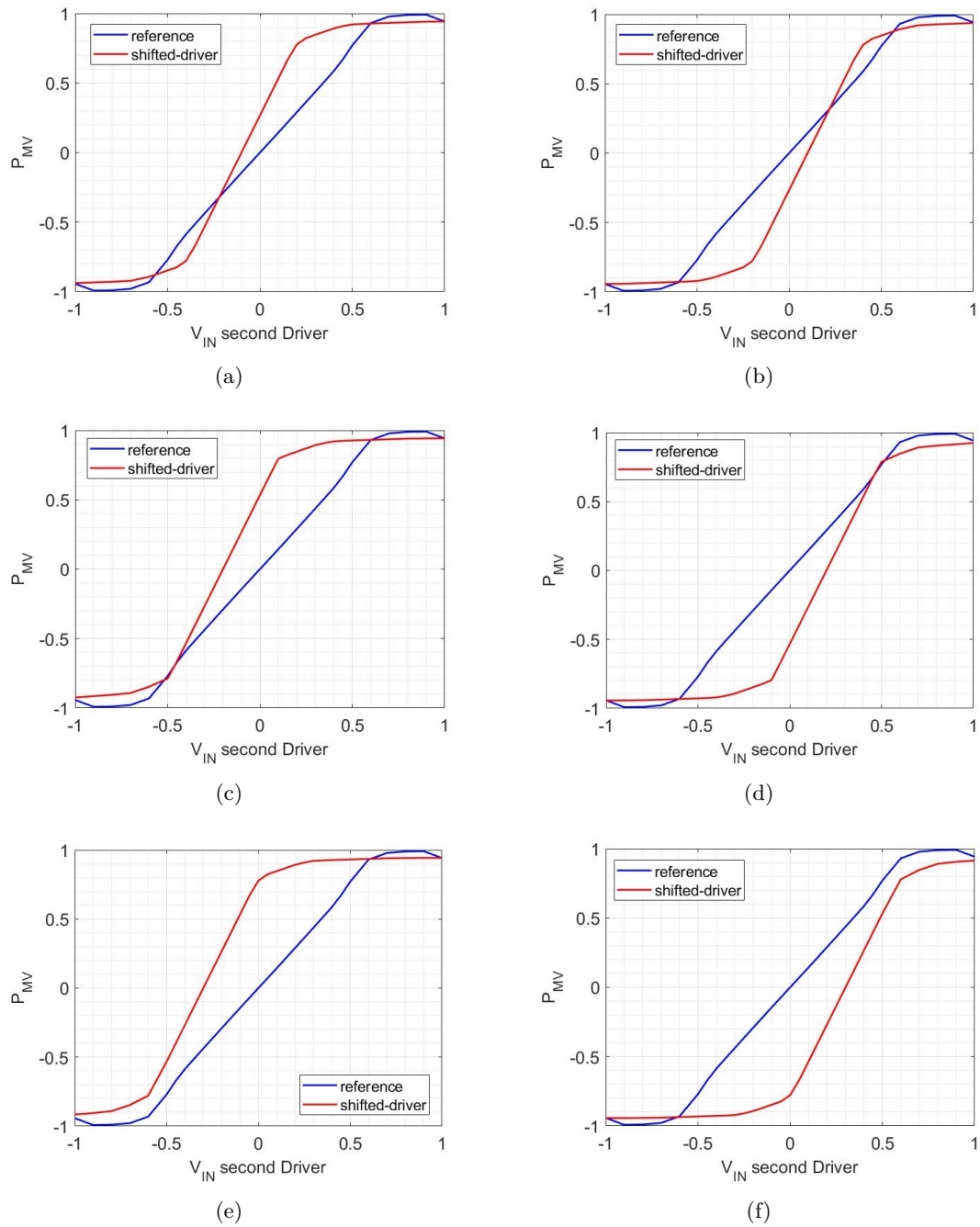


**Figure 5.11:** Polarization of the cell composed by the two drivers versus the input voltage on the second driver when: (a) the first driver is shifted by 0.1 V and the second by -0.1 V, (b) the first driver is shifted by -0.1 V and the second by 0.1 V, (c) the first driver is shifted by 0.2 V and the second by -0.2 V, (d) the first driver is shifted by -0.2 V and the second by 0.2 V, (e) the first driver is shifted by 0.3 V and the second by -0.3 V, (f) the first driver is shifted by -0.3 V and the second by 0.3 V.

The first thing that can be observed is the different slope of the polarization if compared to the reference case in which two bisferrocenes are used. This probably depends on the fact that the slope of the transcharacteristics themselves is different from that of the bisferrocene. The most interesting thing that is noticed is that if no voltage is applied, the shift from the reference curve is exactly that of the transcharacteristics. In this way, the problem highlighted by the use of external voltage on the molecules after the drivers explained in the previous section has therefore been solved. Furthermore, the problem related to the different slope of the curves would be resolved automatically when a saturator was placed after the two drivers, which would behave like a sort of rectifier.

In addition to the characteristics synthesized manually, it has been tried to use the transcharacteristic of the modified bisferrocene in which one of the iron atoms is replaced by a cobalt atom, described in Appendix A. One of the properties of that transcharacteristic was that for zero input voltage, there is a certain charge separation on the two dots, therefore it is like having a shifted characteristic. Since the shift is in one direction, it was decided to rotate one of the two drivers by  $180^\circ$ , to simulate a situation similar to the previous ones. Figure 5.12(a) shows the layout in which the  $180^\circ$  rotation of the first driver is visible, while Figure 5.12(b) shows the polarization curve versus the input voltage on the second driver.

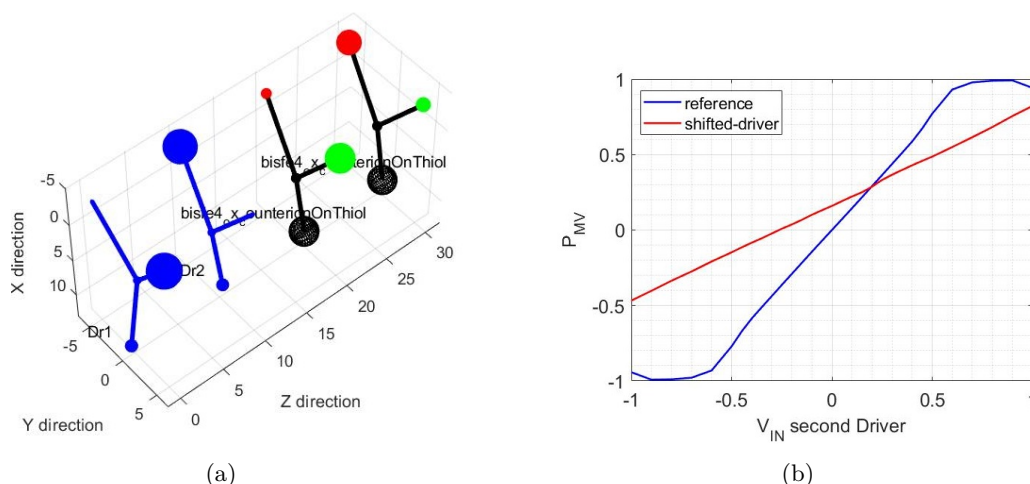


**Figure 5.12:** Study of the threshold mechanism using, as drivers, two bisferrocenes in which one of the iron atom is substituted by a cobalt atom: (a) SCERPA layout which highlight the  $180^\circ$  rotation of the first driver, (b) polarization versus the input voltage on the second driver.

In Figure 5.13(a), instead, the layout is shown in the case in which the rotation of  $180^\circ$  was made on the second driver, and in Figure 5.13(b) the polarization obtained in this case is shown.

It is observed that depending on the diagonal on which the iron and cobalt atoms are

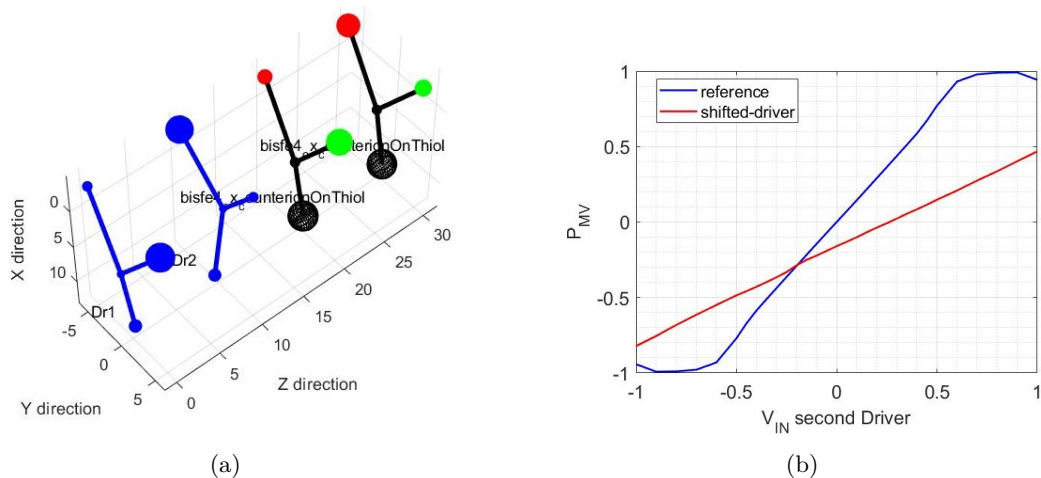


**Figure 5.13:** Study of the threshold mechanism using, as drivers, two bisferrocenes in which one of the iron atom is substituted by a cobalt atom: (a) SCERPA layout which highlight the  $180^\circ$  rotation of the second driver, (b) polarization versus the input voltage on the second driver.

placed, a shift is obtained in one direction rather than the other. The shift value coincides with that of the transcharacteristic, as already observed also with the transcharacteristics synthesized manually. Finally, it is seen that the polarization curve is a straight line as it is also the characteristic of the unsaturated molecules in the voltage range used.

An important consideration to do, for comparing this way of implementing the threshold with that described in the previous section that uses external voltage, concerns programmability. Choosing to implement the threshold through external voltage allows one to change the thresholds even once the circuit has been built. It would be sufficient to change the voltage between the two electrodes. If instead one chooses to use the molecules with the shifted transcharacteristic this is no longer valid: once the circuit is built, the molecules cannot be changed, and among other things, being inside the MV it would also be difficult to position the electrodes to influence the value with an externally applied voltage. In reality, normally the training of the networks almost exclusively changes the weights, therefore as regards the threshold the problem of managing a change is less relevant.

## 5.4 Step 5: toward neurons connected together

Up to now the various parts that make up a neuron have been studied separately. Before connecting multiple neurons, a single neuron made up of all its parts, from the interfaces to the output branch, has been simulated. The structure analysed is the one shown schematically in Figure 5.14(a). The interfaces were each made with two driver molecules, instead of one rotated by  $90^\circ$ . For interface 1, molecules with  $\alpha = 1$  V

were used, whereas, for the other two interfaces, molecules with  $\alpha = 3$  V were used. The two molecules after the central cell of the MV are two bisferrocenes, so it was decided not to use the saturator at this point. Figure 5.14(b) shows the layout obtained with SCERPA.

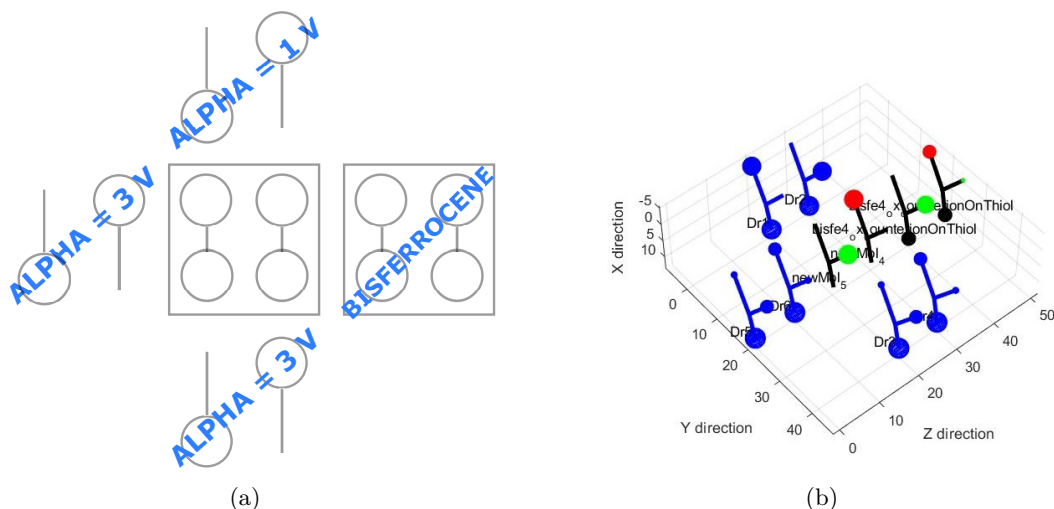


**Figure 5.14:** Layout of the complete neuron: (a) schematic representation, (b) SCERPA representation.

The input voltages on the drivers that make up the three interfaces have been chosen to have  $V_{in1} = +1$  V,  $V_{in2} = -1$  V,  $V_{in3} = -1$  V. Several molecules have been placed in the central cell of the MV, to simulate the behaviour even in the presence of the threshold. In the first case analysed, at the center of the MV, two bisferrocenes were used. With the interface configuration chosen, logic information slightly polarized as interface 1 is expected at the output, as shown in Figure 5.15. From the reference curve shown in the graphs of Figure 5.11 it is possible to evaluate the expected polarization once the voltage on the second molecule at the center of the MV is known. The latter is equal to 0.17 V, which corresponds approximately to  $P_{MV} = 0.2$ . The effective polarization is slightly lower, equal to 0.16.

Maintaining the same configuration of the inputs, it has been tried to put, at the center of the MV, the two molecules which implement a threshold equal to -0.2 V. Therefore the first molecule at the center of the MV will be a molecule with the transcharacteristic shifted of 0.2 V, while the other molecule in that cell will be shifted by -0.2 V. Since the voltage on the second molecule in the standard case with the bisferrocenes was 0.17 V, the sum of the input contributions is expected to be well above the threshold, thus leading to having the same logical information as interface 1, possibly with a greater polarization. In Figure 5.16(a) it is seen that the logical information is correctly calculated. The voltage on the second molecule at the center of the MV is equal to 0.51 V, which corresponds approximately to  $P_{MV} = 0.91$  as seen in Figure 5.11(c). The polarization calculated in this simulation is equal to 0.92, which confirms the correctness

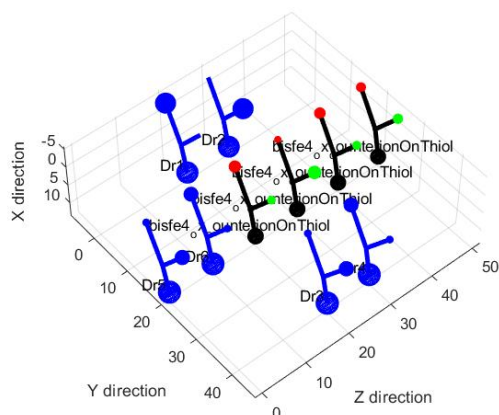


**Figure 5.15:** Simulation result of the neuron structure when the central cell of the MV is composed of bisferrocene molecules, that is threshold is equal to zero.

of the analysis made in the previous section.

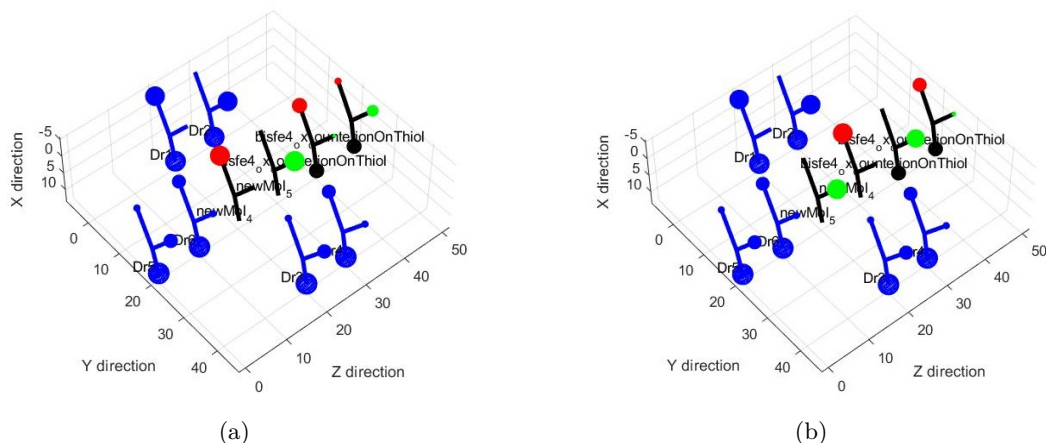


**Figure 5.16:** Simulation result of the neuron structure when: (a) the threshold is equal to  $-0.2$  V, (b) the threshold is equal to  $+0.2$  V.

Then it has been tried to put, at the center of the MV, the two molecules which implement a threshold equal to  $+0.2$  V. Therefore, the two molecules used before have been swapped places. This time the voltage that had been obtained with the bisferrocenes remains below the threshold, even if only slightly. Consequently, logical information opposite to that of the two previous cases is expected. Figure 5.16(b) shows the result of the simulation, which confirms the expectations: the logic information is opposite to that of interface 1.

Until now, interfaces have always been made with ideal drivers. Therefore it must be verified that even if these are non-ideal molecules, free to modify their charge distribution, the system continues to function correctly. The simulated layout scheme is shown in Figure 5.17.

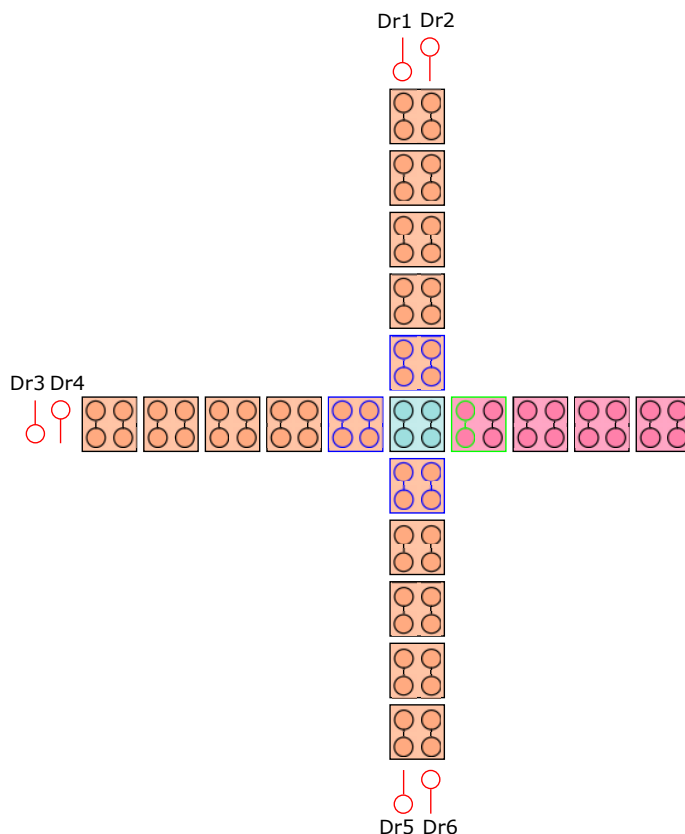
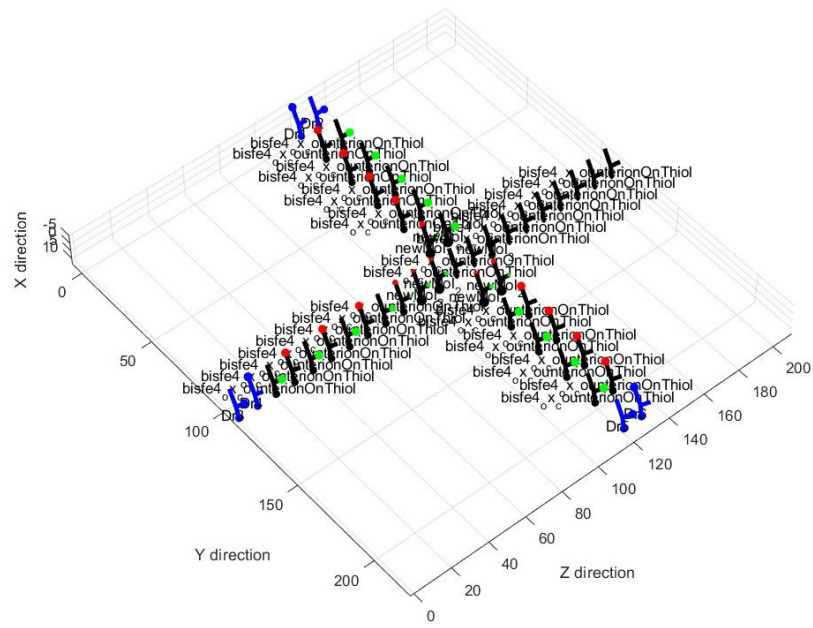


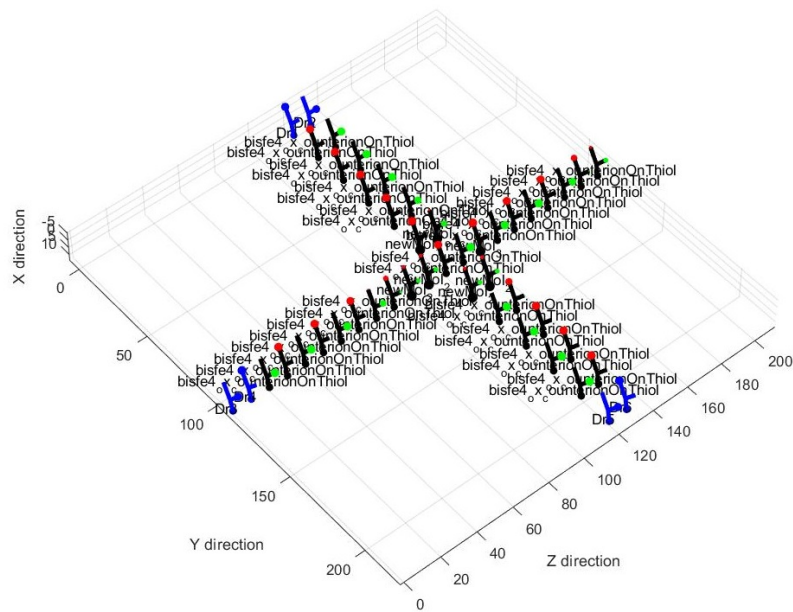
**Figure 5.17:** Schematic representation of the neuron layout with the interfaces connected to the drivers with short wires.

In Figure 5.17, the interfaces have been represented with a blue contour line, while the saturator with a green one. The other molecules are all bisferrocenes, except for the central cell of the MV which, depending on the threshold, has different molecules. The background color of the cells identifies the clock zone to which they belong. In particular, three clock zones were used: one for the inputs (orange), one for the computation of the output (light blue), and one for the propagation of the output (pink).

It was thought to repeat the same three simulations presented previously in this section so that the results obtained in this case could be easily compared. In Figure 5.18(a) and Figure 5.18(b) are shown the *input propagation* step and the *output propagation* step of the case with no threshold and the bisferrocenes molecules in the MV. In Figure 5.19 and Figure 5.20 are shown the same time steps of the case in which the threshold is equal to  $-0.2$  V and  $+0.2$  V, respectively.



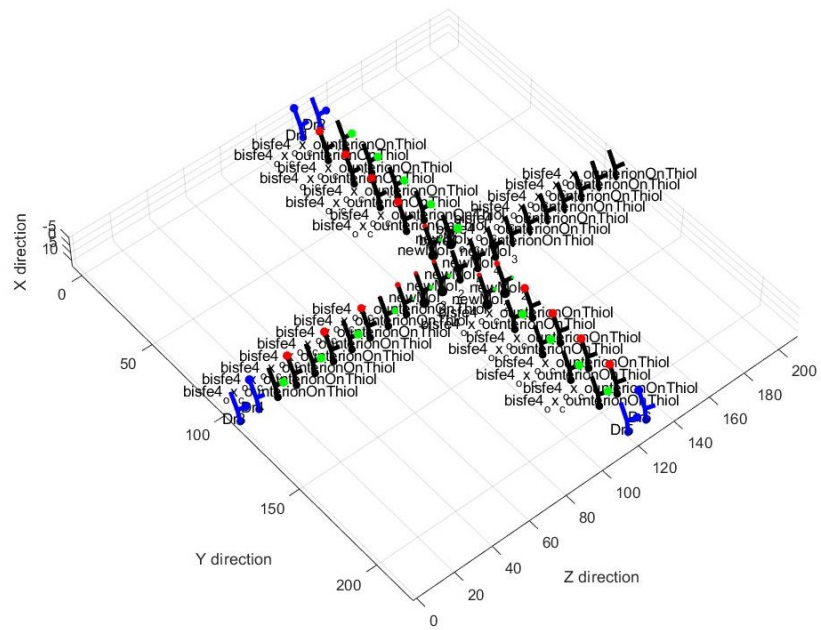
(a)



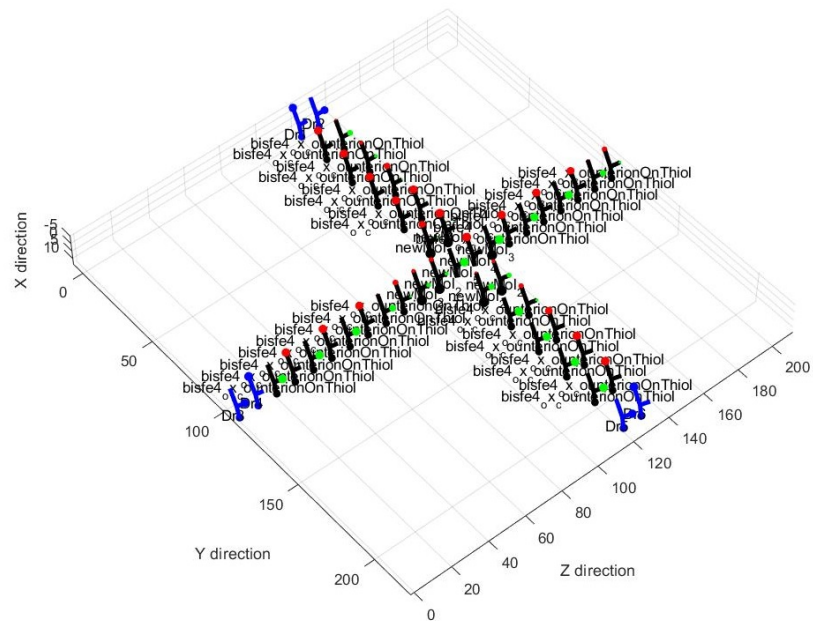
(b)

**Figure 5.18:** Simulation result of the neuron structure when there is no threshold: (a) *input propagation* time step, (b) *output propagation* time step.





(a)



(b)

**Figure 5.20:** Simulation result of the neuron structure when threshold is equal to 0.2 V: (a) *input propagation* time step, (b) *output propagation* time step.

Looking at the figures, it is possible to see that the results are perfectly consistent with what was found using drivers for the interfaces. One thing that can be noticed is that the molecules on the input branch change their charge distribution a lot during the *output propagation* step. This is not a problem that affects the functionality of the system, in fact assuming that one wants to submit a new input, those branches would first be reset, thus returning to the initial condition.



## Chapter 6

# Conclusion

The context in which this work fits includes several aspects. On the one hand, the demand for the implementation of complex tasks employing neural networks is increasingly growing, capable of solving problems other than those of classical computing. Hardware solutions of neural networks offer great advantages compared to the most common software solutions, allowing to complicate models and obtain better performance. The challenges still open are numerous, one of all linked to the enormous energy consumption required by these networks. On the other hand, there is the need to always find new solutions to keep up with technological development, which in recent years has encountered many obstacles to overcome. One of the many proposals made in recent years is the molecular FCN technology. The advantages offered by this technology are manifold, including the reduced energy consumption due to the absence of currents. Furthermore, thanks to the intrinsic characteristics of the molecules, this technology is promising also in the “neuromorphic computation” field.

The problems addressed in this work are related to the optimization of some hardware parameters of neural networks, including the size of a neural network and power consumption. In addition to this, one of the main objectives was to deepen the study of molecules to obtain specific high-level behaviours in circuits implemented in molecular FCN. To address these issues, it was decided to study how to implement a neuron in molecular FCN technology.

The ultimate goal of this work was to create a structure that behaved like an artificial neuron implemented in molecular FCN. To achieve this goal, the standard approach used to study circuits in this technology has been turned upside down. Thanks to a top-down approach, it was possible to understand how molecules must behave electrostatically to obtain specific high-level characteristics. This allows studying complex systems, such as a neuron, from a functional point of view without necessarily having all the specific characteristics of the molecule. In this way, once the properties of the molecule have been established, it is possible to synthesize it ad hoc.

To define a complete neuron, starting from the simple threshold model, the various parts have been analysed separately, from the realization of the synaptic weights up to the analysis of the propagation of the logical output information. Analysing different types of

molecules, it was understood that having molecules with too large an oxidation number generates a strong direct influence between the input and output of a MV, affecting the overall behaviour. In addition to this, it has been shown that it is not strictly necessary to work with oxidized molecules and that even neutral molecules behave similarly, as long as they have two distinct logical states. Again about the weighted inputs, the lower limit that the slope of the transcharacteristic can assume to guarantee correct behaviour was found. This also led to defining the maximum weight that can be obtained with the structure analysed.

Since the calculation of the total input contribution is made by making the molecules work in the linear region, it has been seen that without the presence of a saturator in some cases it was impossible to propagate the information with bistable behaviour. Having found the transcharacteristic that a saturator must have, allows to use it whenever signal regeneration is required, for instance with very long wires or where there are corner or "T" connections.

It has been shown that the threshold mechanism can be inserted in two ways: using an external voltage on the first molecules after the MV, or using particular molecules right inside it. In particular, in the latter case, it has been seen that to make a cell with a stronger logical state than the other, molecules with a transcharacteristic shifted toward the right or left to that of the bisferrocene can be used. It has also been seen that the two molecules within this cell must have opposite shifted transcharacteristics to achieve the desired effect.

Overall, it has come to show the correct behaviour of a neuron, composed of all its parts. Compared to the solutions present in the literature made in this same technology, not only have the various constituent parts of the neuron been studied separately, but they have also been linked together to analyse the complete behaviour. Furthermore, the proposed solution is very compact compared to others made in different technologies, thanks to the use of molecules.

The issues that remain to be explored in this area are many. The first step to deal with will be to connect several neurons and verify the behaviour of a network made of molecular FCN as a whole. Subsequently, it is possible to complicate the neuron model used at this point by also adding a memory mechanism for the realization of SNN. Another important aspect that must be studied concerns learning, therefore the possibility of adjusting the specific parameters of the neuron to allow training and self-learning of the network must be added. For what concerns the structure, a way to create neurons with more than three inputs will have to be studied, including the insertion of multiport devices. In addition to the studies concerning the functionality, in the future, the system should also be studied from the energy consumption point of view, to be able to compare a network implemented in molecular FCN with networks made of silicon, to be able to propose a valid alternative to the solutions presented up to to date.

# Appendix A

## Molecules analysis with orca

A commonly used approach for the study of systems in molecular FCN technology is MoSQuiTo, as described in Section 1.2. Starting from *ab initio* simulations of particular molecules, new figures of merit that describe the system at a higher level are obtained, and finally, the system is studied as a whole at a high level, based on what has been found previously. In this work, the approach used was the opposite: starting from system-level simulations, were obtained characteristics and properties that the underlying molecules should have. This allows directing the research in this field in a more precise way, knowing what are the constraints that must be respected to let the system work properly.

Despite this, it was decided to study, in parallel, some molecules that seemed of particular interest for the realization of neuromorphic computation in molecular FCN. For the *ab initio* simulations made, ORCA was used, which is a package of programs that implement all modern electronic structure methods [67], [68].

### A.1 Toward the characterization of a dendron

One of the interesting ideas touched on in Chapter 3 concerns branched molecules. In that context, what one would like to achieve is a branched molecule that, under certain working conditions, can collect electrons at the base of the trunk. A class of chemical compounds that have a structure similar to this, branched and highly symmetrical, is the so-called *dendrimer* class [65], [66].

In particular, in [69] a dendrimer is presented in which the terminations are ferrocenes or cobaltocenes. Since ferrocenes are groups also present in bisferrocene, which performs particularly well for the molecular FCN, and cobaltocene has the same structure but a cobalt atom in the center, it was decided to study the structure presented in [69] to see if it behaves like the desired one. It was decided to start with the study of only two terminations connected, a ferrocene and a cobaltocene, as shown in Figure A.1(a) and Figure A.1(b).

First, the molecule has been drawn with Avogadro. A first geometry optimization through molecular mechanics has been performed by mean of the *Auto Optimize Tool* provided by Avogadro itself. In particular, it has been used the default force field, which

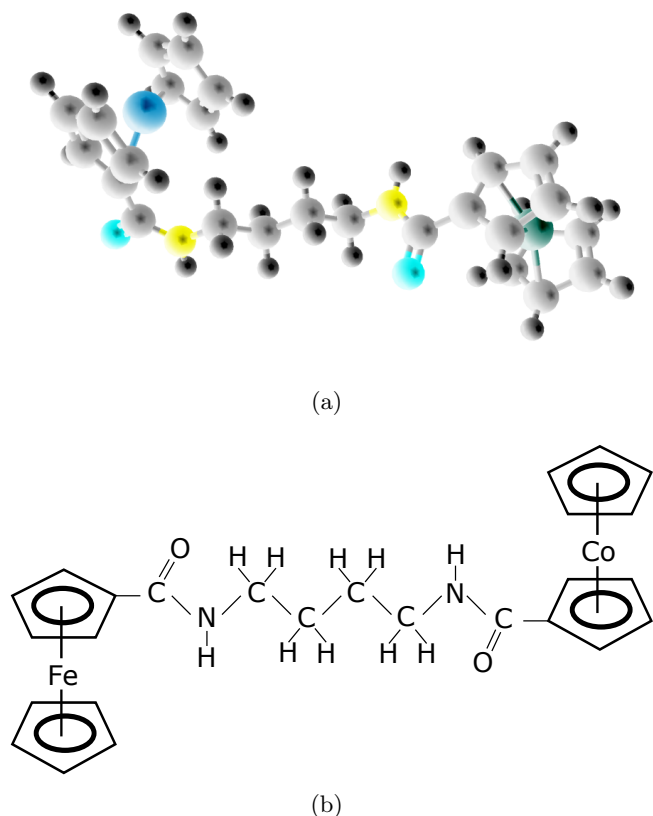


**Figure A.1:** Ferrocene-Cobaltocene molecule: (a) plotted with Avogadro, (b) schematic representation.

is *Universal Force Field (UFF)*, and the *Steepest Descendent* algorithm. Once the energy variation reached zero, the atoms' coordinates have been extracted and used to define the molecule in the input file for ORCA. Then the molecule geometry has been optimized with ORCA, using CAM-B3LYP hybrid functionals, def2-TZVPP basis sets (doubly polarized triple-zeta basis set) and D3 correction. After having reached the convergence, the molecule dipole moment has been characterized in presence of two point-charges, placed on the axis which connect the iron and cobalt atoms: at 4 Å distance from the Fe atom and at 5 Å from the Co atom. These two point-charges were used to emulate the presence of a fixed electric field.

Once the simulations with ORCA were finished, the data obtained were processed in MATLAB. The aggregate charge of ferrocene, cobaltocene, and chain was calculated. The three curves obtained are shown in Figure A.2(a). The input voltage range is quite high mainly because of the proximity of the point-charges from the molecule under test.

As can be seen from Figure A.2(a), the characteristic is not symmetrical concerning the applied voltage. The charge on the central chain remains more or less constant, it increases slightly with increasing voltage. The charge on ferrocene and cobaltocene

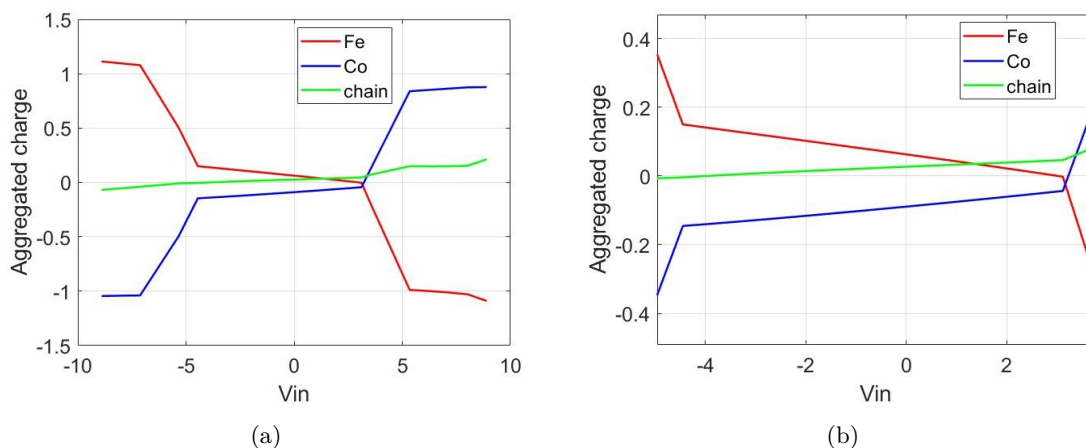


**Figure A.2:** VAC transcharacteristic of the Ferrocene-Cobaltocene molecule: (a) whole transcharacteristic, (b) enlargement of the central region.

varies slightly for voltages between about -4 V and +2 V, as seen from the zoom in Figure A.2(b). For voltages outside that range, the charge undergoes a strong variation, with an opposite sign on the ferrocene with respect to the cobaltocene, and for high voltages, it stabilizes on  $\pm 1$ , i.e. an electron has moved from the ferrocene to the cobaltocene or vice versa. Overall, the charge is always constant equal to zero, consistent with the fact that the studied molecule is neutral.

Another characterization that has been made, involves positioning the point-charges as shown in Figure A.3(a); the point-charges and the iron and cobalt atoms are positioned on the four vertices of a square with a 1.1 nm side.

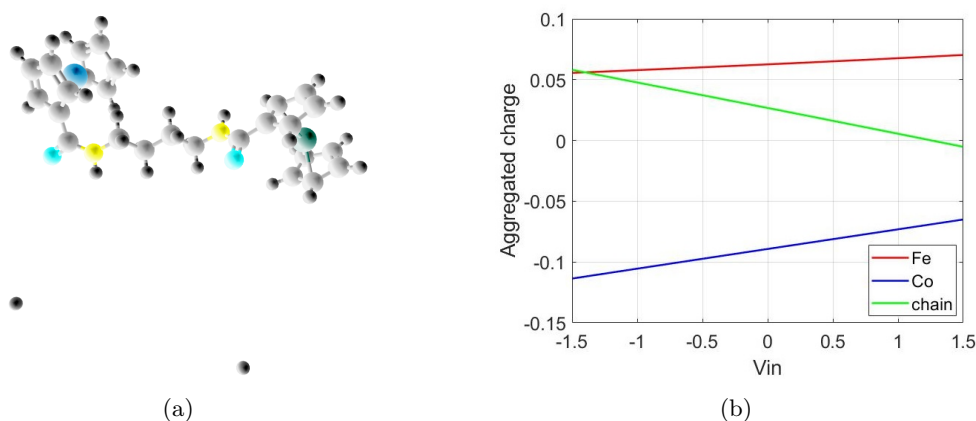


**Figure A.3:** Ferrocene-Cobaltocene molecule: (a) scheme that shows where point-charges have been positioned, (b) VAC transcharacteristic obtained in that case.

In this case, even if the absolute value of the point-charges used were the same as before, the voltage range is smaller, because of the bigger distance between the point-charges and the molecule under test. As can be in Figure A.3(b), charge variation is very small in this case. The aggregated charge on the ferrocene and the chain is always positive, but presents an opposite trend with the voltage increase: the charge on the ferrocene slightly increases, while that on the chain decreases by a greater amount. The aggregated charge on the cobaltocene is instead always negative and tends to reduce, in absolute value, increasing the voltage across the molecule.

Two other simulations have been made. In particular, it has been changed the number of carbon atoms present in the chain, one atom was added in one case, and one atom was removed in the other case. The geometry of the two molecules obtained has not been optimized, simply the metallocenes have been brought closer or further away. This was done to see how the distance between metallocenes affects the overall behaviour of the molecule. In both cases, the point-charges were placed on the same axis that connects ferrocene and cobaltocene, as in the first simulation presented, at a distance of 8 Å from the respective metallocene in both cases. The obtained transcharacteristics are shown in Figure A.4(a) in the case in which a carbon atom has been added to the chain, and in Figure A.4(b) in the case in which instead a carbon atom has been removed from the chain.

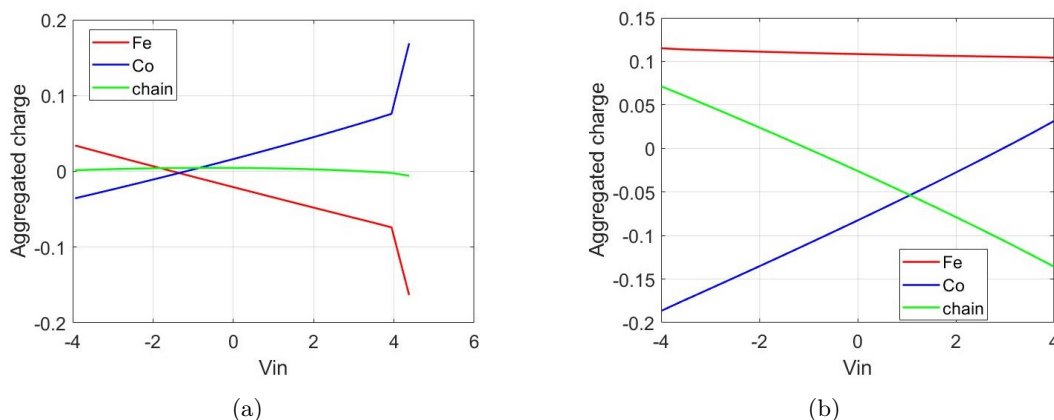


**Figure A.4:** VAC transcharacteristic for: (a) Ferrocene-Cobaltocene molecule with five carbon atoms in the chain, (b) Ferrocene-Cobaltocene molecule with three carbon atoms in the chain.

In the case in which the molecule has a longer chain, the the behaviour of the charge is quite similar to the standard case, only the point of intersection with the axis of the voltages by the charge on the metallocenes changes, which in this case occurs for a negative voltage. If, on the other hand, the chain is shorter, the charge on the ferrocene remains more or less constant, and the charge moves between the cobalt and the chain. However, it is not possible to draw precise conclusions since the geometries of the molecules have not been optimized.

## A.2 *Modified* bisferrocene

To better understand what it means to have different metal atoms in a molecule [70], it was decided to work with the structure of a molecule that has been extensively studied, namely the bisferrocene. In particular, it has been tried to replace one or both iron atoms with cobalt atoms, leaving the structure unchanged, to understand how the behaviour changes in terms of aggregate charge.

First, the structure with both iron atoms was simulated and is shown in Figure A.5. The simulation has been done using B3LYP hybrid functionals, LANL2DZ basis sets and SlowConv option which is recommended in the case of transition metals complexes. To get the transcharacteristics some point-charges have been placed to emulate the presence of electric fields. In particular, six point-charges were arranged. Two to simulate the presence of the clock, which were placed above and below the molecule, at a distance of 5 nm from the center of the molecule. The other four point-charges were used to simulate the presence of another bisferrocene molecule one nanometer away from the molecule under test as if to create a QCA cell.

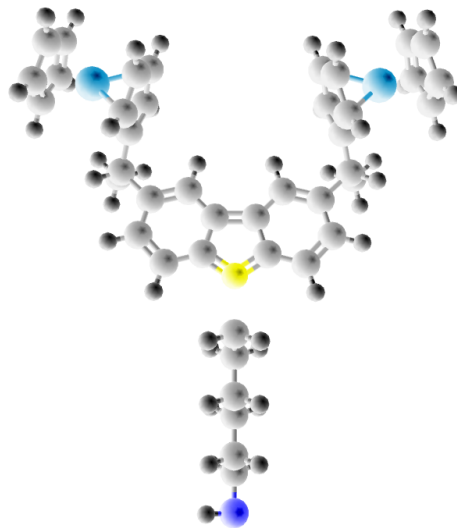


**Figure A.5:** Bis-ferrocene molecule.

The simulation results obtained with ORCA have been elaborated in MATLAB, to calculate the AC and to plot the VACT, for two different clock values, one that simulates the reset condition and the other which favours the presence of the charge in the logic dots. The VACT transcharacteristic has been calculated also in case no clock signal is present. The VACT when the clock signal is equal to +2 V is shown in Figure A.6(a), if the clock signal is equal to 0 V the transcharacteristic is that shown in Figure A.6(b), and if the clock signal is equal to -2 V the aggregated charge behaves like shown in Figure A.6(c).

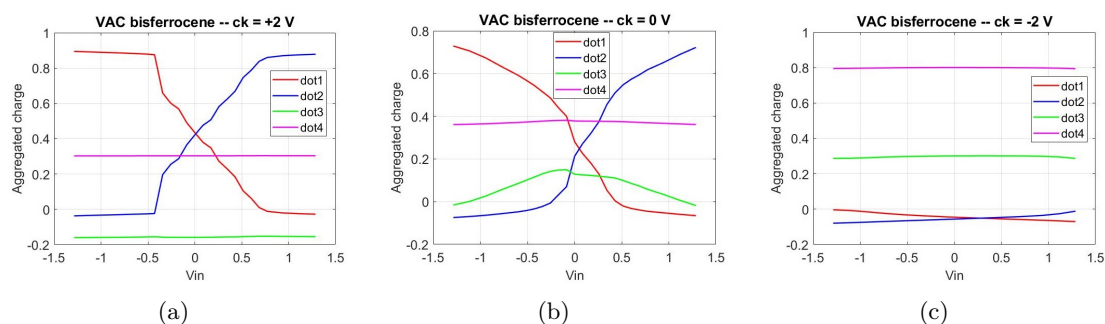


**Figure A.6:** VAC Transcharacteristics obtained from the ORCA data for the bisferrocene molecule when: (a) clock signal is equal to +2 V, (b) clock signal is equal to 0 V, (c) clock signal is equal to -2 V.

The total charge is equal to one since the molecule is oxidized. Without the presence of the clock signal, it can be seen that charge mainly moves between the two ferrocenes. If the clock signal is positive, the separation between the aggregated charge on the two logic dots increases, which justifies the use of the clock field to improve the bistability of the molecule. Around more or less -0.5 V and +0.6 V, charge saturates and stays constant even when increasing the input voltage. When the clock signal is negative on the other side, there is no charge on the logic dots, which is concentrated on Dot 3 and Dot 4.

After that, one of the two iron atoms was changed to a cobalt atom. The resulting structure is shown in Figure A.7. The point-charges were positioned in the same location as in the previous simulation.

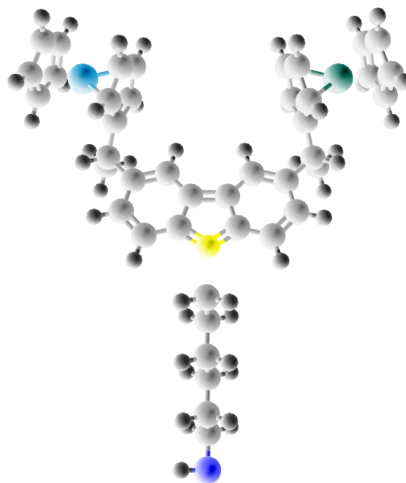


**Figure A.7:** Modified bis-ferrocene molecule with one cobalt atom instead of an iron atom.

Even in this case, the simulation results obtained with ORCA have been elaborated in MATLAB. The VACT when the clock signal is equal to +2 V is shown in Figure A.8(a), if the clock signal is equal to 0 V the transcharacteristic is that shown in Figure A.8(b), and if the clock signal is equal to -2 V the aggregated charge behaves like shown in Figure A.8(c).

The case in which the clock signal is negative the VACT is the same, confirming that this voltage is sufficient to reset the molecule. In the other two cases, the main aspect that can be noticed is that the transcharacteristics are no more symmetrical concerning the input voltage, in fact, with no input voltage there is a charge separation between the ferrocene and the cobaltocene. This means that an asymmetry in the structure corresponds to an asymmetry in the behaviour of the charge. To have the same charge on the two logic dots is necessary an input voltage equal to around 0.3 V if the clock signal is positive, and around 0.8 V if no clock signal is applied. The maximum charge reached by the logic dots doesn't increase with the presence of the clock signal which, in this case just linearizes the characteristics on the logic dots and moves the intersection point between them. Moreover, the positive clock signal leads to a constant negative charge on the Dot 3, whereas influences less the charge on the Dot 4. Finally, it can be seen that with this voltage range, the charge doesn't saturate as it happens in the bisferrocene. Nevertheless, for negative input voltage around -1.5 V it seems that curves begin to bend as if they were about to saturate, whereas for positive voltage this is far to be obtained since charge reaches 0.7 atomic units on the cobaltocene and less than 0.2 atomic units on the ferrocene.

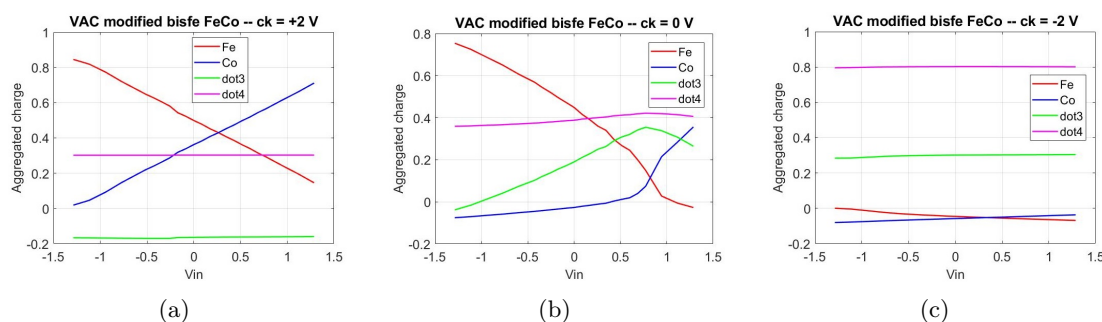


**Figure A.8:** VAC Transcharacteristics obtained from the ORCA data for the bisferrocene molecule with one cobalt atom instead of an iron atom, when: (a) clock signal is equal to +2 V, (b) clock signal is equal to 0 V, (c) clock signal is equal to -2 V.

Finally, the same structure has been characterized in the case in which both iron atoms are replaced by cobalt atoms, shown in Figure A.9. Even in this case, the point-charges were fixed in the same positions as in the other analysed cases.

The VACT obtained from the MATLAB elaboration when the clock signal is equal to +2 V is shown in Figure A.10(a), if the clock signal is equal to 0 V the transcharacteristic is that shown in Figure A.10(b), and if the clock signal is equal to -2 V the aggregated charge behaves like shown in Figure A.10(c).

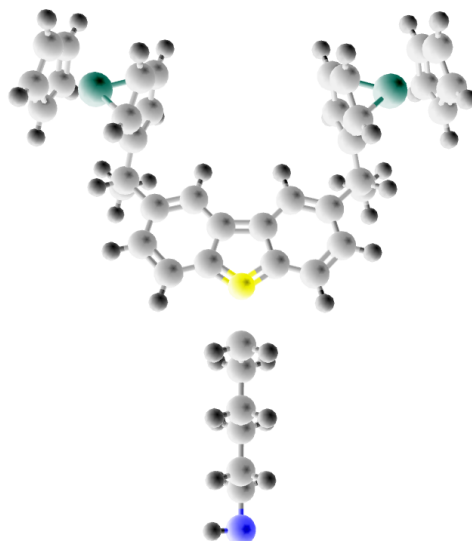


**Figure A.9:** *Modified* bis-ferrocene molecule with both the iron atoms substituted with cobalt atoms.

In this case, it is possible to notice that the transcharacteristic are again symmetrical concerning the input voltage. The main thing that emerges from this simulation is the poor influence of the clock signal on the charge. When it is positive the charge on the logic dots is almost the same as the case in which no clock field is applied, whereas charge on Dot 3 and Dot 4 slightly increase. On the other hand, if the applied clock signal is negative, the charge on the logic dots maintain the same behaviour but shifted downward. Charge on Dot 3 remains almost constant, whereas on Dot 4 charges is constant but at a higher value than of the other cases.

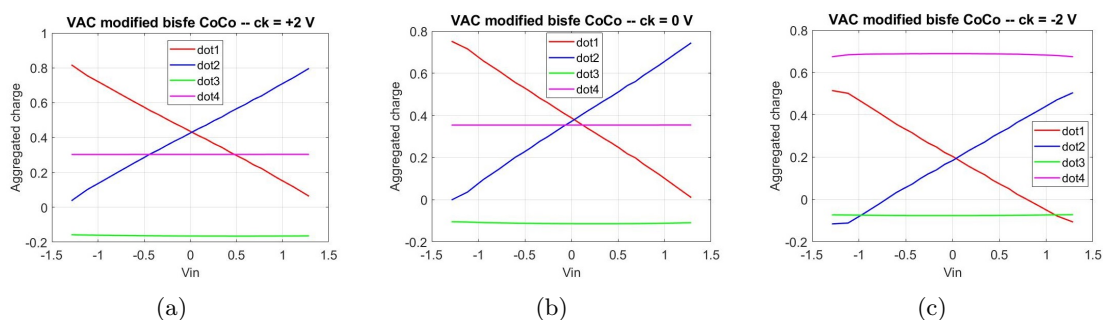


**Figure A.10:** VAC Transcharacteristics obtained from the ORCA data for the bisferrocene molecule with both the iron atoms substituted by cobalt atoms, when: (a) clock signal is equal to +2 V, (b) clock signal is equal to 0 V, (c) clock signal is equal to -2 V.

# Bibliography

- [1] G. E. Moore, “Cramming more components onto integrated circuits”, *Electronics*, vol. 38, no. 8, Apr. 1965.
- [2] M. Roser and H. Ritchie. (2020). Technological progress, [Online]. Available: <https://ourworldindata.org/technological-progress>.
- [3] M. Dubash. (2010). Moore’s law is dead, says gordon moore. Legendary chip man reviews the past, present and future, [Online]. Available: <https://www.techworld.com/news/tech-innovation/moores-law-is-dead-says-gordon-moore-3576581/>.
- [4] International Roadmap Committee. (2015). International technology roadmap for semiconductors 2.0, [Online]. Available: <http://www.itrs2.net/>.
- [5] K. D. Wise, “Microelectronics in the "more than moore" era”, in *68th Device Research Conference*, IEEE, Ed., South Bend, IN, USA, Jun. 2010. DOI: 10.1109/DRC.2010.5551936.
- [6] D. E. Nikonov and I. A. Young, “Overview of beyond-cmos devices and a uniform methodology for their benchmarking”, *Proceedings of the IEEE*, vol. 101, no. 12, pp. 2498–2533, Jun. 2013.
- [7] C. S. Lent, M. Liu, and Y. Lu, “Bennett clocking of quantum-dot cellular automata and the limits to binary logic scaling”, *Nanotechnology*, vol. 17, no. 16, Aug. 2006.
- [8] G. P. Boechler, J. M. Whitney, C. S. Lent, A. O. Orlov, and G. L. Sniderb, “Fundamental limits of energy dissipation in charge-based computing”, *Applied Physics Letters*, vol. 97, no. 10, Jul. 2010.
- [9] Y. Lu and C. S. Lent, “Theoretical study of molecular quantum-dot cellular automata”, *Journal of Computational Electronics*, vol. 4, pp. 115–118, Apr. 2005.
- [10] Y. Wang and M. Lieberman, “Thermodynamic behavior of molecular-scale quantum-dot cellular automata (qca) wires and logic devices”, *IEEE Transactions on Nanotechnology*, vol. 3, no. 3, pp. 368–376, Sep. 2004.
- [11] C. S. Lent, B. Isaksen, and M. Lieberman, “Molecular quantum-dot cellular automata”, *Journal of the American Chemical Society*, vol. 125, no. 4, pp. 1056–1063, Jan. 2003.

- [12] S. Srivastava, S. Sarkar, and S. Bhanja, “Estimation of upper bound of power dissipation in qca circuits”, *IEEE Transactions on Nanotechnology*, vol. 8, no. 1, pp. 116–127, Jan. 2009.
- [13] B. Hoeneisen and C. Mead, “Fundamental limitations in microelectronics—i. mos technology”, *Solid-State Electronics*, vol. 15, no. 7, pp. 819–829, Jul. 1972.
- [14] B. Isaksen and C. Lent, “Molecular quantum-dot cellular automata”, in *Third IEEE Conference on Nanotechnology, 2003. IEEE-NANO 2003.*, IEEE, Ed., vol. 2, San Francisco, CA, USA, Aug. 2003, pp. 5–8.
- [15] R. Wang, A. Pulimeno, M. Ruo Roch, G. Turvani, G. Piccinini, and M. Graziano, “Effect of a clock system on bis-ferrocene molecular qca”, *IEEE Transactions on Nanotechnology*, vol. 45, no. 4, pp. 574–582, Jul. 2016.
- [16] I. Amlani, A. O. Orlov, G. Toth, G. H. Bernstein, C. S. Lent, and G. L. Snider, “Digital logic gate using quantum-dot cellular automata”, *Science*, vol. 284, no. 5412, pp. 289–291, Apr. 1999.
- [17] M. Liu and C. S. Lent, “Reliability and defect tolerance in metallic quantum-dot cellular automata”, *Journal of Electronic Testing*, vol. 23, 211–218, Mar. 2007.
- [18] M. Governale, M. Macucci, G. Iannaccone, and C. Ungarelli, “Modeling and manufacturability assessment of bistable quantum-dot cells”, *Journal of Applied Physics*, vol. 85, no. 5, pp. 2962–2971, Feb. 1999.
- [19] R. P. Cowburn and M. E. Welland, “Room temperature magnetic quantum cellular automata”, *Science*, vol. 287, no. 5457, pp. 1466–1468, Feb. 2000.
- [20] J. Y. Cheng, F. Zhang, V. P. Chuang, and C. A. Mayes Anne M. Ross, “Self-assembled one-dimensional nanostructure arrays”, *Nano Letters*, vol. 6, no. 9, pp. 2099–2103, Aug. 2006.
- [21] V. Arima, M. Iurlo, L. Zoli, S. Kumar, M. Piacenza, F. Della Sala, F. Matino, G. Maruccio, R. Rinaldi, F. Paolucci, M. Marcaccio, P. G. Cozzi, and A. P. Bramanti, “Toward quantum-dot cellular automata units: Thiolated-carbazole linked bisferrocenes”, *Nanoscale*, vol. 4, pp. 813–823, 2012.
- [22] E. P. Blair, E. Yost, and C. S. Lent, “Power dissipation in clocking wires for clocked molecular quantum-dot cellular automata”, *Journal of Computational Electronics*, vol. 9, pp. 49–55, Mar. 2010.
- [23] Y. Lu, M. Liu, and C. S. Lent, “Molecular electronics - from structure to circuit dynamics”, in *2006 Sixth IEEE Conference on Nanotechnology*, IEEE, Ed., Cincinnati, OH, USA, Oct. 2006, pp. 62–65.
- [24] B. Schneider, S. Demeshko, S. Neudeck, S. Dechert, and F. Meyer, “Mixed-spin  $[2 \times 2]$  fe4 grid complex optimized for quantum cellular automata”, *Inorganic Chemistry*, vol. 52, no. 22, pp. 13 230–13 237, Oct. 2013.

- 
- [25] J. Jiao, G. J. Long, L. Rebbouh, F. Grandjean, A. M. Beatty, and T. P. Fehlner, “Properties of a mixed-valence (feii)2(feiii)2 square cell for utilization in the quantum cellular automata paradigm for molecular electronics”, *Journal of the American Chemical Society*, vol. 127, no. 50, pp. 17 819–17 831, Nov. 2005.
- [26] A. Pulimeno, M. Graziano, and G. Piccinini, “Molecule interaction for qca computation”, in *2012 12th IEEE International Conference on Nanotechnology (IEEE-NANO)*, IEEE, Ed., Birmingham, UK, Aug. 2012, pp. 1–5.
- [27] A. Pulimeno, M. Graziano, R. Wang, D. Demarchi, and G. Piccinini, “Charge distribution in a molecular qca wire based on bis-ferrocene molecules”, in *2013 IEEE/ACM International Symposium on Nanoscale Architectures (NANOARCH)*, IEEE, Ed., Brooklyn, NY, USA, Jul. 2013, pp. 42–43.
- [28] A. Pulimeno, M. Graziano, A. Sanginario, V. Cauda, D. Demarchi, and G. Piccinini, “Bis-ferrocene molecular qca wire: Ab initio simulations of fabrication driven fault tolerance”, *IEEE Transactions on Nanotechnology*, vol. 12, no. 4, pp. 498 – 507, May 2013.
- [29] Y. Ardesi, A. Pulimeno, M. Graziano, F. Riente, and G. Piccinini, “Effectiveness of molecules for quantum cellular automata as computing devices”, *Journal of Low Power Electronics and Applications*, vol. 8, no. 24, Jul. 2018.
- [30] Y. Ardesi, R. Wang, G. Turvani, G. Piccinini, and M. Graziano, “Scerpa: A self-consistent algorithm for the evaluation of the information propagation in molecular field-coupled nanocomputing”, *IEEE Transactions on Computer-Aided Design of Integrated Circuits and Systems*, Dec. 2019.
- [31] A. Pulimeno, M. Graziano, D. Demarchi, and G. Piccinini, “Towards a molecular qca wire: Simulation of write-in and read-out systems”, *Solid-State Electronics*, vol. 77, pp. 101–107, Nov. 2012.
- [32] E. P. Blair, “Quantum-dot cellular automata: A clocked architecture for high-speed, energy-efficient molecular computing”, in *Unconventional Computation and Natural Computation*, M. J. Patitz and M. Stannett, Eds., Cham: Springer International Publishing, 2017, pp. 56–68, ISBN: 978-3-319-58187-3.
- [33] W. S. McCulloch and W. Pitts, “A logical calculus of the ideas immanent in nervous activity”, *Bulletin of Mathematical Biophysics*, vol. 5, 115–133, Dec. 1943.
- [34] K. Gurney, *An introduction to neural networks*. UCL Press, 1997.
- [35] R. Agundez. (Mar. 2018). Multi-threshold neuron model, [Online]. Available: <https://blog.godatadriven.com/rod-multi-threshold-neuron>.
- [36] R. Ghasemiyeh, R. Moghdani, and S. Sana, “A hybrid artificial neural network with metaheuristic algorithms for predicting stock price”, *Cybernetics and Systems*, pp. 1–28, Mar. 2017.
- [37] V. K. Ojha, A. Abraham, and V. Snášel, “Metaheuristic design of feedforward neural networks: A review of two decades of research”, *Engineering Applications of Artificial Intelligence*, vol. 60, pp. 97–116, Apr. 2017.

- [38] A. Dey, “Machine learning algorithms: A review”, (*IJCSIT*) *International Journal of Computer Science and Information Technologies*, vol. 7, no. 3, pp. 1174–1179, 2016.
- [39] B. Krose and P. van der Smagt, *An introduction to Neural Networks*. University of Amsterdam, Nov. 1996.
- [40] H. Jang, O. Simeone, B. Gardner, and A. Grüning, “An introduction to probabilistic spiking neural networks. probabilistic models, learning rules, and applications”, *IEEE SIGNAL PROCESSING MAGAZINE*, 2019.
- [41] H. Paugam-Moisy, “Spiking neuron networks a survey”, 2006. [Online]. Available: <http://infoscience.epfl.ch/record/83371>.
- [42] W. M. Kistler, W. Gerstner, and J. L. v. Hemmen, “Reduction of the hodgkin-huxley equations to a single-variable threshold model”, *Neural Computation*, vol. 9, no. 5, pp. 1015–1045, 1997. DOI: 10.1162/neco.1997.9.5.1015. [Online]. Available: <https://doi.org/10.1162/neco.1997.9.5.1015>.
- [43] J. Vreeken, “Spiking neural networks, an introduction”, Adaptive Intelligence Laboratory, Intelligent Systems Group, Institute for Information and Computing Sciences, Utrecht University, Tech. Rep., 2003.
- [44] J. Misra and I. Saha, “Artificial neural networks in hardware: A survey of two decades of progress”, *Neurocomputing*, vol. 74, 239–255, May 2010.
- [45] J.-H. Chung, H. Yoon, and S. R. Maeng, “A systolic array exploiting the inherent parallelisms of artificial neural networks”, *Microprocessing and Microprogramming*, vol. 33, no. 3, pp. 145–159, May 1992.
- [46] H. Amin, K. Curtis, and B. Hayes Gill, “Two-ring systolic array network for artificial neural networks”, *IEE Proceedings - Circuits, Devices and Systems*, vol. 146, no. 5, 225 – 230, Oct. 1999.
- [47] Holler, Tam, Castro, and Benson, “An electrically trainable artificial neural network (etann) with 10240 ‘floating gate’ synapses”, in *International 1989 Joint Conference on Neural Networks*, IEEE, Ed., Washington, DC, USA, 1989, pp. 191–196.
- [48] M. Milev and M. Hristov, “Analog implementation of ann with inherent quadratic nonlinearity of the synapses”, *IEEE Transactions on Neural Networks*, vol. 14, no. 5, pp. 1187 –1200, Sep. 2003.
- [49] P. Masa, K. Hoen, and H. Wallinga, “A high-speed analog neural processor”, *IEEE Micro*, vol. 14, no. 3, pp. 40 –50, Jun. 1994.
- [50] R. Douglas, M. Mahowald, and K. Martin, “Hybrid analog-digital architectures for neuromorphic systems”, in *Proceedings of 1994 IEEE International Conference on Neural Networks (ICNN’94)*, IEEE, Ed., vol. 3, Orlando, FL, USA, 1994, pp. 1848–1853.

- 
- [51] Y. Maeda and T. Tada, “Fpga implementation of a pulse density neural network with learning ability using simultaneous perturbation”, *IEEE Transactions on Neural Networks*, vol. 14, no. 3, pp. 688–695, May 2003.
- [52] M. Krips, T. Lammert, and A. Kummert, “Fpga implementation of a neural network for a real-time hand tracking system”, in *Proceedings First IEEE International Workshop on Electronic Design, Test and Applications 2002*, IEEE, Ed., Christchurch, New Zealand, New Zealand, 2002, pp. 313–317.
- [53] T. J. Koickal, L. C. Gouveia, and A. Hamilton, “A programmable spike-timing based circuit block for reconfigurable neuromorphic computing”, *Neurocomputing*, vol. 72, no. 16-18, pp. 3609–3616, Oct. 2009.
- [54] T. Schoenauer, S. Atasoy, N. Mehrtash, and H. Klar, “Neuropipe-chip: A digital neuro-processor for spiking neural networks”, *IEEE Transactions on Neural Networks*, vol. 13, no. 1, pp. 205–213, Jan. 2002.
- [55] P. D. Moerland, E. Fiesler, and I. Saxena, “Incorporation of liquid-crystal light valve nonlinearities in optical multilayer neural networks”, *Applied Optics*, vol. 35, no. 26, pp. 5301–5307, 1996.
- [56] F. T. S. Yu, T. Lu, X. Yang, and D. A. Gregory, “Optical neural network with pocket-sized liquid-crystal televisions”, *Optics Letters*, vol. 15, no. 15, pp. 863–865, 1990.
- [57] J. Gupta and D. Koppad, “Artificial neural network hardware implementation: Recent trends and application”, in *Computational Vision and Bio-Inspired Computing*, S. Smys, J. Tavares, V. Balas, and A. Ilyasu, Eds., 2020, pp. 345–354.
- [58] S. Wang, L. Cai, H. Cui, C. Feng, and X. Yang, “Three-dimensional quantum cellular neural network and its application to image processing”, in *2017 IEEE/ACIS 16th International Conference on Computer and Information Science (ICIS)*, IEEE, Ed., Wuhan, China, 2017, pp. 411–415.
- [59] A. Jaiswal, S. Roy, G. Srinivasan, and K. Roy, “Proposal for a leaky-integrate-fire spiking neuron based on magnetoelectric switching of ferromagnets”, *IEEE Transactions on Electron Devices*, vol. 64, no. 4, pp. 1818–1824, Apr. 2017.
- [60] E. P. Blair and S. Koziol, “Neuromorphic computation using quantum-dot cellular automata”, in *2017 IEEE International Conference on Rebooting Computing (ICRC)*, IEEE, Ed., Washington, DC, USA, 2017, pp. 1–4.
- [61] M. Prezioso, “Experimental analog implementation of neural networks on integrated metal-oxide memristive crossbar arrays”, in *2016 IEEE 16th International Conference on Nanotechnology (IEEE-NANO)*, IEEE, Ed., Sendai, Japan, 2016, pp. 276–279.
- [62] S. Duan, X. Hu, Z. Dong, L. Wang, and P. Mazumder, “Memristor-based cellular nonlinear/neural network: Design, analysis, and applications”, *IEEE Transactions on Neural Networks and Learning Systems*, vol. 26, no. 6, pp. 1202–1213, Jun. 2015.

- [63] Y. Ardesi, M. Graziano, and G. Piccinini. (Dec. 2018). System level bistability of molecular field-coupled nanocomputing, [Online]. Available: [https://www.researchgate.net/publication/329814354\\_System\\_level\\_bistability\\_of\\_molecular\\_Field-Coupled\\_Nanocomputing](https://www.researchgate.net/publication/329814354_System_level_bistability_of_molecular_Field-Coupled_Nanocomputing).
- [64] V. Beiu, J. Quintana, and M. Avedillo, “Vlsi implementations of threshold logic-a comprehensive survey”, *IEEE Transactions on Neural Networks*, vol. 14, no. 5, pp. 1217–1243, Sep. 2003.
- [65] L. L. Miller, R. G. Duan, D. C. Tully, and D. A. Tomalia, “Electrically conducting dendrimers”, *Journal of the American Chemical Society*, vol. 119, no. 5, pp. 1005–1010, Feb. 1997.
- [66] A.-M. Caminade, D. Yanc, and D. K. Smithd, “Dendrimers and hyperbranched polymers”, *Chemical Society Reviews*, vol. 44, pp. 3870–3873, May 2015.
- [67] F. Neese, “Software update: The orca program system, version 4.0”, *WIREs Computational Molecular Science*, vol. 8, no. 1, Feb. 2018.
- [68] F. Neese and F. Wennmohs, *Orca - an ab initio, dft and semiempirical scf-mo package, Version 4.0.1 - release*, 2017. [Online]. Available: [https://cec.mpg.de/fileadmin/media/Forschung/ORCA/orca\\_manual\\_4\\_0\\_1.pdf](https://cec.mpg.de/fileadmin/media/Forschung/ORCA/orca_manual_4_0_1.pdf).
- [69] C. M. Casado, B. G. I. Cuadrado, B. Alonso, M. Morán, and J. Losada, “Mixed ferrocene–cobaltocenium dendrimers: The most stable organometallic redox systems combined in a dendritic molecule”, *Angewandte Chemie International Edition*, vol. 39, no. 12, pp. 2135–2138, Jun. 2000.
- [70] H. Bauer, J. Weismann, D. Saurenz, C. Farber, M. Schar, W. Gidt, I. Schadlich, G. Wolmershäuser, Y. Sun, S. Harder, and H. Sitzmann, “Chromocene, ferrocene, cobaltocene, and nickelocene derivatives with isopropyl and methyl or trimethylsilyl substituents”, *Journal of Organometallic Chemistry*, vol. 809, pp. 63–73, May 2016.